THREE-DIMENSIONAL GROUND-WATER FLOW MODEL OF THE WATER-TABLE AQUIFER IN VEGA ALTA, PUERTO RICO

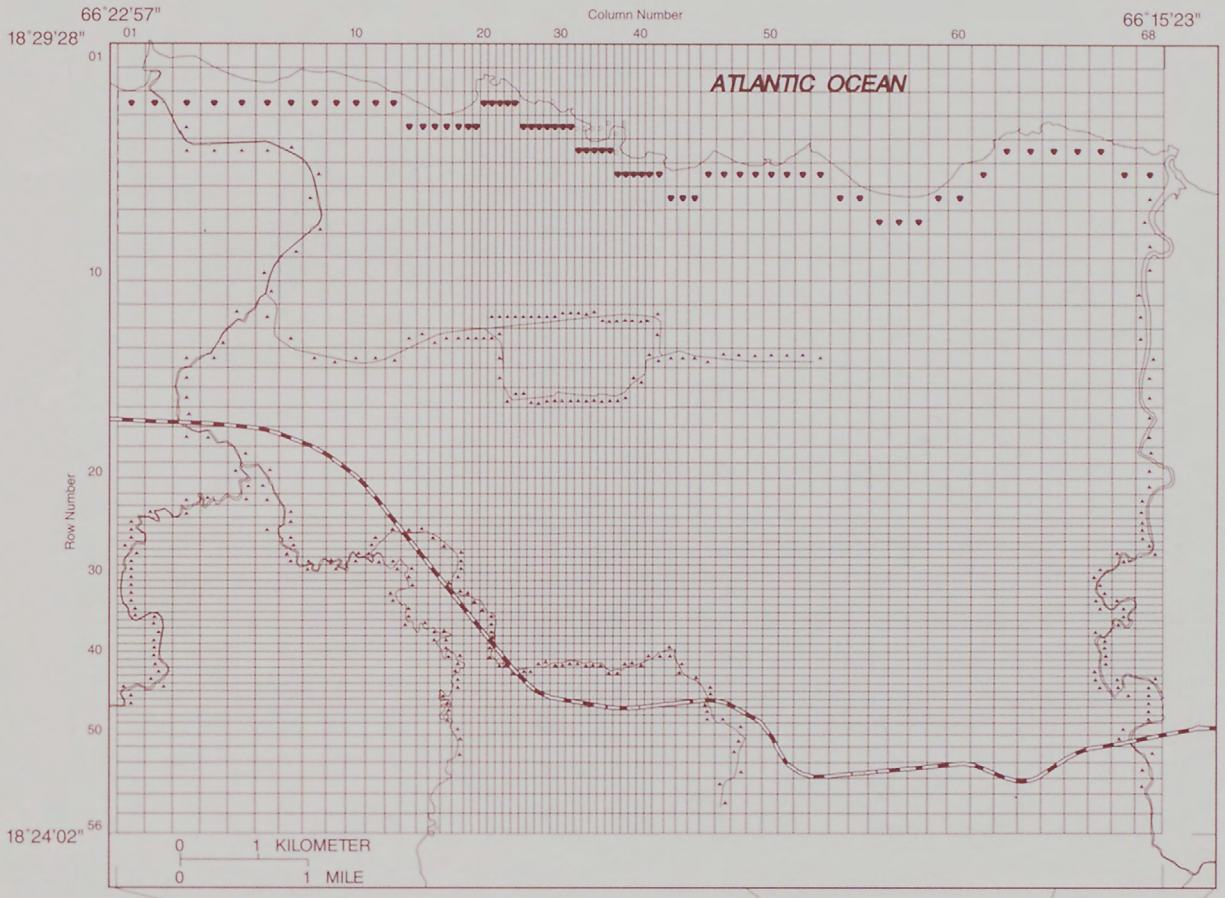

U.S. GEOLOGICAL SURVEY
Water-Resources Investigations
Report 95-4184

Prepared in cooperation with the
PUERTO RICO INDUSTRIAL DEVELOPMENT COMPANY

THREE-DIMENSIONAL GROUND-WATER FLOW MODEL OF THE WATER-TABLE AQUIFER IN VEGA ALTA, PUERTO RICO

By Nicasio Sepúlveda

U.S. GEOLOGICAL SURVEY

Water-Resources Investigations Report 95-4184

Prepared in cooperation with the

PUERTO RICO INDUSTRIAL DEVELOPMENT COMPANY

San Juan, Puerto Rico
1996

U.S. DEPARTMENT OF THE INTERIOR

BRUCE BABBITT, Secretary

U.S. GEOLOGICAL SURVEY

Gordon P. Eaton, Director

For additional information write to:

District Chief
U.S. Geological Survey
GSA Center
651 Federal Drive, Suite 400-15
San Juan, Puerto Rico 00965

Copies of this report can be purchased from:

U.S. Geological Survey
Earth Science Information Center
Open-File Reports Section
Box 25286, MS 517
Denver Federal Center
Denver, CO 80225

CONTENTS

FIGURES

TABLES

CONVERSION FACTORS, ABBREVIATED WATER-QUALITY UNITS, AND ACRONYMS

Multiply	By	To obtain
cubic foot per second (ft^3/s)	0.028317	cubic meter per second
foot (ft)	0.3048	meter
foot per day (ft/d)	0.3048	meter per day
foot squared per day (ft^2/d)	0.092903	meter squared per day
gallon (gal)	0.0037854	cubic meter
gallon per minute (gal/min)	0.063091	liter per second
inch (in.)	2.540	centimeter
inch per year (in/yr)	2.540	centimeter per year
mile (mi)	1.6093	kilometer
pound per square inch (lb/in^2)	6,894.8	Pascals
pound per square inch per foot [$(lb/in^2)/ft$]	22,615	Pascals per meter
square mile (mi^2)	2.5916	square kilometer

Abbreviated water-quality units used in report:

gram per milliliter (g/mL)

milligram per liter (mg/L)

microgram per liter (µg/L)

Acronyms used in report:

U.S. Geological Survey (USGS)

U.S. Environmental Protection Agency (EPA)

Puerto Rico Industrial Development Company (PRIDCO)

National Oceanic and Atmospheric Administration (NOAA)

Three-Dimensional Ground-Water Flow Model of the Water-Table Aquifer in Vega Alta, Puerto Rico

By Nicasio Sepúlveda

Abstract

A transient three-dimensional ground-water flow model is presented for the water-table aquifer in Vega Alta, Puerto Rico, using MODFLOW, the finite-difference modular model developed by the U.S. Geological Survey. The model simulates the period extending from February 1983 to April 1992. Slug tests were conducted in wells with access to multiple pumping ports (multiport wells) installed in the water-table aquifer to define horizontal and vertical variations in hydraulic conductivity for the area. Specific-capacity tests were also conducted in single-port wells to improve the definition of the transmissivity map. Vertical hydraulic gradients prevailing in the vicinity of the multiport wells were used to extrapolate variations of water levels with depth in areas away from the locations of these multiport wells. The process used to assign values for specific yield, rainfall recharge, riverbed conductance, and areal, as well as vertical distribution of hydraulic conductivity, is discussed in this report. The initial water level distribution for the ground-water flow simulation discussed in this report was generated using water levels measured during February 1983. The simulated period is divided into 12 stress periods of variable duration. The last five of these stress periods were chosen to end in January 1991, May 1991, August 1991, January 1992, and April 1992, coinciding with five rounds of water-level measurements performed in the area. The reasonable agreement between the measured and simulated water levels obtained for these five stress periods assesses the reliability of the values assigned to the hydraulic properties that characterize the ground-water flow of the Vega Alta water-table aquifer.

INTRODUCTION

The development of a transient three-dimensional ground-water flow model for the Vega Alta water-table aquifer has been conducted by the U.S. Geological Survey (USGS) in cooperation with the Puerto Rico Industrial Development Company (PRIDCO). The Vega Alta water-table aquifer is located approximately 20 mi west of San Juan, Puerto Rico. This aquifer is approximately 51.35 mi^2 in extent, including areas of the municipalities of Vega Baja, Vega Alta, and Dorado (fig. 1). Even though this water-table aquifer exists in parts of three municipalities, it will be referred to in this report as the Vega Alta water-table aquifer. A ground-water flow model for this water-table aquifer is presented based on MODFLOW, the USGS modular three-dimensional finite-difference ground-water flow model (McDonald and Harbaugh, 1988). This model is based on the solution of the ground-water flow equation using finite differences and a block-centered formulation, where the nodes for which water levels are simulated are located at the center of the grid cells. These cells are the smallest volumetric units over which the hydraulic properties are assumed constant.

Trichloroethylene, C_2HCl_3, is a volatile organic compound commonly denoted as TCE. In March 1983, the USGS (Guzmán-Ríos and Quiñones-Márquez, 1984) detected TCE concentrations of 84 and 412 µg/L in water samples taken from wells 65 and 86, respectively. All wells from which hydraulic or water-quality data were obtained are shown in figure 2 and listed in table 1. The detection of TCE in water samples from wells 65 and 86, as well as additional analyses of other samples, led to the designation of a section of the Vega Alta water-table aquifer as a Superfund site (NUS Corporation, 1986) by the U.S. Environmental Protection Agency (EPA). In this report, the ground-water flow model for the Vega Alta water-table aquifer is presented.

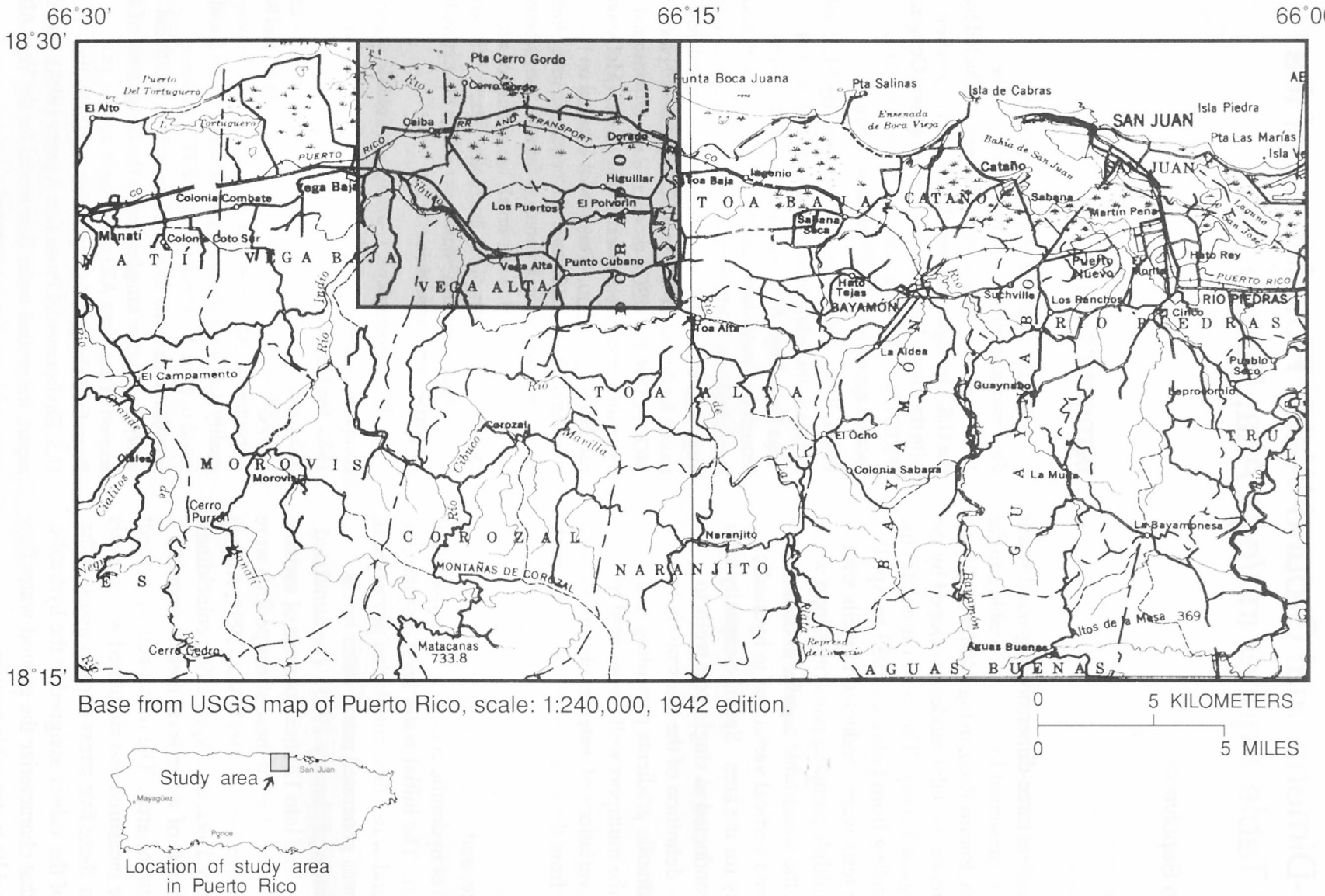

Figure 1. Location of study area and municipalities of Vega Baja, Vega Alta, and Dorado with respect to San Juan, Puerto Rico.

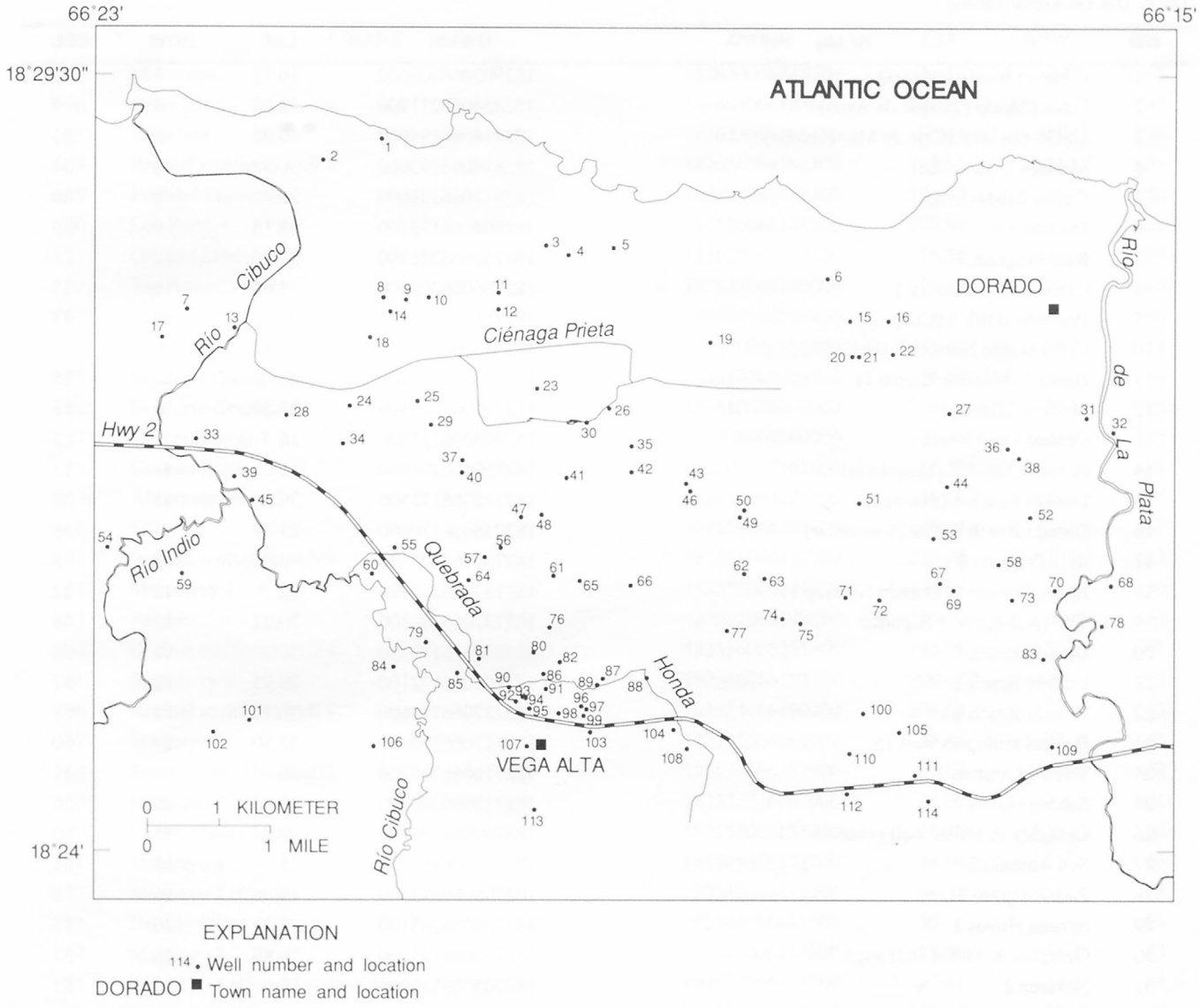

Figure 2. Location of wells referenced in the ground-water flow model.

Table 1. List of wells referenced in the ground-water flow model of the Vega Alta water-table aquifer

[Well numbers 19, 86, and 107 represent a group of two or more neighboring wells; WN, well number; NAME, well name; GWSIN, Ground-Water Site Inventory Number; LSE, land surface elevation (in feet above mean sea level); ROW, grid row number; COL, grid column number; obs, observation; USGS, U.S. Geological Survey]

WN	NAME	GWSIN	LSE	ROW	COL
1	Cibuco (Tomás Jiménez)	182903066205300	16.78	3	13
2	Finca Cibuco (Tanque de Agua)	182854066211900	28.08	4	9
3	USGS obs well (Caja de Mar-Navedo)	182818066194000	46.95	8	31
4	Morales 1 (Baudilio)	182814066193000	36.52	8	34
5	Castro 2 (Máximo)	182817066191000	36	8	40
6	Dorado Air	182804066173500	62.15	9	55
7	Rice Program 4	182751066221900	11.36	10	4
8	Cerro Gordo Nursery 1	182756066205200	43.65	10	13
9	Pennock Gard. 3 (Chepo 4)	182755066204200	39	10	15
10	Cerro Gordo Nursery 2 (Beli)	182756066203200	44.44	10	17
11	Breña 1 (Máximo Castro 1)	182758066200100	46	10	25
12	Medina 2 (Harry)	182751066200100	27.50	10	25
13	Central San Vicente	182743066215800	16	11	5
14	Pennock Gard. 2 (Maquintín)	182750066204900	16	11	13
15	Dorado Beach 4 (Sunway)	182746066172500	39.36	11	56
16	Dorado Beach 7 (USGS recorder)	182746066170800	23.79	11	58
17	Rice Program 5	182739066223000	6.60	12	3
18	Jardín Dorado 1 (Dorado Nursery 1)	182739066205800	22	12	12
19	TW-1A,2-8,PW-1 Higuillar	182737066182700	20.93	12	48
20	Dorado Beach 5	182731066172400	30.28	12	56
21	Dorado Beach 8	182731066172100	29.95	12	57
22	Dorado Beach 6	182732066170600	20.73	12	58
23	Bechtel multiport well 15	182717066194400	32.30	14	30
24	Warner Lambert 1	182710066210700	26	15	11
25	Sabana Hoyos 2	182712066203700	15.30	15	16
26	Geraghty & Miller well point	182709066191200	9.24	15	40
27	San Antonio 2	182707066164100	15	15	61
28	Rice Program 3	182706066213500	13	16	8
29	Sabana Hoyos 1	182702066203100	18.14	16	17
30	Geraghty & Miller staff gage	182703066192200	10.88	16	37
31	Nevarez 2	182705066154000	16	16	67
32	Central Constancia 1 (Trigo Hermanos)	182659066152800	20.45	16	68
33	Ceiba 1 (USGS Ceiba)	182656066221500	22.96	17	4
34	Sabana Hoyos 3 (Carmelita)	182654066211000	25.71	17	10
35	Arenas Procesadas (Empresas Terrassa)	182653066190200	213	17	42
36	San Antonio 1	182652066161500	16.93	17	64
37	Sabana Hoyos (USGS recorder)	182647066201700	35.39	18	20
38	San Antonio 3	182648066161000	18.88	18	64
39	Ceiba 2 (Carmelita Monserrate)	182640066215800	25.91	19	5
40	Bechtel multiport well 16	182642066201700	62.02	19	20
41	Bechtel multiport well 5	182640066193100	153	19	34
42	Tropigardens	182642066190200	150	19	42
43	Bechtel multiport well 17	182637066183800	192.82	19	47
44	Higuillar	182636066164200	55	19	61

Table 1. List of wells referenced in the ground-water flow model of the Vega Alta water-table aquifer--Continued

WN	NAME	GWSIN	LSE	ROW	COL
45	Monserrate	182630066215000	31.78	20	6
46	Santa Rosa 1	182634066183600	132	20	47
47	Regadera	182623066195100	185.98	21	28
48	Bechtel multiport well 2	182624066194200	185.63	21	31
49	Forestal Marismina	182623066181400	191.77	21	50
50	Los Puertos	182626066181200	195.90	21	50
51	Gramas Lindas 4	182629066172100	55.56	21	57
52	San Antonio Dairy	182623066160500	28.18	21	65
53	Gramas Lindas 2	182614066164800	31	23	60
54	Planta de Filtros (La Trocha)	182610066225400	45.90	24	1
55	Manatí 2 (Santa Rosa 2)	182610066204700	45.60	24	14
56	El Morro Corrugated	182610066200000	194.99	24	25
57	Owens Illinois 1	182606066200700	171.54	26	23
58	Gramas Lindas 3	182603066161900	35.12	27	63
59	Almirante Norte 3	182559066222100	118.16	28	4
60	IT-3	182559066205700	40.63	28	12
61	Bechtel multiport well 9	182558066193700	210.46	28	32
62	Monterrey 1	182559066181200	149.65	28	50
63	Reyes	182557066180300	120	28	52
64	Bechtel multiport well 4	182556066201400	145.91	29	21
65	Monterrey 2	182556066192500	209.07	29	36
66	Bechtel multiport well 8	182554066190200	204.08	29	42
67	Maguayo 6	182555066164500	35.46	29	61
68	Santa Elena (Fonalleda)	182554066152900	23.63	29	68
69	Maguayo 7	182552066163900	28.07	30	61
70	Cuatro Calles Dairy	182552066155400	25.36	30	66
71	Maguayo 4	182549066172700	88.08	31	56
72	Maguayo 5 (Coto)	182548066171200	58.37	31	58
73	Dorado Dairy	182548066161300	30	31	64
74	Maguayo 2	182540066175500	125.09	34	53
75	Maguayo 3 (New Maguayo 3)	182538066174700	91.31	34	54
76	Bechtel multiport well 3	182536066193800	189.75	35	32
77	Bechtel multiport well 13	182535066182000	172.13	35	49
78	Nevarez 1 (Media Luna Fonalleda)	182537066153300	26	35	68
79	Bajura 5 (New Bajura 3)	182530066203300	48.36	37	16
80	Bechtel multiport well 11	182526066194500	145.82	38	30
81	Bechtel multiport well 10	182523066200900	66.49	39	23
82	Bechtel multiport well 12	182522066193400	98.04	39	33
83	Rubero	182523066155900	31.32	39	65
84	Bechtel multiport well 18	182520066204700	46.53	40	14
85	Bajura 1	182517066201900	51.18	41	20
86	Bechtel multiport well 6 (Ponderosa, P wells 1, 2, and 3)	182517066194102	80.88	41	31
87	Bechtel multiport well 19	182515066191500	105.74	41	39
88	Santa Ana	182515066185500	98.52	41	43

Table 1. List of wells referenced in the ground-water flow model of the Vega Alta water-table aquifer--Continued

WN	NAME	GWSIN	LSE	ROW	COL
89	Alta Nursery	182512066191700	97.54	42	38
90	GE 2 (Bajura 4)	182511066195600	71.89	43	27
91	Bechtel multiport well 14	182510066194000	83.21	43	31
92	GE B3	182505066195300	81	44	27
93	GE 1 (Bajura 3)	182507066195000	75.53	44	28
94	Bechtel multiport well 1	182506066194900	78.57	44	29
95	Harman 1	182502066194700	83	45	29
96	Geraghty & Miller multiport well 1	182503066192400	111.26	45	36
97	Bechtel multiport well 22	182502066192200	115.75	45	37
98	Levi 1 (G&M Cash and Carry 1)	182500066193400	98.40	46	33
99	Geraghty & Miller multiport well 2	182459066192300	111.17	46	36
100	La Calandria (New)	182500066171900	167.50	46	57
101	Arraiza	182457066215100	220	47	6
102	Almirante Norte 2	182452066220700	231.61	48	5
103	Geraghty & Miller multiport well 3	182452066192000	128.21	48	37
104	Serrano e Hijos	182453066184300	150	48	46
105	Cantera Dorado	182452066170300	229.60	48	59
106	Cibuco Spring	182446066205600	65.62	50	12
107	Vega Alta 1, 2	182446066194800	106.69	50	29
108	Nieves Dairy 3	182445066183700	180	50	47
109	Maguayo Spring	182446066155500	49.31	50	66
110	La Calandria (Old)	182443066172500	249.32	51	56
111	Nieves Dairy 1	182434066165600	248	52	60
112	Nieves Dairy 2	182426066172600	297	53	56
113	Bechtel multiport well 20	182419066194500	254.14	54	30
114	Díaz, Gilberto (Barrio Espinosa)	182423066165000	228.24	54	60

Purpose and Scope

The purpose of this report is to describe the hydraulic properties needed by MODFLOW (McDonald and Harbaugh, 1988) to develop a three-dimensional ground-water flow model for the Vega Alta water-table aquifer and to evaluate the performance of the model by comparing simulated and measured water levels at various wells for several stress periods. Presentation of the algorithms used to estimate the main hydraulic variables affecting the ground-water flow in this water-table aquifer establishes the basis for the development of a solute-transport model for the EPA Superfund site in the Vega Alta area.

In this report, an attempt is made to present a systematic analysis of the main hydraulic variables that govern the ground-water flow in the Vega Alta area. Whenever possible, an analytical derivation of all numerical results obtained from the algorithms herein derived is presented. The ground-water flow model presented here makes use of data collected by the USGS as well as data collected by Bechtel Environmental, Inc. (1990) and Geraghty & Miller, Inc. (1991, 1992).

Previous Studies

Several previous ground-water investigations were conducted in the Vega Alta area. Gómez-Gómez and Torres-Sierra (1988) developed a two-dimensional ground-water flow model for the Vega Alta water-table aquifer simulating the period from predevelopment (1930) to February 1983. A ground-water investigation conducted by NUS Corporation (1986) concentrated primarily on the area around the industrial park in the Quebrada Honda karst valley, where TCE concentrations were detected originally. Bechtel Environmental, Inc. (1990) installed 20 multiport wells and conducted extensive water-quality analysis of water samples from wells located in the Vega Alta area and developed three-dimensional ground-water flow and solute transport models based on water-level and TCE-concentration data. Geraghty & Miller, Inc. (1992) conducted comprehensive water-level and water-quality data measurements in the area, installed three additional multiport wells in the vicinity of the TCE plume, and developed ground-water flow and solute-transport models for the water-table aquifer. The purpose of those models was to develop a remedial scheme designed to reclaim the water-table aquifer for public-water supply usage.

Acknowledgments

The author wants to thank Brian Smith of Geraghty & Miller, Inc., for his assistance in performing the slug tests on the multiport wells installed in the water-table aquifer.

DESCRIPTION OF STUDY AREA

The study area mainly falls within the Vega Alta 7 1/2-minute quadrangle. The generalized surficial geology of this quadrangle is shown in figure 3. The area simulated in the ground-water flow model presented in this report extends a maximum distance of 30,000 ft from north to south from the Atlantic Ocean coast to the Cibao Formation boundary, and a maximum distance of 40,000 ft from west to east from the Río Indio boundary to the Río de La Plata boundary. The location of the multiport wells installed in the area and the main physiographic regions of the study area are shown in figure 4.

The study area lies within the North Coast Limestone region of Puerto Rico (Giusti and Bennett, 1976). The main physiographic regions of the study area are: the southern karst uplands, the broad karst uplands plateau, three alluvial valleys formed by the Río de La Plata, Río Cibuco, and Río Indio, a karst valley that has been filled with blanket sand deposits (Giusti, 1978) through which the creek of Quebrada Honda flows, and the coastal plain, which includes the marsh of Ciénaga Prieta. The main geologic formations in the study area are, from oldest to youngest, the Cibao Formation, the Aguada Limestone, and the Aymamón Limestone. The outcrop of the Cibao is marked by gently rolling hills and by gentle slopes leading up to cliff faces where the Aguada Limestone crops out. The Aguada Limestone, which overlies the Cibao Formation, has higher clay content in the southern karst uplands than in the Quebrada Honda karst valley or in the karst uplands plateau (figs. 3 and 4). In contrast to the abundant deep sinkholes in the adjacent Aguada Limestone, the few sinks in the Aymamón Limestone are all gentle depressions. Detailed descriptions of these Tertiary geologic units present within the Vega Alta quadrangle map are given by Monroe (1980). The Quaternary formations of interest in the study area are the blanket sands and alluvial deposits shown in figure 3.

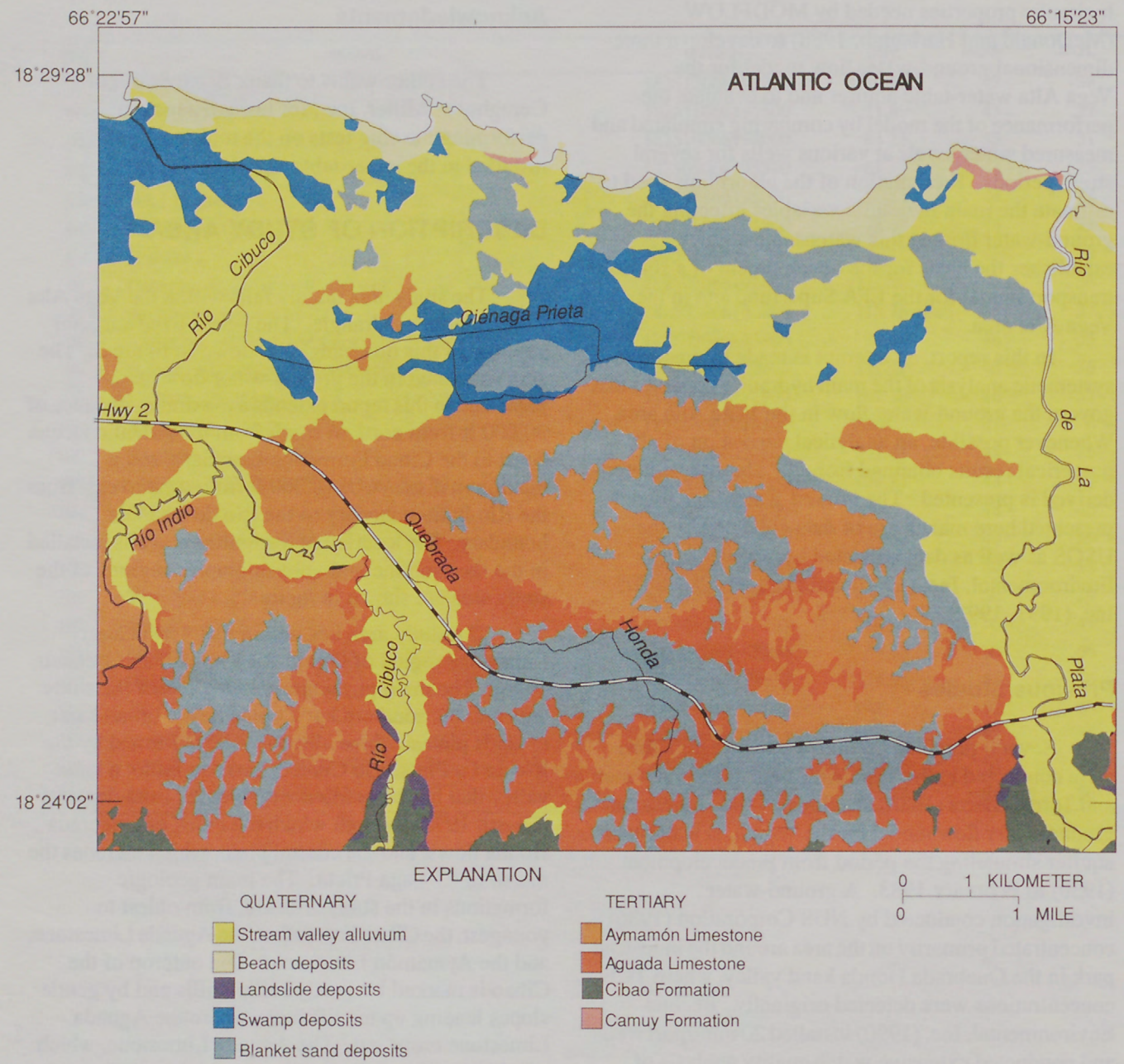

Figure 3. Generalized surficial geology of the ground-water flow model area.

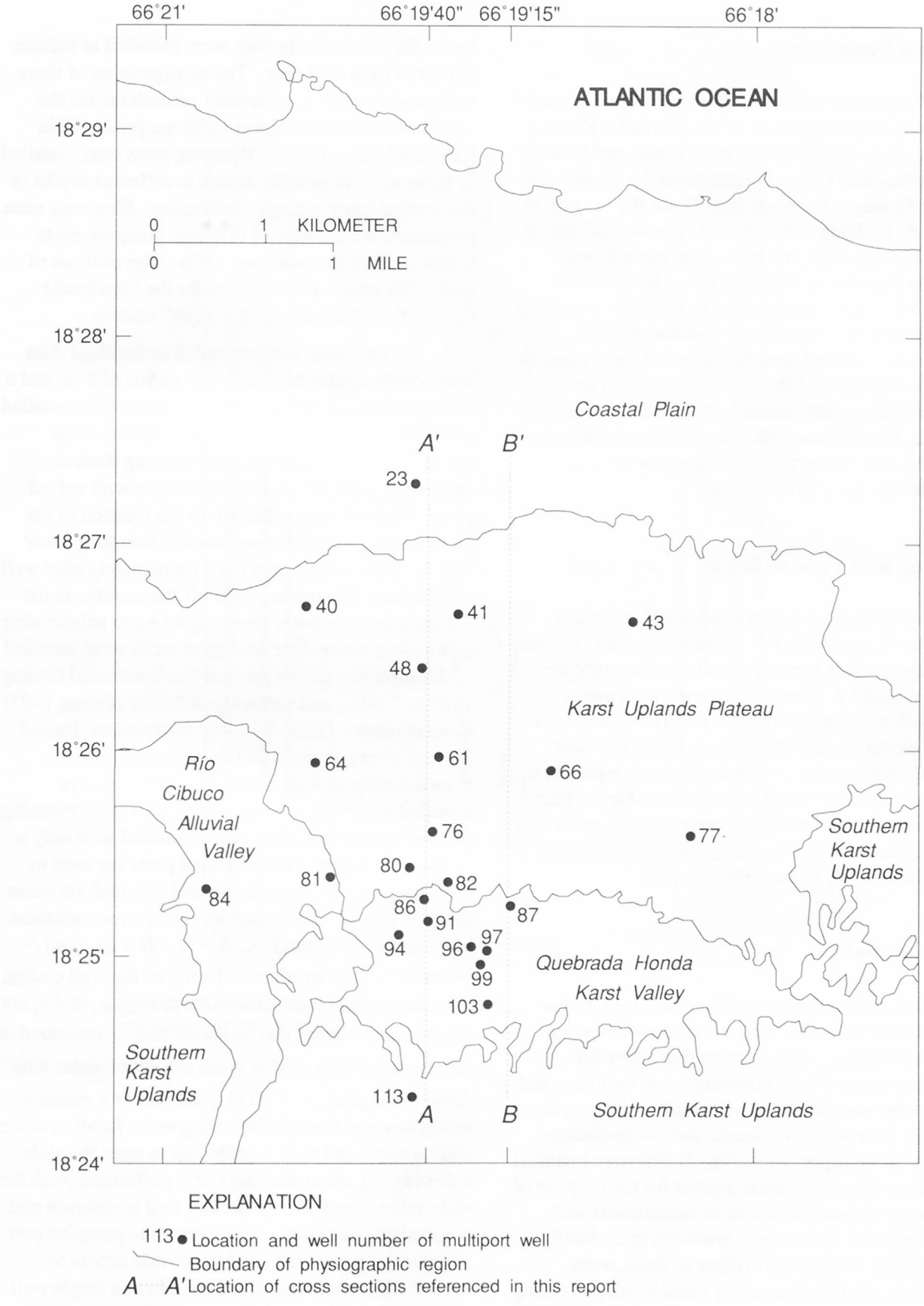

Figure 4. Location and well number of multiport wells in the modeling area.

Physical Boundaries

The ground-water flow simulation area, or model area, extends from just east of the Río de La Plata to just west of the Río Indio and Río Cibuco, and from the low-permeability Cibao Formation to the south to the Atlantic Ocean to the north (fig. 3). In the vicinity of the Río de La Plata delta, as well as in the vicinity of the Río Cibuco delta, the river stage has a lower elevation than the surrounding water levels in the water-table aquifer. In these areas, the water is seeping from the aquifer to the rivers. A constant-head boundary is assumed near the Atlantic Ocean coast at the north boundary of the simulation area. The Ciénaga Prieta marsh channels, Quebrada Honda creek channels, Río Cibuco, Río de La Plata, as well as the Río Indio, a tributary to Río Cibuco, are the river channels simulated in this model.

Location and Type of Wells

All wells from which water level, hydraulic conductivity, ground-water withdrawals, and chloride-concentration data were obtained for this study are shown in figure 2. The well number, well name, Ground-Water Site Inventory (GWSI) number, land-surface elevation, and the corresponding row and column number of the well in the grid developed for the ground-water flow model are listed in table 1. The land-surface elevation of a number of these wells was obtained from surveyors' reports listed in Appendix D of the Geraghty & Miller (1991) report.

Multiport Wells

The term multiport well is introduced in this report to refer to a well with a multiple number of measurement and pumping ports that allow for measuring water levels, pumping water volumes, and taking water samples at various depths. Among the 114 wells from which hydraulic data were obtained, there are 23 multiport wells (fig. 4) that were installed in the Vega Alta water-table aquifer for the purpose of monitoring vertical variations in water levels and measuring areal and vertical gradients in hydraulic conductivity. During the drilling of these wells, monitoring ports for measuring water levels and taking water samples as well as pumping ports for performing hydraulic conductivity tests were installed at various depths in each drill hole. The configuration of these wells and general development procedures for the installation of the multiport wells are presented in Black and others (1986). Pumping ports were installed in these wells to provide access to different depths in the aquifer using a single well casing. Slug tests were performed at a number of different pumping ports within each of the multiport wells. The analysis of these slug tests is discussed under the "Hydraulic Conductivity Results of Slug Tests" section.

All multiport wells installed in the Vega Alta water-table aquifer have a screen radius of 2 in. and a casing radius of 0.854 in. The multiport wells installed in the Vega Alta water-table aquifer are modular multiple-level ground-water monitoring devices employing a single, closed access tube with valved ports. Water is pumped down to the location of the packer and directed through a valve into the packer (fig. 5). This is done only once immediately after well installation. The packer seals off the annulus in the borehole to keep water from migrating to neighboring monitoring zones. The multiport wells were installed for General Electric by Bechtel Environmental (during 1989 and 1990) and Geraghty & Miller (during 1993) using equipment from Westbay Instruments, Inc. Vertical intervals separated by packers are herein named multiport well zones. Some zones were installed with both, a measurement port and a pumping port, whereas other zones were installed with only a measurement port. Measurement ports are used to compute water pressure levels and to withdraw water samples (fig. 6). The water level h at a measurement port can be computed from $h = M - D + (p_o - p_i)/w$, where M is the elevation of the top of the well casing, D is the depth to water inside the casing, p_o and p_i are the pressures outside and inside the casing, measured in lb/in^2 respectively, and w is the weight of water with density of 1 g/mL, or 0.4335 $(lb/in^2)/ft$. An open/close tool is lowered through the casing to the location of the sliding valve and then is pulled up to open the slide valve (fig. 7). After the slug test is performed (with the slide valve open), the open/close tool is reversed and dropped onto the slide valve to close the pumping port. The pumping ports are used to provide access to several different levels of a drill hole in a single well casing.

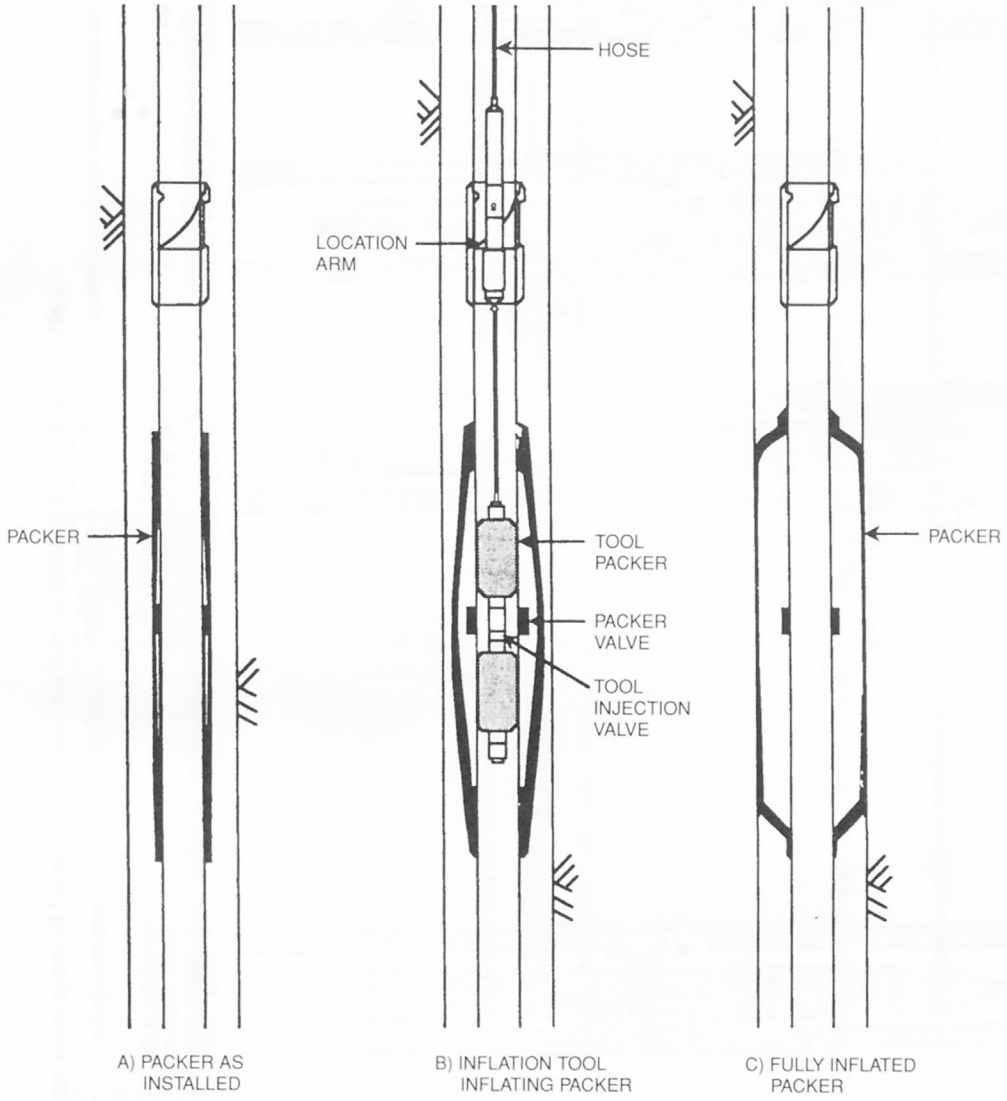

Figure 5. Packer inflation process performed in multiport wells to isolate monitoring zones (from Black and others, 1986).

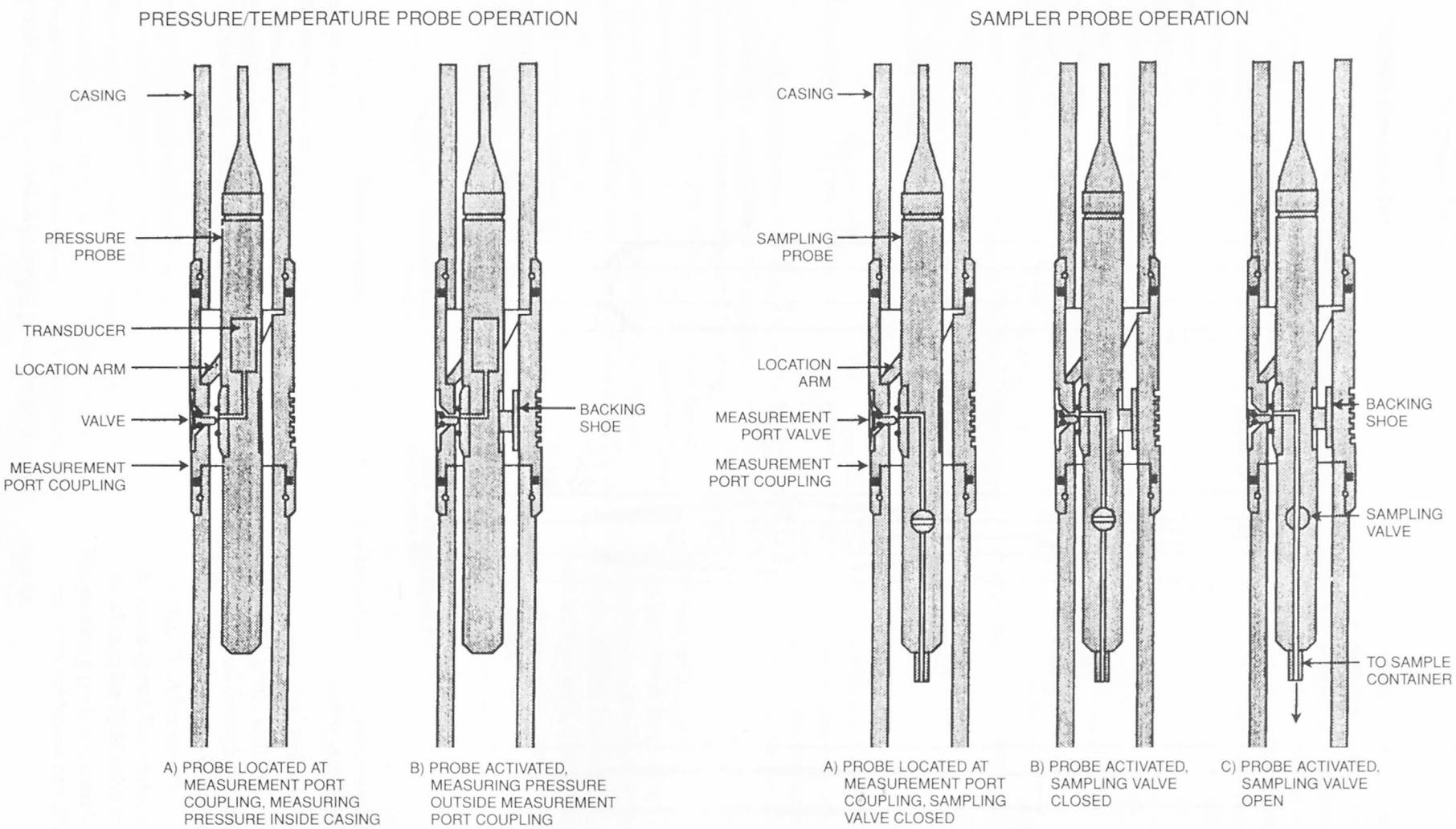

Figure 6. Measurement port operation in multiport wells showing pressure and sampler probes (from Black and others, 1986).

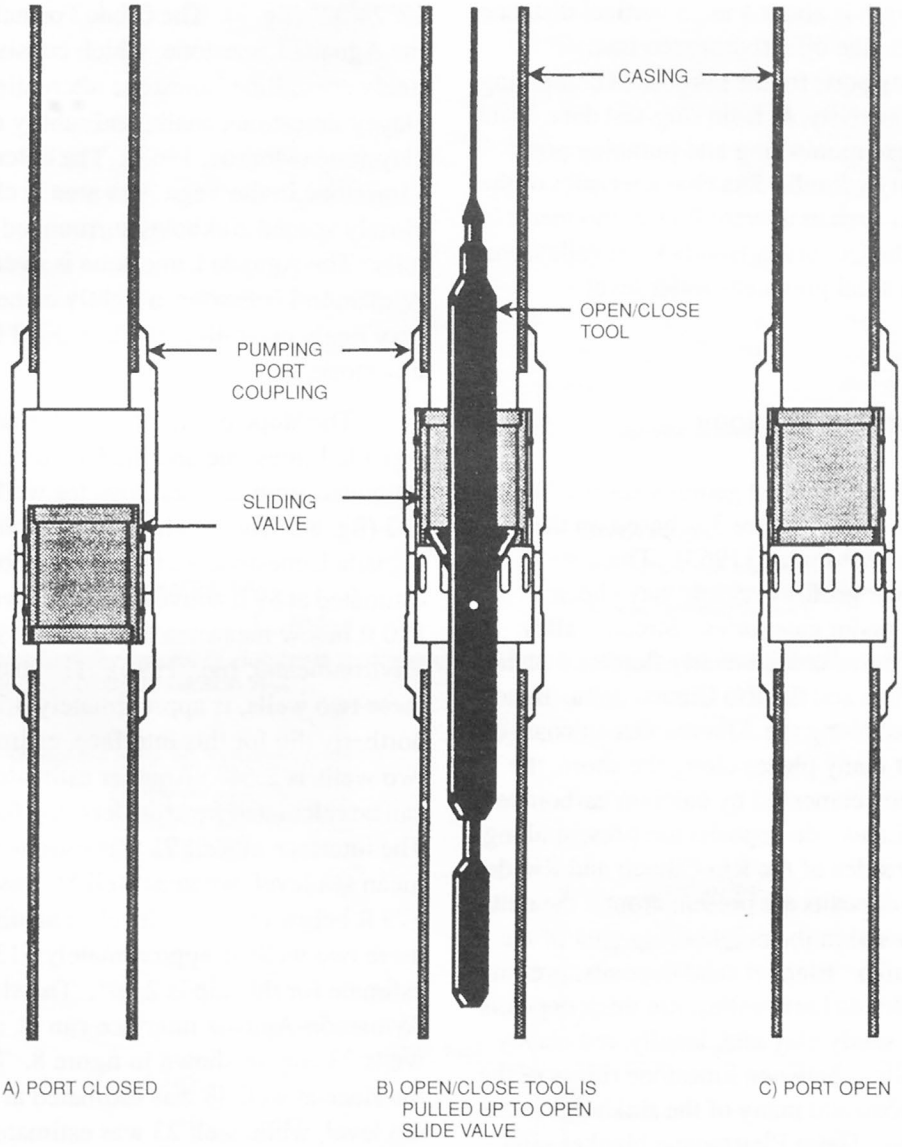

Figure 7. Closing and opening of a pumping port in multiport wells (from Black and others, 1986).

The casing radius, the screen radius, and the screen interval of these multiport wells were used as input to the computer program developed to analyze the slug-test data (Sepúlveda, 1992). Although the screen interval length is about 1 in., a vertical distance of 10 ft was used as the effective screen interval for zones with pumping ports for the purpose of computing the hydraulic conductivity, *K*, from slug-test data. Data collected from these monitoring and pumping ports revealed important hydraulic data characteristics of the water-table aquifer such as upward flow components in some sections of the Quebrada Honda karst valley, and vertical as well as areal prevalent water level variations.

Generalized Surficial Geology

The generalized surficial geology for the Vega Alta quadrangle shown in figure 3 is based on the geology described by Monroe (1963). The predominant surface geology regions have been grouped into nine major categories. Stream valley alluvium deposits surround the nearly flat flood plains of the Río de La Plata and the Río Cibuco delta. Beach deposits are present along the Atlantic Ocean coast of the study area. At many places along the shore, the beach sand has been cemented by calcium carbonate into beach rock. Landslide deposits are present along parts of the valley sides of the Río Cibuco and Río de La Plata. Swamp deposits are present around the delta of the Río Cibuco and in the neighboring area of the Ciénaga Prieta marsh. Blanket sand deposits, present in the Quebrada Honda karst valley, are thick deposits of orange- to red- sandy clay and, locally, red clayey sand present in valleys between limestone ridges of the Aymamón Limestone and many of the sinkholes in the Aguada Limestone. These Pleistocene blanket sand deposits are much older than the recent alluvium deposits.

Monroe (1963) observed the presence of extensive deposits of residual clays overlying karstic limestone throughout the southern karst uplands of the Vega Alta area. The only multiport well installed in this area, (well 113, fig. 4), had very low hydraulic conductivity values at all four aquifer zones tested; these zones were characterized by overdamped well-aquifer responses. The most extensive bedrock formations in the Vega Alta quadrangle are the Cibao Formation, the Aguada Limestone, and the Aymamón Limestone. The Camuy Limestone is present only to the west of the Río de La Plata delta. The top of the Cibao Formation, characterized by calcareous claystone, is at the land surface south of latitude 18°24′02″ (fig. 3). The Cibao Formation is overlain by the Aguada Limestone, which consists of rubbly to finely crystalline limestone alternating with beds of clayey limestone, chalk, and rubbly calcareous claystone (Monroe, 1963). The outcrop of the Aguada Limestone in the Vega Alta area is characterized by closely spaced sinkholes surrounded by low rolling hills. The Aguada Limestone is overlain by the Aymamón Limestone, a tightly cemented, dense to very finely crystalline thick-bedded fossiliferous limestone.

The slope or dip of the interface between the Aguada Limestone and the Cibao Formation can be estimated from drillers' logs for wells 86, 91, 94, and 113 (fig. 8). The depth of the contact between the Aguada Limestone and the Cibao Formation was estimated at 89 ft above mean sea level at well 113, and 130 ft below mean sea level at well 94 (Bechtel Environmental, Inc., 1990). The distance between these two wells, is approximately 4,756 ft. Thus, the northerly dip for this interface, estimated from these two wells is 2.64°. Another estimate of the same dip can be calculated from drillers' log for wells 86 and 91. The interface at well 91 was estimated at 147 ft below mean sea level, whereas well 86 was estimated at 179 ft below mean sea level. The distance between these two wells is approximately 613 ft. A second estimate for this dip is 2.99°. The slope of the Aymamón-Aguada interface can be estimated from wells 23 and 48 shown in figure 8. The depth of this interface at well 48 was estimated at 46 ft above mean sea level, while well 23 was estimated at 193 ft below mean sea level (Bechtel Environmental, Inc., 1990). The distance between these wells is approximately 5,349 ft. Therefore, the northerly dip of the Aymamón-Aguada interface is estimated to be 2.56°. Analogous calculations from data obtained from wells 82, 87, and 97 (fig. 9) produced dips of 2.67° and 2.89° for the contact between the Cibao Formation and the Aguada Limestone. Monroe (1963) estimated the slope of the Cibao-Aguada and Aguada-Aymamón interfaces to range from 2 to 5 degrees. The dip estimates computed here, shown in figure 8, tend to agree more with the lower range of values estimated by Monroe (1963).

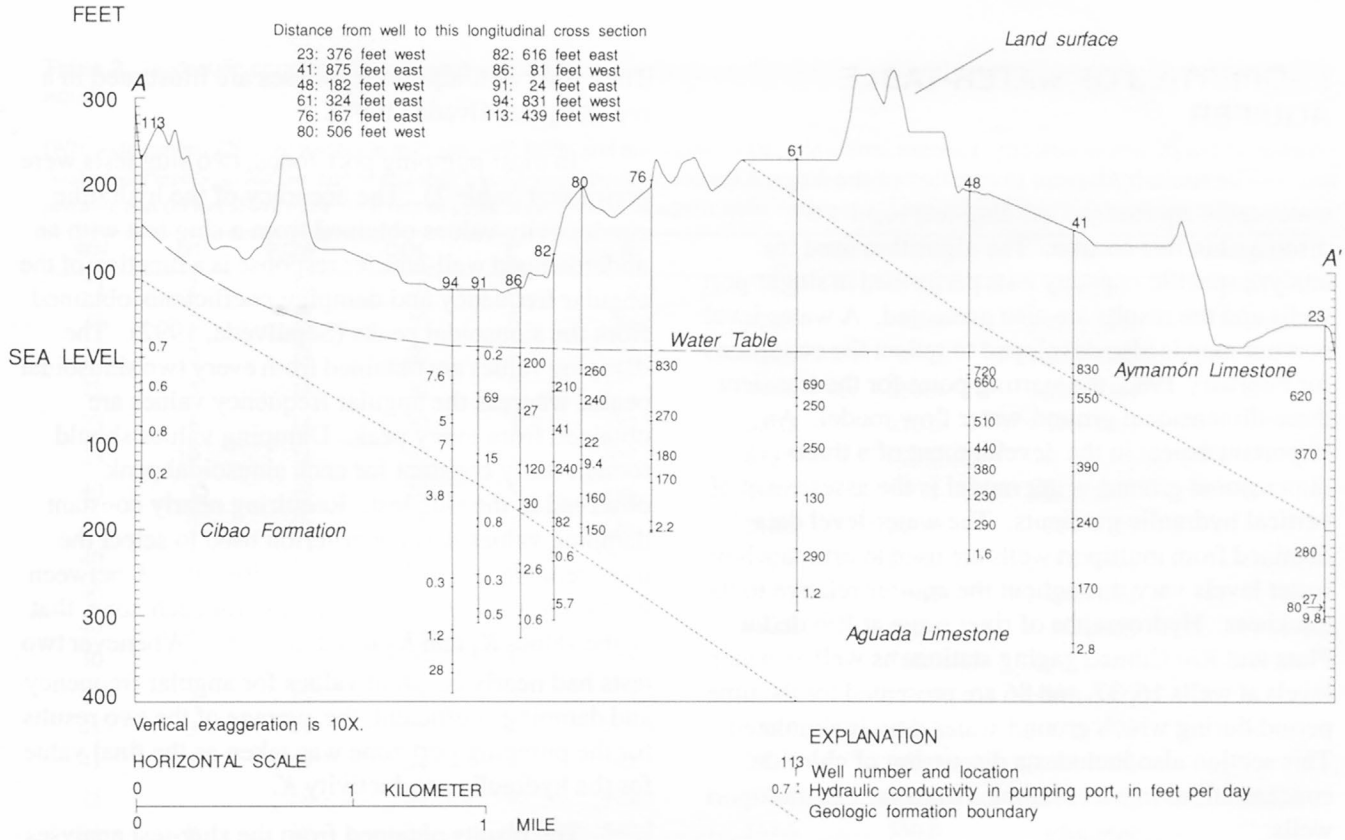

Figure 8. Hydraulic conductivity results of slug tests performed in multiport wells, shown along longitude 66°19′40″ (refer to figure 4 for location of cross section *A-A′*).

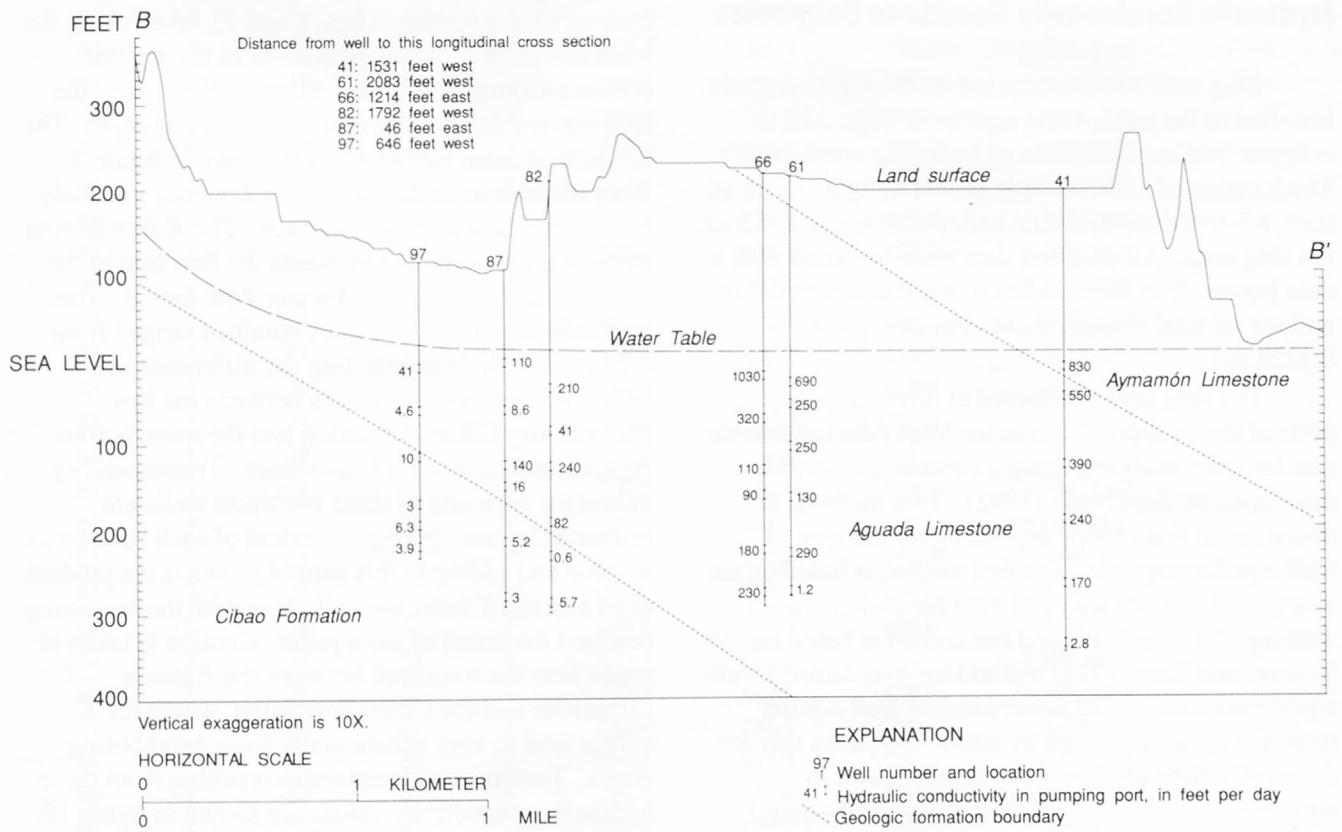

Figure 9. Hydraulic conductivity results of slug tests performed in multiport wells, shown along longitude 66°19′15″ (refer to figure 4 for location of cross section *B-B′*).

PROPERTIES OF WATER-TABLE AQUIFER

The main hydraulic properties of the Vega Alta water-table aquifer and the slug-test results are discussed in this section. The algorithm used to analyze specific-capacity tests performed in single-port wells and the results are also presented. A water-level contour map is also developed to reflect the conditions for February 1983, the starting point for the transient three-dimensional ground-water flow model. An important aspect in the development of a three-dimensional ground-water model is the assessment of vertical hydraulic gradients. The water-level data obtained from multiport wells are used to estimate how water levels vary throughout the aquifer relative to its thickness. Hydrographs of river stage at Río de La Plata and Río Cibuco gaging stations as well as water levels at wells 16, 37, and 86 are presented for the time period during which ground-water flow is simulated. This section also includes a discussion of chloride concentrations in water samples from various multiport wells.

Hydraulic Conductivity Results of Slug Tests

Slug tests were conducted in 23 multiport wells installed in the water-table aquifer in Vega Alta to estimate vertical variations of hydraulic conductivity. The location of these wells is shown in figure 4. In all tests, a 3-foot-long cylindric bailer was used to conduct the slug tests. All slug-test data were recorded with a data logger. The inner radius of the bailer was 0.5 in. making its total displacement volume equal to 0.1224 gal.

The slug tests conducted at different pumping ports of the multiport wells in the Vega Alta water-table aquifer were analyzed using a computer algorithm developed by Sepúlveda (1992). Two methods are discussed in this report, depending on the type of well-aquifer response. The first method is based on the analysis of van der Kamp (1976) for underdamped well-aquifer responses, and the second is based on the Bouwer and Rice (1976) method for overdamped well-aquifer responses. The underdamped well-aquifer response is characterized by sinusoidal peaks that are damped in time until the oscillations return to equilibrium, whereas the overdamped well-aquifer response is characterized by an exponential decay. These two well-aquifer responses are illustrated in a report by Sepúlveda (1992).

In most pumping port zones, two slug tests were performed (table 2). The accuracy of the hydraulic conductivity values obtained from a slug test with an underdamped well-aquifer response is a function of the angular frequency and damping coefficients obtained from the sinusoidal peaks (Sepúlveda, 1992). The damping values are obtained from every two sinusoidal peaks, whereas the angular frequency values are obtained from every peak. Damping values should remain fairly constant for each sinusoidal peak observed in the slug test. Requiring nearly constant damping values was the criterion used to select the most reliable hydraulic conductivity value K between the two results generally available for each zone, that is, the values K_1 and K_2 listed in table 2. Whenever two tests had nearly constant values for angular frequency and damping coefficient, the average of the two results for the pumping port zone was taken as the final value for the hydraulic conductivity K.

The results obtained from the slug-test analyses were compiled in two different hydrogeologic sections of the Vega Alta water-table aquifer. These two hydrogeologic sections (figs. 8 and 9), taken along the main direction of water movement in the aquifer (Gómez-Gómez and Torres-Sierra, 1988), show the slug-test results as a function of latitude and depth. The location of these two sections is shown in figure 4. Both sections indicate that higher K values generally occur near the water-table surface. The K distribution in these cross sections represents the first step in the development of the ground-water flow model. The hydraulic conductivity values obtained ranged from 0.2 to 960 ft/d, demonstrating the difference in hydraulic conductivity values between the low-permeability Cibao Formation and the more porous Aguada and Aymamón Limestones. Transmissivity values for each one of these multiport wells are estimated by multiplying the extent of each zone by its K value and adding to this sum of products the product of an average K value over all zones with the remaining untested thickness of the aquifer. Caution is taken at zones near the transition between the Aguada Limestone and the Cibao Formation, where the K values tend to vary substantially from neighboring zones. Transmissivity estimates resulting from these hydraulic conductivity values are shown in figure 10. The only multiport well located in the southern karst

Table 2. Hydraulic conductivity values obtained from slug tests performed in multiport wells of the Vega Alta water-table aquifer

[WN, well number; ZN, zone number in multiport well; ROW, grid row number; COL, grid column number; L, grid layer number; K_1 and K_2, hydraulic conductivity results (in feet per day) of slug tests 1 and 2, respectively; K, rounded average from slug-test results K_1 and K_2; PD, packer depth interval of pumping port (in feet above mean sea level); S, saline water present; A, aquifer under confined conditions; NT, no second slug test was performed]

WN	ZN	ROW	COL	L	K_1	K_2	K	PD	Remarks
23	1	14	30	6	9.3	10.3	9.8	[-303,-293]	S
23	2	14	30	6	84.5	76.1	80.0	[-291,-285]	S
23	3	14	30	6	28.4	24.9	27.0	[-281,-275]	S
23	5	14	30	5	273.6	292.6	280.0	[-228,-218]	S
23	8	14	30	3	382.8	367.5	370.0	[-116,-106]	
23	10	14	30	1	608.6	623.5	620.0	[-46,-36]	
40	1	19	20	5	146.2	170.5	160.0	[-243,-233]	S
40	2	19	20	5	180.1	212.7	200.0	[-228,-218]	
40	3	19	20	4	202.8	199.5	200.0	[-203,-193]	
40	5	19	20	3	287.4	271.1	280.0	[-136,-126]	
40	7	19	20	2	481.9	492.0	490.0	[-76,-66]	
40	9	19	20	1	777.7	752.1	760.0	[-9,1]	
41	1	19	34	6	2.5	3.2	2.8	[-342,-332]	S
41	3	19	34	6	202.3	143.2	170.0	[-272,-262]	S
41	5	19	34	4	242.3	242.5	240.0	[-197,-187]	
41	7	19	34	3	422.8	353.1	390.0	[-132,-122]	
41	9	19	34	1	540.7	557.6	550.0	[-52, -42]	
41	10	19	34	1	845.2	816.5	830.0	[-17,-7]	
43	1	19	47	5	605.0	435.6	520.0	[-210,-200]	
43	2	19	47	4	122.4	111.9	120.0	[-185,-175]	
43	3	19	47	3	351.8	320.9	340.0	[-155,-145]	
43	5	19	47	2	261.4	311.5	290.0	[-95,-85]	
43	7	19	47	1	799.3	771.8	790.0	[-35,-25]	
43	8	19	47	1	418.2	374.3	400.0	[-10,0]	
48	1	21	31	5	1.6	NT	1.6	[-231,-227]	
48	2	21	31	4	300.7	278.0	290.0	[-199,-189]	
48	3	21	31	4	229.4	231.4	230.0	[-164,-154]	
48	4	21	31	3	376.1	392.9	380.0	[-134,-124]	
48	5	21	31	3	449.2	422.2	440.0	[-109,-99]	
48	6	21	31	2	489.3	529.2	510.0	[-79,-69]	
48	7	21	31	1	684.2	643.0	660.0	[-34,-24]	
48	8	21	31	1	744.2	700.5	720.0	[-14,-4]	
61	1	28	32	6	1.2	1.2	1.2	[-279,-269]	
61	3	28	32	5	306.2	269.8	290.0	[-234,-224]	
61	5	28	32	4	127.3	125.2	130.0	[-169,-159]	
61	7	28	32	3	237.3	252.8	250.0	[-109,-99]	
61	9	28	32	2	252.1	245.3	250.0	[-59,-49]	
61	10	28	32	1	676.8	708.5	690.0	[-34,-24]	
64	5	29	21	4	103.3	137.5	120.0	[-199,-189]	
64	7	29	21	3	117.2	144.8	130.0	[-144,-134]	
64	9	29	21	2	244.9	236.5	240.0	[-74,-64]	
64	11	29	21	1	959.2	955.2	960.0	[-19,-9]	
66	1	29	42	6	228.1	225.4	230.0	[-281,-271]	
66	3	29	42	5	146.1	204.2	180.0	[-231,-221]	
66	5	29	42	4	90.0	94.3	90.0	[-166,-156]	

Table 2. Hydraulic conductivity values obtained from slug tests performed in multiport wells of the Vega Alta water-table aquifer--Continued

WN	ZN	ROW	COL	L	K_1	K_2	K	PD	Remarks
66	6	29	42	3	124.4	101.0	110.0	[-136,-126]	
66	8	29	42	2	282.2	352.1	320.0	[-76,-66]	
66	10	29	42	1	988.8	1,070.4	1,030.0	[-26,-16]	
76	1	35	32	4	2.3	2.2	2.2	[-200,-190]	
76	3	35	32	3	156.5	182.6	170.0	[-145,-135]	
76	4	35	32	3	206.0	158.8	180.0	[-116,-109]	
76	6	35	32	2	293.1	238.4	270.0	[-73,-63]	
76	8	35	32	1	838.0	826.8	830.0	[-14,-4]	
77	1	35	49	6	3.0	3.4	3.2	[-272,-262]	A
77	3	35	49	5	242.8	355.3	300.0	[-217,-207]	
77	5	35	49	4	680.8	501.1	590.0	[-157,-147]	
77	7	35	49	2	532.2	692.7	610.0	[-97,-87]	
77	9	35	49	1	752.6	700.6	730.0	[-37,-27]	
77	10	35	49	1	796.6	844.4	820.0	[-17,-7]	
80	1	38	30	4	151.0	145.0	150.0	[-204,-194]	
80	3	38	30	4	162.3	149.0	160.0	[-169,-159]	
80	5	38	30	3	9.1	9.7	9.4	[-129,-119]	
80	6	38	30	2	21.7	22.6	22.0	[-104,-94]	
80	8	38	30	1	241.2	236.5	240.0	[-54,-44]	
80	9	38	30	1	262.7	262.8	260.0	[-29,1]	
81	1	39	23	5	1.6	2.0	1.8	[-228,-218]	
81	2	39	23	4	81.3	79.7	80.0	[-203,-193]	
81	3	39	23	4	84.3	64.3	74.0	[-176,-166]	
81	5	39	23	3	140.4	137.5	140.0	[-126,-116]	
81	6	39	23	3	157.1	160.4	160.0	[-106,-96]	
81	8	39	23	1	178.9	172.6	180.0	[-49,-39]	
82	1	39	33	6	5.3	6.1	5.7	[-291,-281]	A
82	3	39	33	5	0.5	0.7	0.6	[-236,-226]	
82	4	39	33	4	86.7	78.8	82.0	[-196,-186]	
82	6	39	33	3	237.0	248.5	240.0	[-131,-121]	
82	7	39	33	2	39.6	42.6	41.0	[-89,-79]	
82	8	39	33	1	215.0	213.3	210.0	[-49,-19]	
84	1	40	14	5	1.8	1.5	1.6	[-219,-209]	
84	2	40	14	4	2.4	1.6	2.0	[-199,-189]	
84	3	40	14	4	0.5	NT	0.5	[-179,-169]	
84	4	40	14	4	88.0	88.5	88.0	[-159,-149]	
84	6	40	14	3	113.5	120.4	120.0	[-114,-104]	
84	7	40	14	2	151.9	156.4	150.0	[-89,-79]	
86	1	41	31	6	0.6	NT	0.6	[-310,-300]	A
86	3	41	31	5	2.1	3.1	2.6	[-250,-240]	A
86	5	41	31	4	28.3	32.1	30.0	[-175,-165]	
86	6	41	31	3	123.1	128.7	120.0	[-135,-125]	
86	8	41	31	2	26.0	27.9	27.0	[-65,-55]	
86	10	41	31	1	186.2	204.8	200.0	[-20,10]	

Table 2. Hydraulic conductivity values obtained from slug tests performed in multiport wells of the Vega Alta water-table aquifer--Continued

WN	ZN	ROW	COL	L	K_1	K_2	K	PD	Remarks
87	1	41	39	6	2.9	3.1	3.0	[-284,-274]	A
87	3	41	39	5	5.3	5.2	5.2	[-219,-209]	A
87	5	41	39	3	15.9	16.4	16.0	[-154,-144]	
87	6	41	39	3	133.7	142.8	140.0	[-129,-119]	
87	8	41	39	2	8.5	8.8	8.6	[-64,-54]	
87	10	41	39	1	111.2	100.1	110.0	[-19,6]	
91	1	43	31	6	0.5	NT	0.5	[-302,-292]	A
91	2	43	31	6	0.3	NT	0.3	[-262,-252]	A
91	4	43	31	4	0.4	1.2	0.8	[-197,-187]	
91	6	43	31	3	14.1	15.6	15.0	[-122,-112]	
91	8	43	31	1	66.7	70.6	69.0	[-62,-32]	
91	10	43	31	1	0.2	NT	0.2	[-2,8]	
94	2	44	29	6	30.6	27.5	28.0	[-366,-356]	A
94	4	44	29	6	1.2	1.2	1.2	[-326,-316]	A
94	6	44	29	6	0.3	0.3	0.3	[-266,-256]	A
94	9	44	29	4	3.9	3.6	3.8	[-166,-156]	
94	10	44	29	3	6.6	7.3	7.0	[-106,-96]	
94	11	44	29	2	4.9	5.1	5.0	[-76,-66]	
94	13	44	29	1	7.3	7.8	7.6	[-26,-16]	
96	2	45	36	3	2.9	3.1	3.0	[-149,-139]	
96	5	45	36	2	4.5	5.0	4.8	[-99,-89]	
96	8	45	36	1	2.1	1.3	1.7	[-54,-44]	
96	9	45	36	1	49.2	51.1	50.0	[-39,-29]	
96	11	45	36	1	46.5	59.6	53.0	[-12,-2]	
97	1	45	37	5	3.5	4.3	3.9	[-225,-215]	A
97	2	45	37	4	8.0	4.6	6.3	[-200,-190]	A
97	3	45	37	4	2.6	3.5	3.0	[-175,-165]	A
97	5	45	37	3	10.3	10.4	10.0	[-120,-110]	
97	7	45	37	2	4.8	4.5	4.6	[-65,-55]	
97	9	45	37	1	46.7	36.3	41.0	[-30,0]	
99	2	46	36	3	10.5	13.4	12.0	[-131,-121]	
99	4	46	36	2	1.8	2.2	2.0	[-86,-76]	
99	6	46	36	2	3.6	3.8	3.7	[-56,-46]	
99	7	46	36	1	2.1	2.0	2.0	[-41,-31]	
99	8	46	36	1	7.3	7.2	7.2	[-26,-16]	
103	1	48	37	2	2.1	1.7	1.9	[-96,-86]	
103	2	48	37	2	1.5	0.9	1.2	[-66,-56]	
103	3	48	37	1	1.6	1.9	1.8	[-31,-21]	
103	4	48	37	1	8.7	12.8	11.0	[-11,-1]	
103	5	48	37	1	1.5	2.0	1.8	[9,19]	
113	1	54	30	3	0.2	0.3	0.2	[-141,-131]	A
113	3	54	30	2	0.8	0.9	0.8	[-91,-81]	A
113	5	54	30	1	0.5	0.7	0.6	[-39,-29]	
113	7	54	30	1	0.4	0.9	0.7	[8,18]	

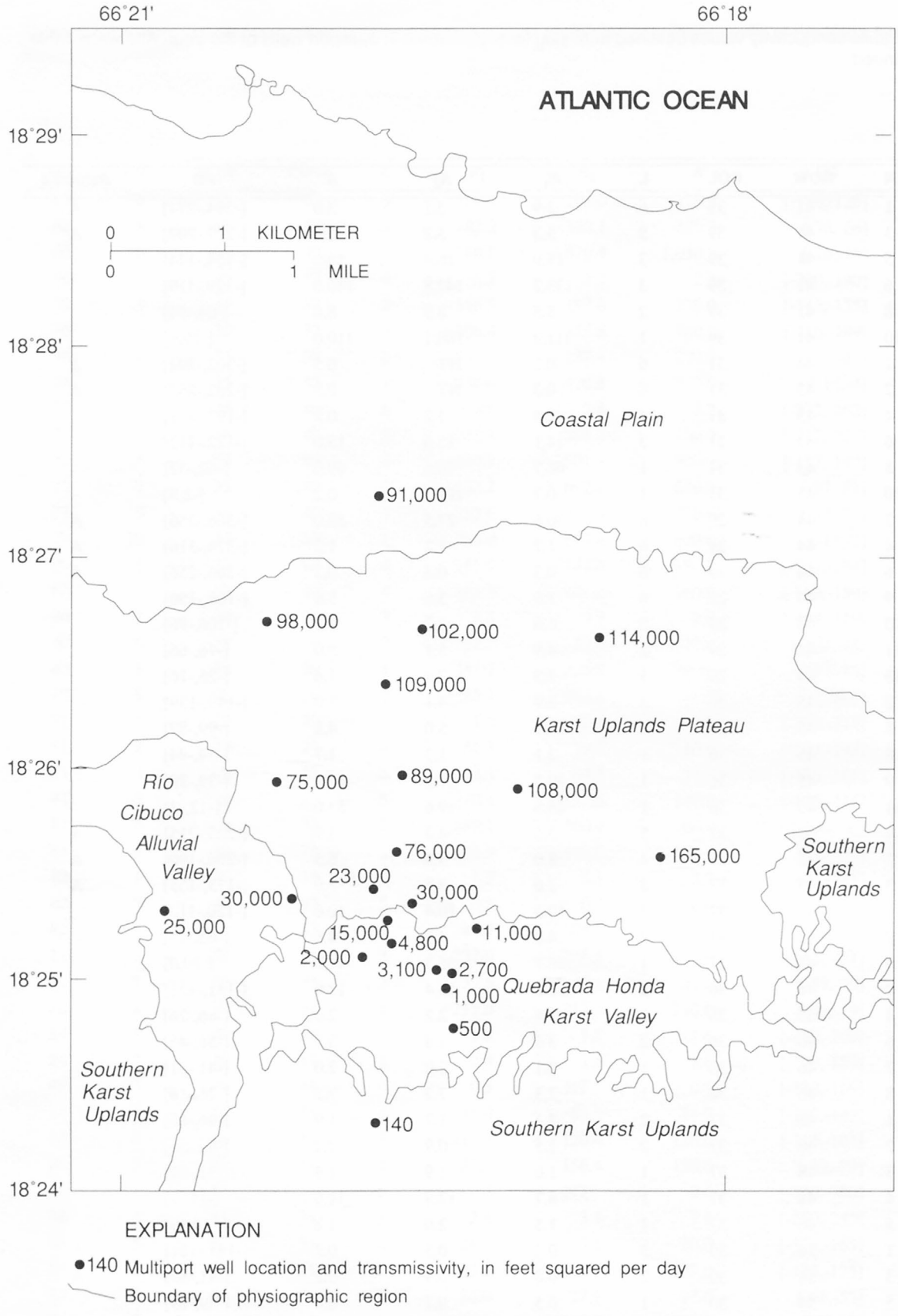

Figure 10. Transmissivity estimates based on slug tests performed in multiport wells.

uplands, well 113, showed very low K values at all four aquifer zones tested. This indicates a state of highly dense and undissolved limestone. Wells 81 and 84, which lie within the Río Cibuco alluvial valley, have higher hydraulic conductivity values at shallow zones, that is at depths of about 120 ft below mean sea level or less, than at deeper zones. For example, the bottom three zones of well 84 had overdamped well-aquifer responses, whereas the upper zones had underdamped responses. The overdamped well-aquifer responses are indicative of lower hydraulic conductivity values than the underdamped well-aquifer responses. Of all six zones tested in well 81, only the bottom zone had an overdamped response, indicating that the transmissivity in the vicinity of well 81 is higher than that around well 84. Well 23, located in the coastal plain, has only two zones completed in the fresh section of the water-table aquifer; the transmissivity of the aquifer at well 23, from about 150 ft below mean sea level to the water-table surface, is about 91,000 ft^2/d.

Most of the multiport wells lie within the karst uplands plateau and Quebrada Honda karst valley (fig. 10). High transmissivity values in the karst uplands plateau (at wells 40, 41, 43, 48, 61, 64, 66, 76, 77, 80, and 82) resulted from the high hydraulic conductivity values, K, computed at depths of 30 ft below mean sea level to the water table. All T values obtained from these wells exceeded 20,000 ft^2/d. Most of the slug tests performed in this plateau produced underdamped well-aquifer responses. The consistently high K values at zones near the water-table surface indicate a high porosity at near-surface depths within this plateau. The storage coefficient value used for slug tests with underdamped well-aquifer responses was derived using a specific storage value of 6.4×10^{-6}/ft.

The Quebrada Honda karst valley (fig. 4), characterized by its numerous blanket sand deposits, acts as a transition zone between the southern karst plateau and the karst uplands plateau. Transmissivity values in the Quebrada Honda karst valley (at wells 86, 87, 91, 94, 96, 97, 99, and 103) ranged from 500 to 15,000 ft^2/d; the closer to the karst uplands plateau, the higher the transmissivity. These transmissivities generally agree with those reported by Gómez-Gómez and Torres-Sierra (1988). The low K values at various depths indicate the presence of either clay lenses or very dense limestone. From the Quebrada Honda karst valley north to the karst uplands plateau, the K values for all zones generally increase (table 2), indicating a high level of karstic dissolution.

Transmissivity Results of Specific-Capacity Tests

In addition to the slug tests performed in the multiport wells, some specific-capacity tests were performed in "single-screened" wells within the water-table aquifer with the purpose of obtaining transmissivity values for areas where multiport wells were not present. An efficient and rapidly converging numerical algorithm that computes transmissivity values from specific-capacity data obtained from these single-screened wells was used. The assumptions made in the derivation of the Theis ground-water solution (Theis, 1963) were taken into account in the analysis of specific-capacity tests. If the well is not open to the entire thickness of the aquifer, then early-time drawdown data may reflect the transmissivity of only that section of the aquifer that is screened. Neighboring wells screened at different depths yielded contrasting transmissivity values, results that were easily reconciled by a careful study of the well logs and observation of lengths of screened intervals. Only specific-capacity data from wells open to most of the aquifer thickness are analyzed and presented here.

The transmissivity value at a given well was obtained from the solution of the nonlinear Theis equation:

$$T - \frac{Q}{4\pi s}\int_{u}^{\infty}\frac{exp\,(-\tau)}{\tau}d\tau = T - \frac{Q}{4\pi s}W(u) = 0 \qquad (1)$$

where

T is the transmissivity in ft^2/d;

Q is the well discharge in ft^3/s;

s is the drawdown in ft;

$u = \frac{r^2 S}{4tT}$, r is the radial distance from the well;

S is the dimensionless storage coefficient;

t is the time in days; and

$W(u)$ is the well function.

The storage coefficient value used for the specific-capacity test was 0.10, which was the average specific-yield value assigned to the study area. The radial distance from the center of the well to the outside well bore is the radius used in the specific-capacity tests.

The Newton numerical algorithm (Conte and de Boor, 1980) for finding the root of a nonlinear equation was used to solve equation (1) for the value of T. Note that the application of Leibnitz rule of differentiation under the integral sign to equation (1) gives:

$$\frac{dW(u)}{dT} = -\frac{exp(-u)}{u}\frac{du}{dT} = \frac{exp(-u)}{T}. \quad (2)$$

If T_{i+1} and T_i represent the transmissivity values of iterations $i + 1$ and i, then the iterative equation to be solved becomes:

$$T_{i+1} = T_i - \frac{T_i - \frac{Q}{4\pi s}W(u)}{1 - \frac{Q}{4\pi Ts}exp(-u)}. \quad (3)$$

The solution to equation (3) is achieved when an index n is found satisfying the convergence criterion given by:

$$|T_{n+1} - T_n| < \varepsilon \quad (4)$$

where ε is a threshold chosen by the hydrologist. If the value for T is in ft^2/d, a value of $\varepsilon = 0.10$ is a reasonable threshold to choose.

The data needed to obtain T from the solution of equation (3) consist of well discharge Q in gal/min, drawdown s in ft after pumping at constant rate for time t (in d), well radius r in ft, and a storage coefficient estimate S of 0.10. These data are listed in table 3 for each well for which a specific-capacity test was performed. The location of these specific-capacity test sites with the corresponding T values obtained from the application of this algorithm, and the T estimates obtained from the slug tests performed on multiport wells are shown in figure 11. The initial value T_0 used in the iteration process established by equation (3) is obtained from the equation:

$$T_0 = \frac{Q}{s}\{K_0 - 264[log(5S) - log(t)]\}, \quad (5)$$

Table 3. Transmissivity values obtained from specific-capacity tests conducted in several wells of the Vega Alta water-table aquifer

[WN, well number; Q, well discharge (in gallons per minute); s, drawdown (in feet); t, pumping duration (in days); r, outside screen radius (in feet); T, rounded transmissivity value (in feet squared per day)]

WN	Q	s	t	r	T
6	75	33.00	0.250	0.417	320
18	150	4.50	0.292	0.333	6,600
20	300	15.00	0.042	0.583	2,700
25	600	2.00	1.208	0.583	71,000
27	750	4.00	1.833	0.500	45,000
29	360	1.00	1.000	0.500	88,000
32	1,500	6.50	0.083	0.500	45,000
33	600	1.70	1.000	0.500	86,000
36	1,000	3.00	2.014	0.500	84,000
38	604	2.00	0.666	0.667	68,000
45	800	2.00	0.500	0.833	87,000
54	200	1.25	0.250	0.833	30,000
72	700	1.50	1.000	0.667	111,000
75	400	2.50	0.500	0.833	32,000
79	400	2.00	1.000	0.500	47,000
93	300	7.00	1.375	0.583	8,900
98	220	6.00	1.000	0.448	7,700
107	280	22.00	2.000	0.458	2,600
110	100	13.00	0.396	0.833	1,100
111	225	15.00	0.416	0.417	2,700

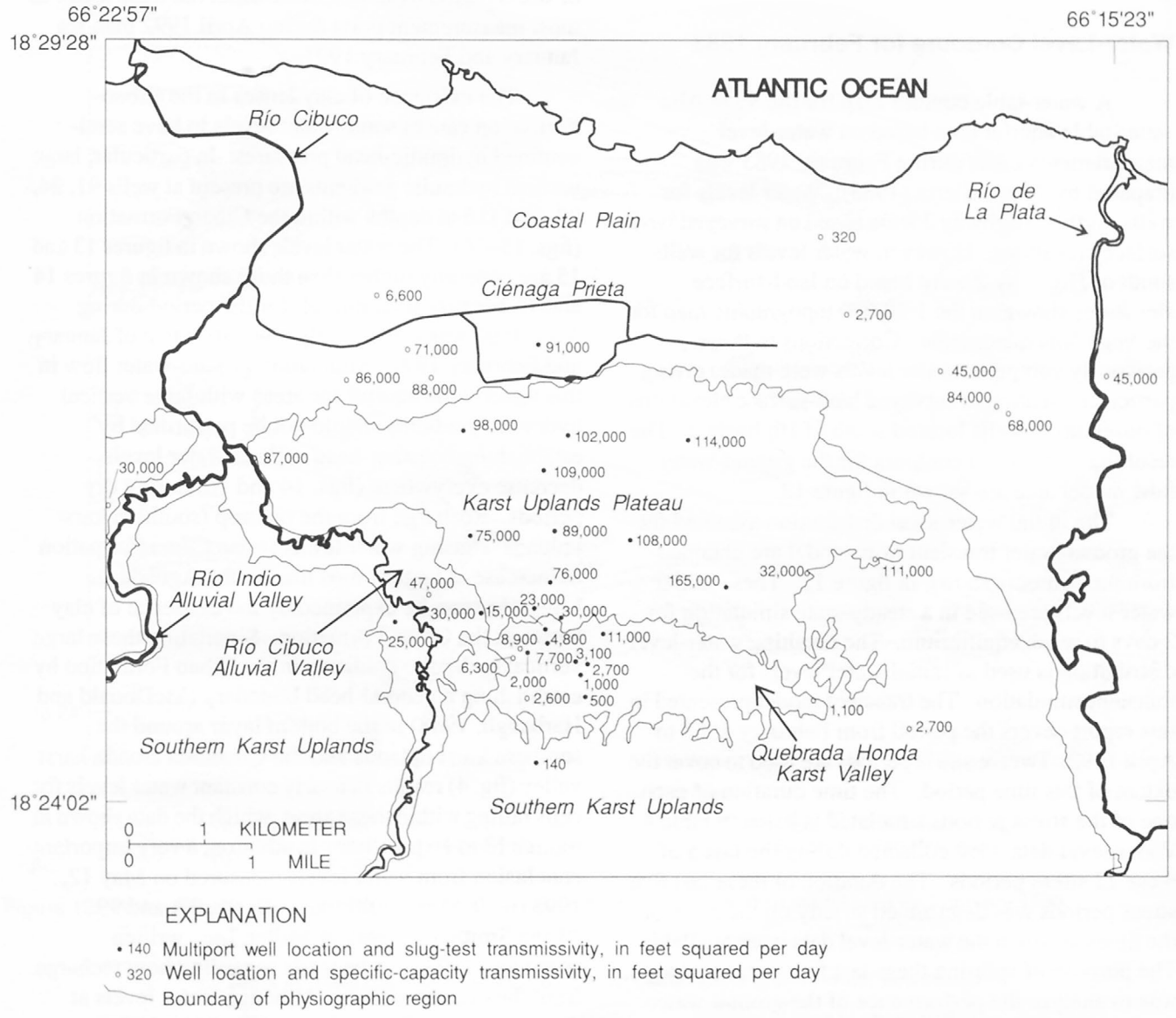

Figure 11. Transmissivity estimates from slug and specific-capacity tests.

where, K_0 is given by:

$$K_0 = -66 - 264\,[log\,(3.74r^2 \times 10^{-6})]\,. \qquad (6)$$

Equations (5) and (6) were derived from Theis (1963).

Water-Level Contours for February 1983

A water-table contour map for the Vega Alta water-table aquifer area based on water-level measurements made during February 1983 was prepared by Torres-Sierra (1985). Water levels for wells north of Highway 2 were based on surveyed land-surface elevations. However, water levels for wells south of Highway 2 were based on land-surface elevations shown on the 1:20,000 topographic map for the Vega Alta quadrangle. Corrections to these previously computed water levels were made, giving particular attention to surveyed land-surface elevations of observation wells located south of Highway 2. The resulting water-level contours for the ground-water flow model area are shown in figure 12.

The initial water-level distribution assumed for the ground-water transient flow model are obtained from the contours shown in figure 12. These initial water levels are used in a steady-state simulation for 2 days to reach equilibrium. The resulting water-level distribution is used as initial water levels for the transient simulation. The transient model presented in this report covers the period from February 1983 to April 1992. Twelve stress periods are used to cover the extent of this time period. The time duration of each one of the stress periods simulated is listed in table 4. Water-level data were collected during the last 5 of these 12 stress periods. The duration of these last five stress periods was determined strictly on the basis of the times at which the water-level data were available. The purpose of splitting these last five stress periods was to analyze the performance of the ground-water flow model during time intervals that included both dry and wet periods.

Vertical Hydraulic Gradients

The development of a three-dimensional ground-water flow model requires an assessment of water level variations with depth in the aquifer. Water levels obtained from measurement ports in the multiport wells provided the data needed to develop a three-dimensional model. The measured water levels in these multiport wells are illustrated (figs. 13–16) along the two longitudinal cross sections shown in figure 4. These water levels indicate larger vertical hydraulic gradients in the Cibao Formation than in the Aguada Limestone (figs. 13–16). Water levels shown at the end of stress period 8 (table 4) were observed to be lower in most measurement ports during April 1992 than for January and February 1991.

The existence of clay lenses in the Cibao Formation causes some water levels to have semi-confined hydraulic-head pressures. In particular, large vertical hydraulic gradients are present at wells 91, 94, 97, and 113 at depths within the Cibao Formation (figs. 13–16). The water levels shown in figures 13 and 15 are generally higher than those shown in figures 14 and 16 because total rainfall for the period during April 1992 was significantly lower than that of January and February 1991. Simulating ground-water flow in this water-table aquifer for areas with large vertical hydraulic gradients should not be performed by establishing constant-head cells as water levels decrease everywhere (figs. 14 and 16) during dry periods. Recharge from the outcrop (southern karst uplands) causing water levels in the Cibao Formation to increase at larger ratios than in the Aguada Limestone can be explained by the existence of clay lenses in the Cibao Formation. Simulating these large vertical hydraulic gradients in the Cibao Formation by establishing a general-head boundary (McDonald and Harbaugh, 1988) in the bottom layer around the southern karst uplands and the Quebrada Honda karst valley (fig. 4) results in nearly constant water levels for cells falling within these areas, which the data shown in figures 13 to 16 preclude. In addition, a very important conclusion from water levels measured on May 12, 1993 (table 5) on multiport wells 96, 97, and 99 (Brian Smith, Geraghty & Miller, Inc., written commun., 1993) can be made regarding how recharge from the outcrop occurs. Although water levels at depths near mean sea level at wells 96 and 97 show semi-confined pressures, measured water levels from deeper measurement ports do not show semi-confined pressures. Water levels for well 99 indicate smaller vertical hydraulic gradients that do not necessarily increase as depth increases. These water levels indicate that what causes water levels at various depths to increase relative to the aquifer thickness is the recharge from the southern karst uplands (outcrop). These findings also preclude the simulation of the ground-water flow in these areas as flux from the underlying confined aquifer.

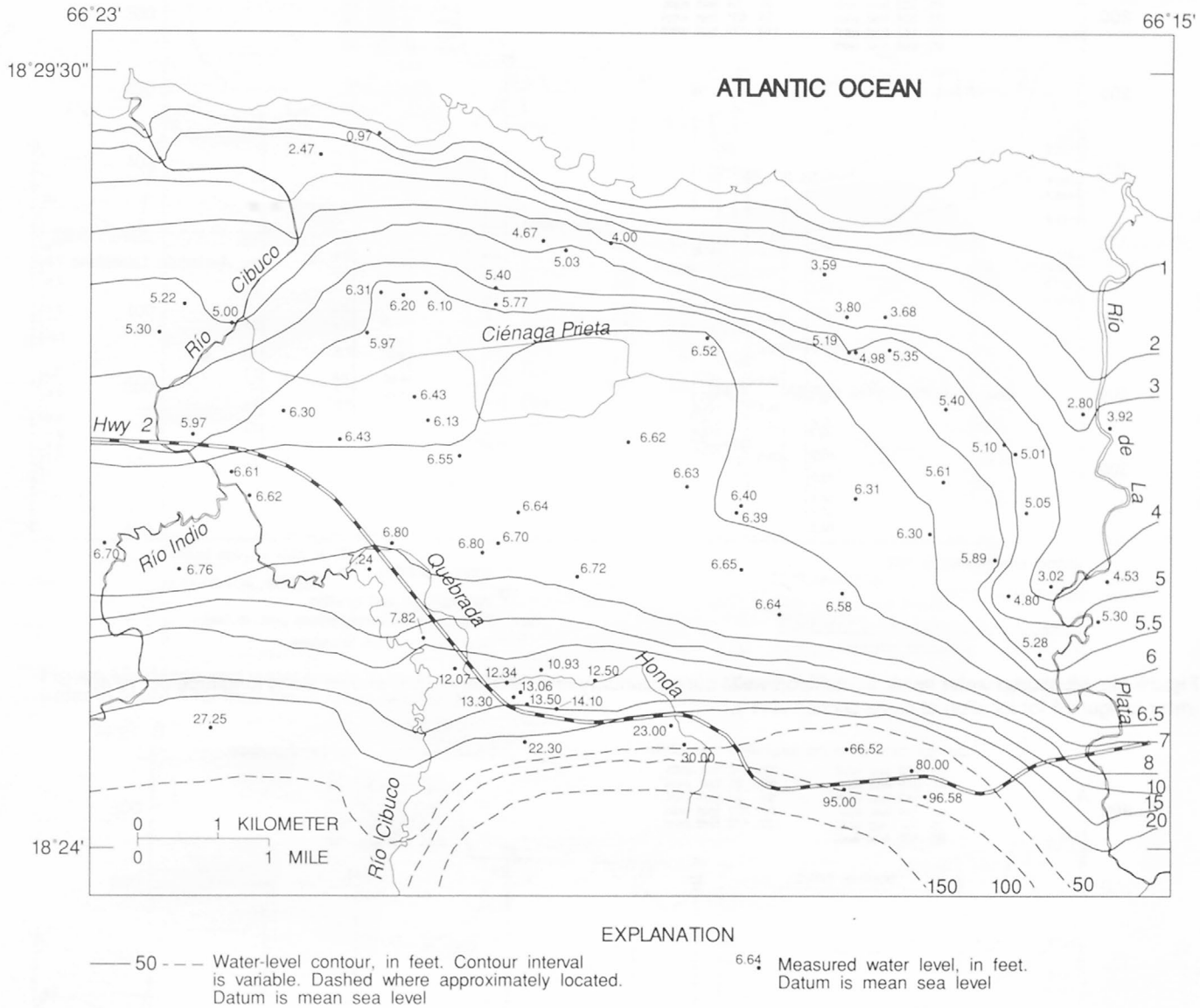

Figure 12. Water-level contours and measured water levels in the ground-water flow model area for February 1983.

Table 4. Time duration of stress periods simulated in the ground-water flow model

Stress period number	Time interval	Number of days in stress period
1	02-01-83 to 12-31-83	334
2	01-01-84 to 12-31-84	366
3	01-01-85 to 12-31-85	365
4	01-01-86 to 12-31-86	365
5	01-01-87 to 12-31-87	365
6	01-01-88 to 12-31-88	366
7	01-01-89 to 12-31-89	365
8	01-01-90 to 01-15-91	380
9	01-16-91 to 05-15-91	120
10	05-16-91 to 08-15-91	92
11	08-16-91 to 01-15-92	153
12	01-16-92 to 04-30-92	106

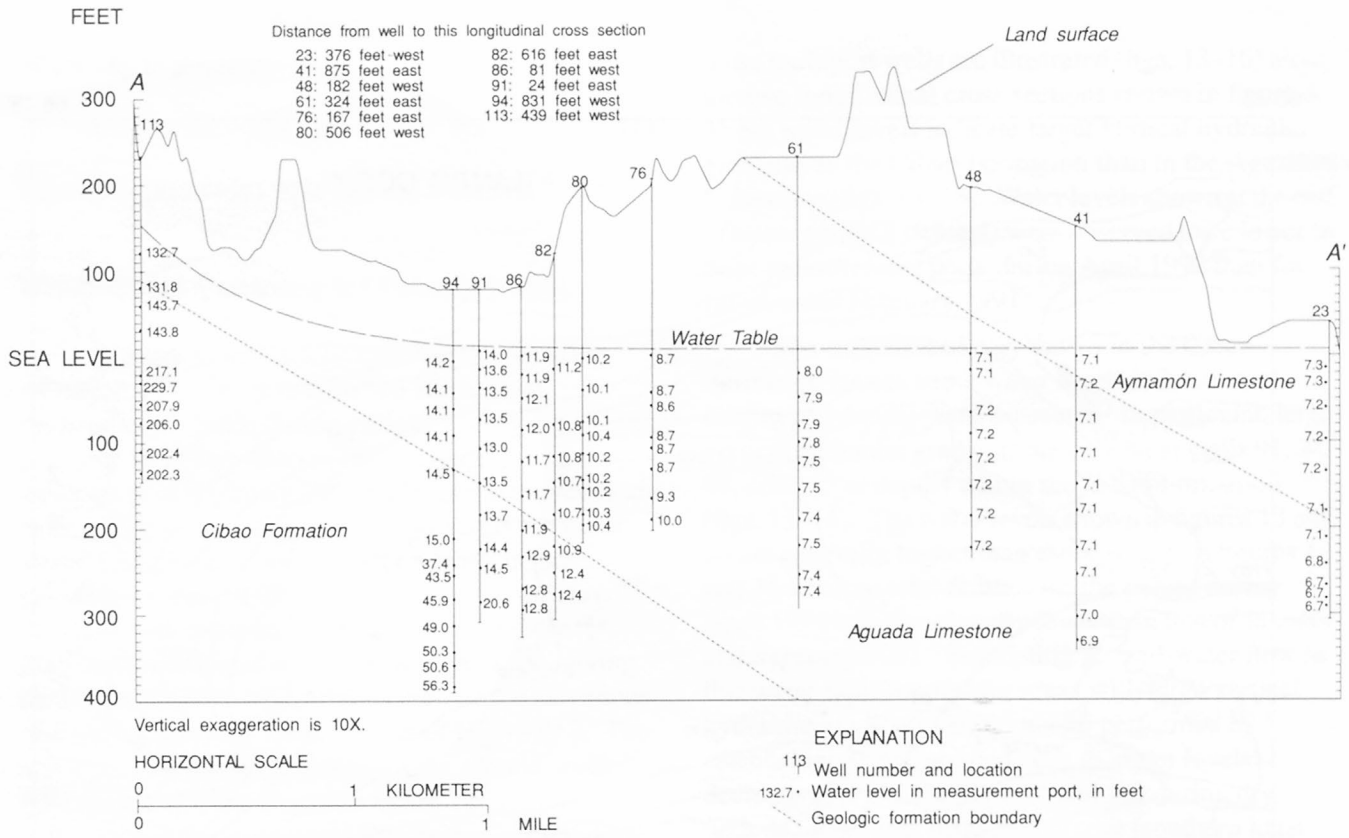

Figure 13. Measured water levels in multiport wells during January and February 1991, shown along longitude 66°19′40″ (refer to figure 4 for location of cross section *A-A′*).

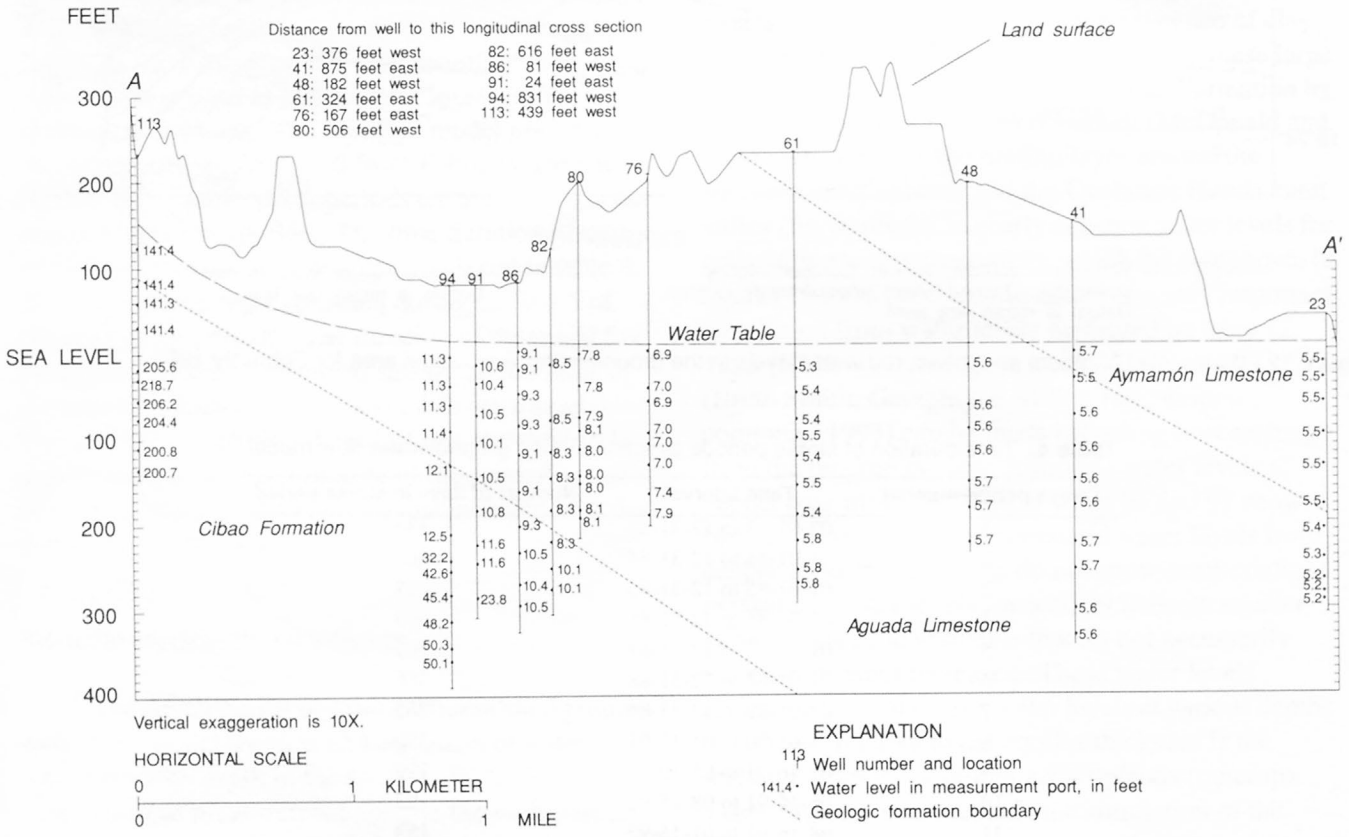

Figure 14. Measured water levels in multiport wells during April 1992, shown along longitude 66°19′40″ (refer to figure 4 for location of cross section *A-A′*).

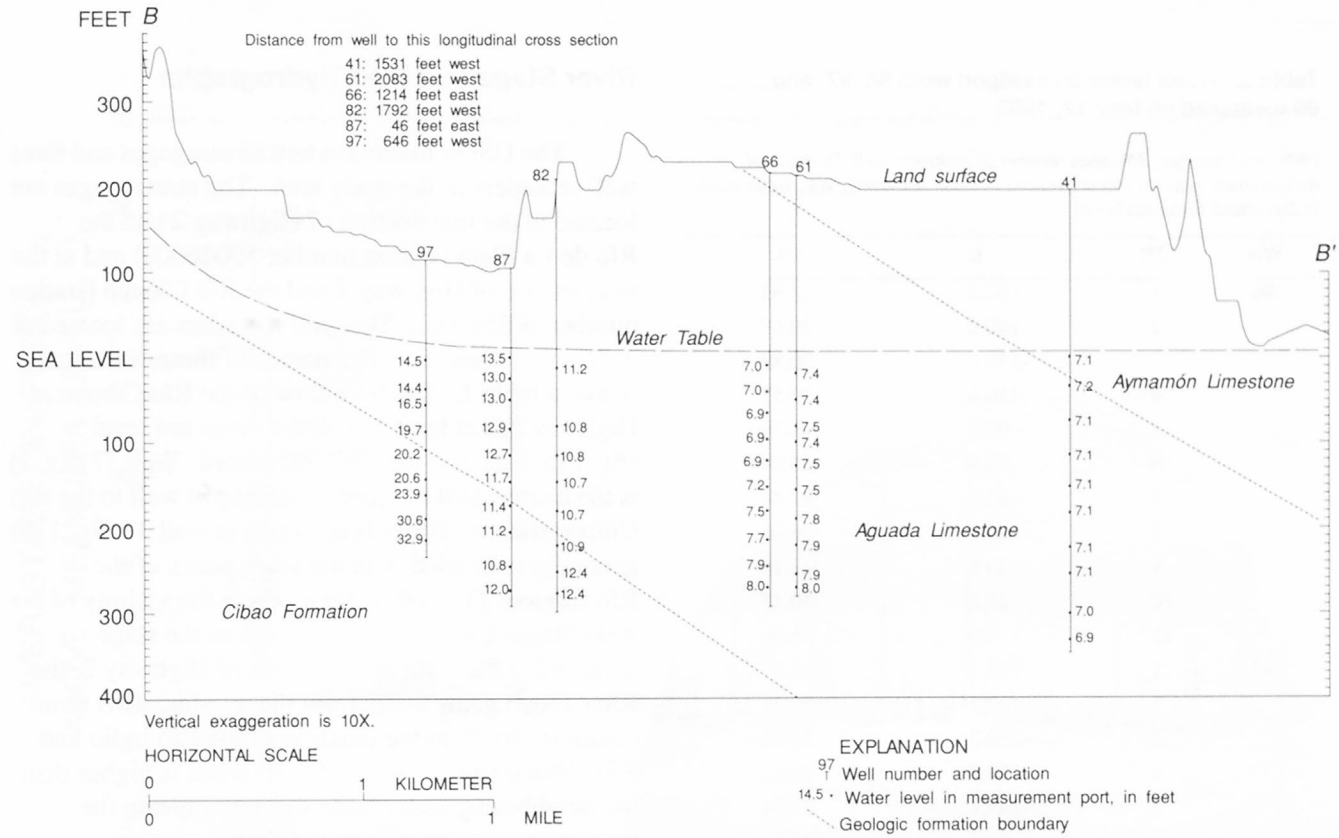

Figure 15. Measured water levels in multiport wells during January and February 1991, shown along longitude 66°19′15″ (refer to figure 4 for location of cross section *B-B′*).

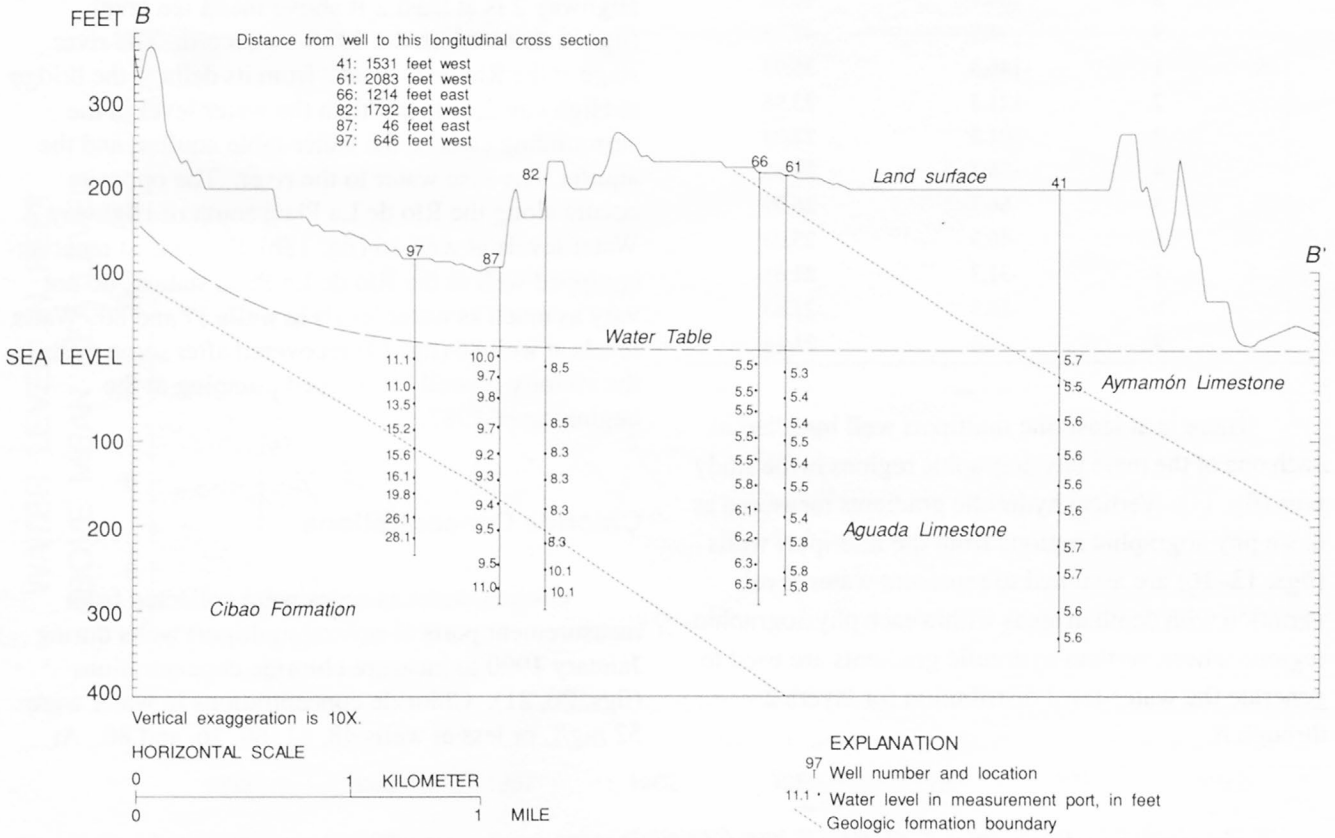

Figure 16. Measured water levels in multiport wells during April 1992, shown along longitude 66°19′15″ (refer to figure 4 for location of cross section *B-B′*).

Table 5. Water levels on multiport wells 96, 97, and 99 measured on May 12, 1993

[WN, well number; ZN, zone number in multiport well; D, depth of measurement port (in feet referenced to mean sea level); WL, water level, in feet above mean sea level]

WN	ZN	D	WL
96	1	-160.6	24.63
	2	-140.6	20.69
	3	-130.6	20.89
	4	-110.6	20.57
	5	-90.6	16.34
	6	-70.6	16.64
	7	-60.6	17.44
	8	-45.6	56.06
	9	-30.6	42.18
	10	-25.6	40.45
	11	-3.6	56.04
97	1	-214.7	34.07
	2	-189.7	31.21
	3	-159.7	25.21
	4	-139.7	21.13
	5	-109.7	20.74
	6	-84.7	20.21
	7	-54.7	18.01
	8	-34.7	15.02
	9	-4.7	47.58
99	1	-146.3	35.93
	2	-121.3	22.96
	3	-101.3	22.94
	4	-76.3	27.55
	5	-66.3	26.99
	6	-46.3	25.03
	7	-31.3	21.68
	8	-16.3	21.83
	9	-1.3	21.14

There is at least one multiport well installed in each one of the main physiographic regions in the study area (fig. 11). Vertical hydraulic gradients measured at these physiographic regions from the multiport wells (figs. 13–16) are assumed to represent water-level variation with depth in areas within each physiographic region. These vertical hydraulic gradients are used to generate the water-level distribution for layers 2 through 6.

River Stage and Well Hydrographs

The USGS maintains two streamgages and three well recorders in the study area. The streamgages are located at the intersection of Highway 2 and the Río de La Plata (station number 50046000) and at the intersection of Highway 2 and the Río Cibuco (station number 50039500). The well recorders are located at wells 16, 37, and 86. The names of these wells are listed in table 1. The base flow of the Río Cibuco at Highway 2 is at least 4 ft above mean sea level (fig. 17a) based on the 1985–92 record. Well 37 (fig. 2) is the nearest USGS recorder-equipped well to the Río Cibuco station. Water-level peaks at well 37 (fig. 17b) generally coincided with the stage peaks of the Río Cibuco. Ground-water levels in the vicinity of the Río Cibuco are generally higher than the stage recorded at the station, thus north of Highway 2, the Río Cibuco gains water from the aquifer. This trend continues south to the junction of the Río Indio and Río Cibuco (fig. 2), where the riverbed is higher than the neighboring water-table surface, causing the aquifer to gain water from the river.

The base flow of the Río de La Plata at Highway 2 is at least 2 ft above mean sea level (fig. 18a), based on the 1985–92 record. The river stage at the Río de La Plata, from its delta to the bridge at Highway 2, is lower than the water level in the surrounding cells of the water-table aquifer, and the aquifer may lose water to the river. The opposite occurs along the Río de La Plata south of Highway 2. Water levels at well 16 (fig. 18b), the nearest recorder-equipped well to the Río de La Plata station, do not vary as much as water levels in wells 37 and 86. Water levels at well 86 (fig. 19) recovered after some wells in the vicinity of well 86 stopped pumping at the beginning of 1987.

Chloride Concentrations

Ground-water samples were collected from measurement ports at several multiport wells during January 1990 to measure chloride concentrations (figs. 20, 21). Chloride concentrations in water were 52 mg/L or less at wells 48, 61, 66, 76, and 80. At

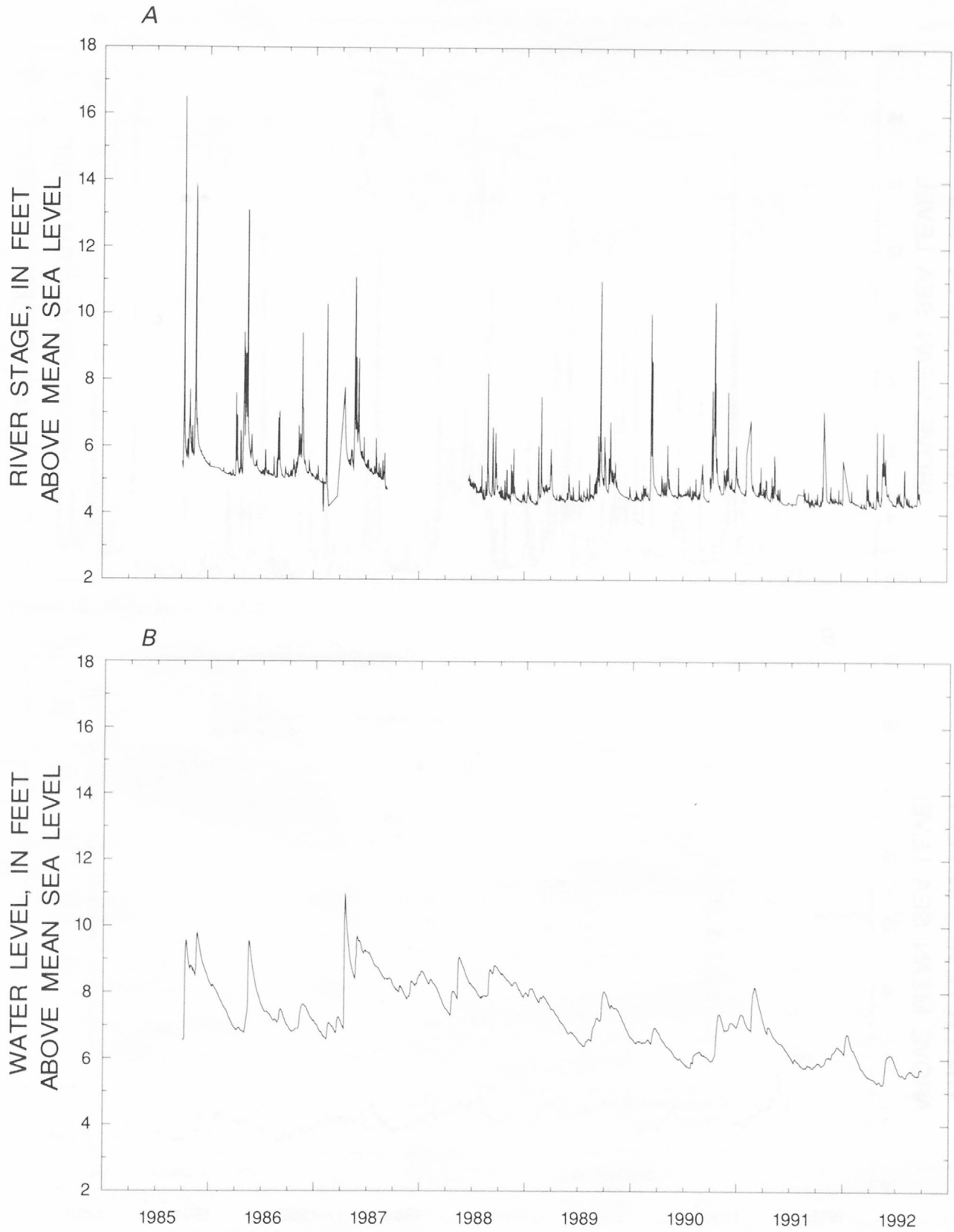

Figure 17. *A,* River stage at Río Cibuco (station number 50039500), and *B,* water level at well 37 (gaps indicate that no data were available).

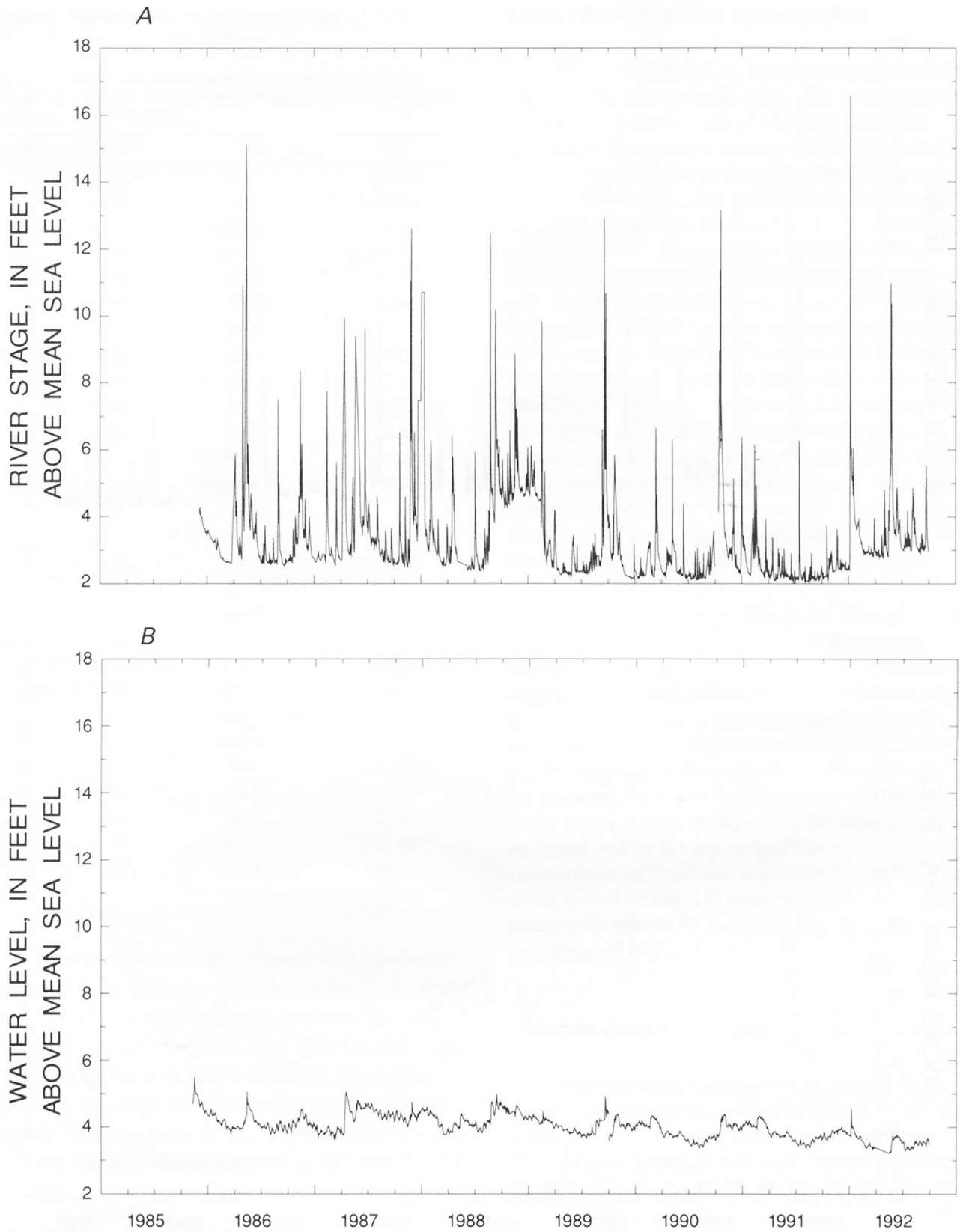

Figure 18. *A*, River stage at Río de La Plata (station number 50046000), and *B*, water level at well 16 (gaps indicate that no data were available).

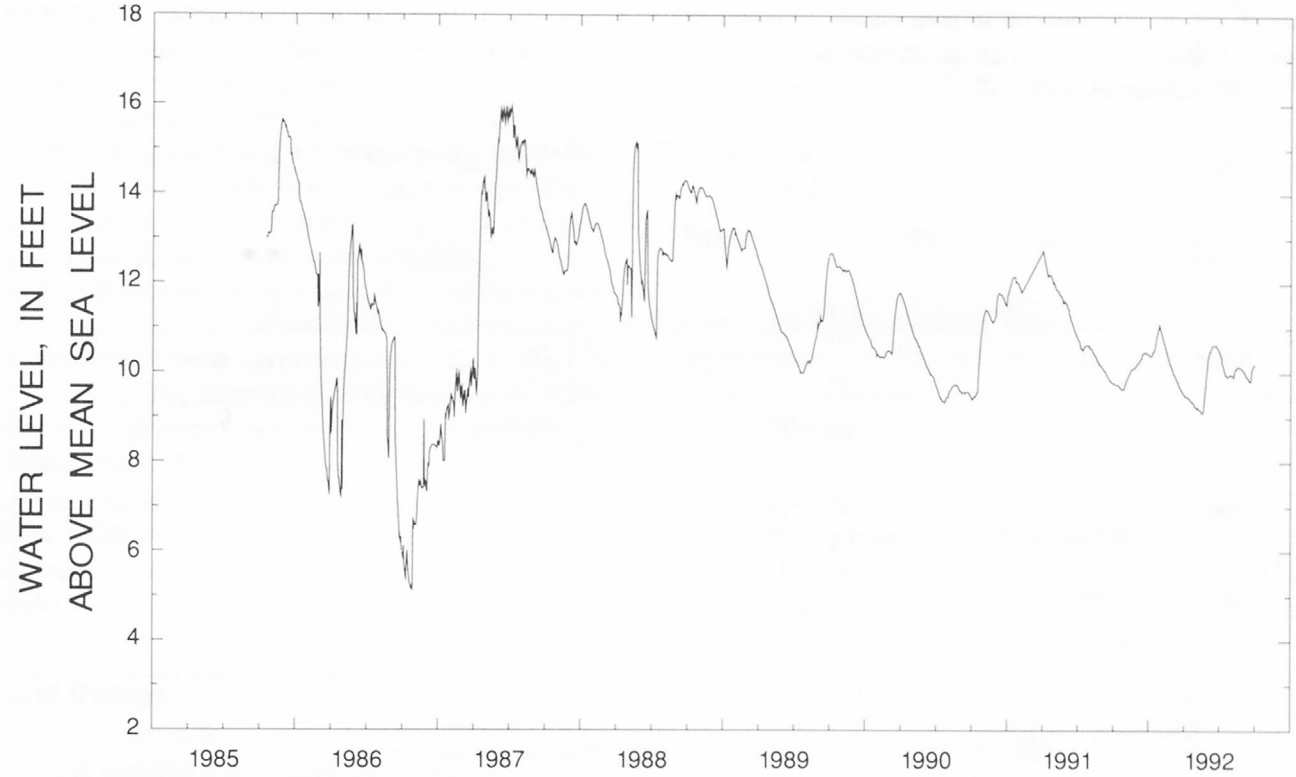

Figure 19. Water level at well 86.

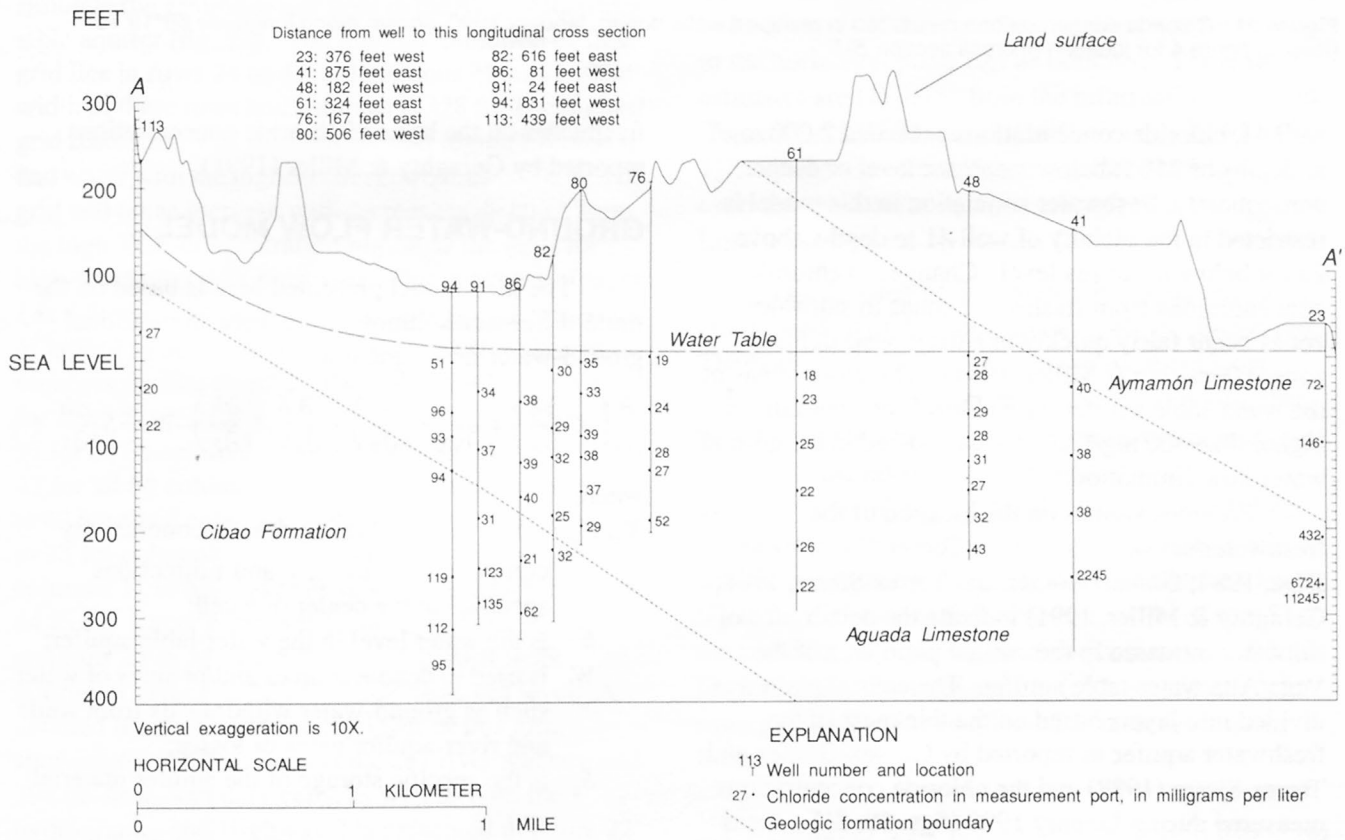

Figure 20. Chloride concentrations measured in multiport wells during January 1990, shown along longitude 66°19′40″ (refer to figure 4 for location of cross section *A-A′*).

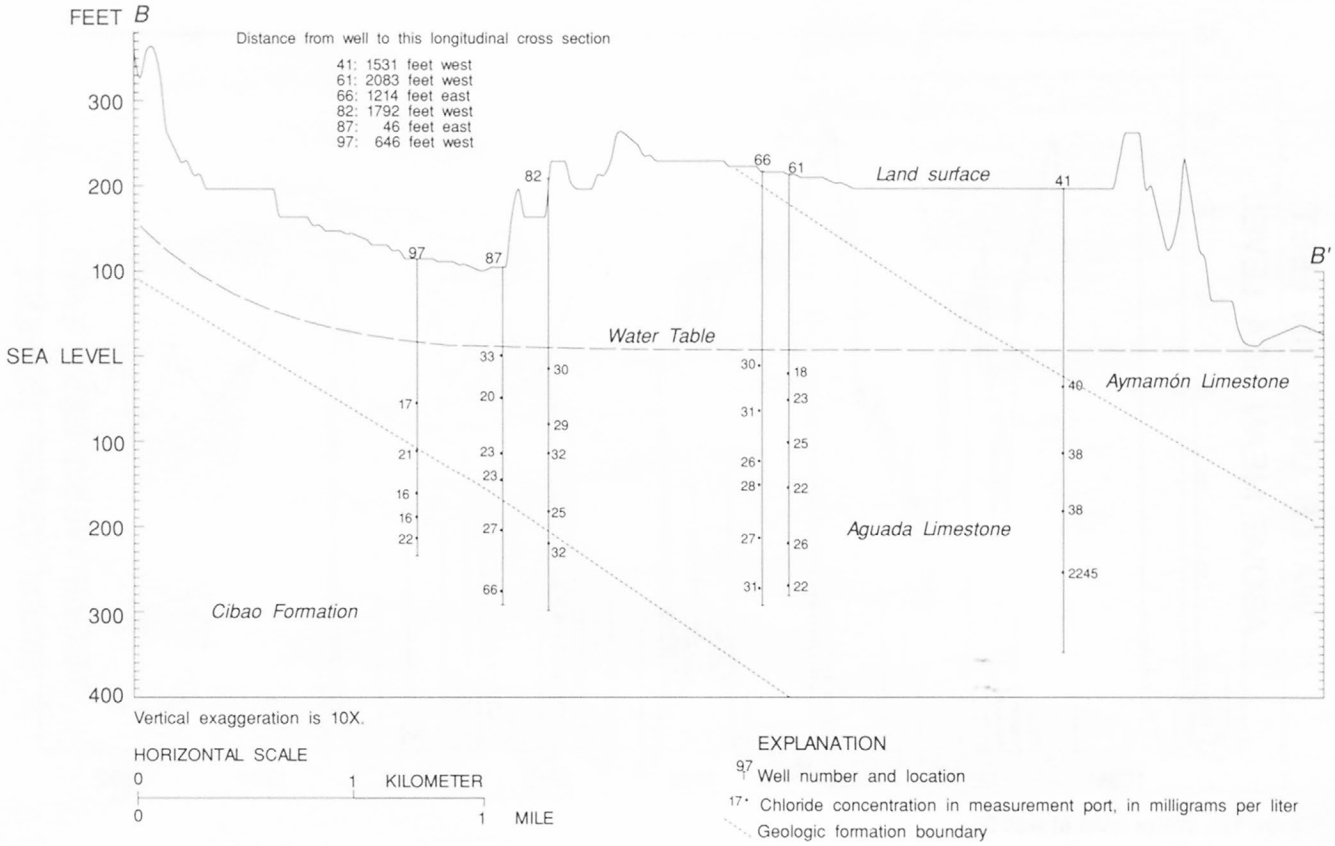

Figure 21. Chloride concentrations measured in multiport wells during January 1990, shown along longitude 66°19′15″ (refer to figure 4 for location of cross section *B-B′*).

well 41, chloride concentrations exceeded 2,000 mg/L at depths of 250 ft below mean sea level or deeper; consequently, freshwater simulation in this model is restricted in the vicinity of well 41 to depths above 250 ft below mean sea level. Changes in chloride concentrations from freshwater zones to saltwater zones occur fairly quickly in narrow well-defined zones (Geraghty & Miller, 1991). Therefore, areas in the water-table aquifer with chloride concentrations higher than 400 mg/L are not considered in the ground-water flow simulation.

Previous studies on the location of the freshwater/saltwater interface (Torres-González and Díaz, 1984; Gómez-Gómez and Torres-Sierra, 1988; Geraghty & Miller, 1991) indicate the occurrence of saltwater intrusion in the coastal plain area of the Vega Alta water-table aquifer. The coastal plain was divided into layers based on the thickness of the freshwater aquifer as reported by Gómez-Gómez and Torres-Sierra (1988) and the chloride concentrations measured during January 1990 (figs. 20, 21). Areas outside the coastal plain were divided into layers of freshwater on the basis of chloride concentrations reported by Geraghty & Miller (1991).

GROUND-WATER FLOW MODEL

The flow model presented here is based on the finite-difference solution of the three-dimensional ground-water flow equation:

$$\frac{\partial}{\partial x}\left(K_x\frac{\partial h}{\partial x}\right)+\frac{\partial}{\partial y}\left(K_y\frac{\partial h}{\partial y}\right)+\frac{\partial}{\partial z}\left(K_z\frac{\partial h}{\partial z}\right)-W=S_s\frac{\partial h}{\partial t} \quad (7)$$

where

K_x, K_y, and K_z are the three hydraulic conductivity components in the x, y, and z directions specified at the center of a cell;

h is the water level in the water-table aquifer;

W is used to denote sources and/or sinks of water such as ground-water withdrawals from wells and river-aquifer gains or losses;

S_s is the specific storage of the aquifer material; and

t represents time.

MODFLOW (McDonald and Harbaugh, 1988) uses a block-centered formulation, in which all hydraulic properties are specified at the center of the cell. The main hydraulic variables that need to be measured to develop the ground-water flow model for the Vega Alta water-table aquifer are indicated by equation (7). These are the hydraulic conductivity, the recharge from rainfall, the ground-water withdrawals from wells, the specific storage (specific yield for a water-table aquifer), riverbed conductance and stage values, and the initial water-level distribution for a transient simulation. The calibration of a ground-water flow model involves an iterative process in which the values assigned to K_x, K_y, K_z, S_s, rainfall recharge, and riverbed conductance are modified to reduce the error between the h values obtained for the solution of equation (7) and the measured water levels at the wells.

Grid Design

A variably spaced grid composed of 56 rows, 68 columns, and 6 layers was designed to simulate the ground-water flow in the Vega Alta water-table aquifer (fig. 22). The highest resolution of this grid lies in rows 24 to 49 and columns 18 to 41. The width of these rows and columns is 328 ft. The highest grid resolution was selected for that region because it had water with the highest concentrations of TCE. The grid cell areas increase with increasing distance from the high TCE-concentration region as the need for high-resolution data decreases. The thickness of layer 1 is a function of the water-table surface. The bottom of layer 1 is 50 ft below mean sea level for all row numbers smaller than 52. The bottom of layer 1 varied for rows 52 or larger. Layer 2 extends from rows 9 to 51 for all 68 columns. Layer 3 extends from rows 11 to 47 for all 68 columns. Layer 4 extends from rows 12 to 44 for all 68 columns. Layer 5 extends from rows 18 to 33 for columns 1 to 10, from rows 15 to 40 for columns 11 to 63, and from rows 18 to 33 for columns 64 to 68. Layer 6 extends from rows 21 to 36 for columns 25 to 58. Layers 2 to 5 are 50-ft thick. The bottom of layer 6 is 325 ft below mean sea level. A detailed illustration of the top layer of this grid, showing 68 constant-head cells, 291 river reaches, and 398 no-flow boundary cells, as well as both the hydrography and Highway 2 is presented in figure 22 to provide a frame of reference. The grid extends west to east from the vicinity of the Río Indio to the Río de La Plata, and north to south from the Atlantic Ocean coast to the areas where the Cibao Formation is exposed (fig. 3).

Division of Aquifer Thickness into Layers

The thickness of the Vega Alta water-table aquifer varies areally. A large region of the karst uplands plateau has an aquifer thickness of as much as 330 ft. The region is illustrated in figure 23 by the rectangle where six layers are simulated in the ground-water flow model. Water under semi-confined conditions is present at depths of 287 ft below mean sea level or lower in multiport well 91, at depths of 241 ft below mean sea level or lower in multiport well 94, and at depths of 18 ft below mean sea level or lower in multiport well 113. These depths are estimates based on vertical hydraulic gradient changes in water levels at those wells (Geraghty & Miller Inc., 1992). The distance between wells 91 and 94 is 956 ft and between wells 91 and 113 is 5,167 ft. Based on these distances, two estimates of the dip of the artesian aquifer relative to the horizontal plane can be obtained. These two estimates are (1) 2.75° from the information obtained for wells 91 and 94 and (2) 2.98° from wells 91 and 113. These dip estimates are similar to the dips estimated earlier for the Cibao Formation, the Aguada Limestone, and the Aymamón Limestone.

The division of the aquifer thickness into layers is independent of the slopes of the geologic formations. The bottom of the first layer in the southern karst uplands was computed based on the assumption that the slope of the confining unit of the water-table aquifer relative to the horizontal is estimated at 2.86°, an average value of the two previously computed slope values. At well 113, the bottom of the water-table aquifer is estimated to be at 8 ft above mean sea level. If y is the distance, in feet, from the center of row 51 to the center of any row larger than 52, then y = 2,050 ft for well 113. The thickness, z, (in feet) of layer 1 for rows greater than or equal to 52 is then determined from:

$$z = (tan 2.86°)\, y + 8.0 - (tan 2.86°) \times 2,050 \quad (8)$$
$$= 0.04996y - 94.$$

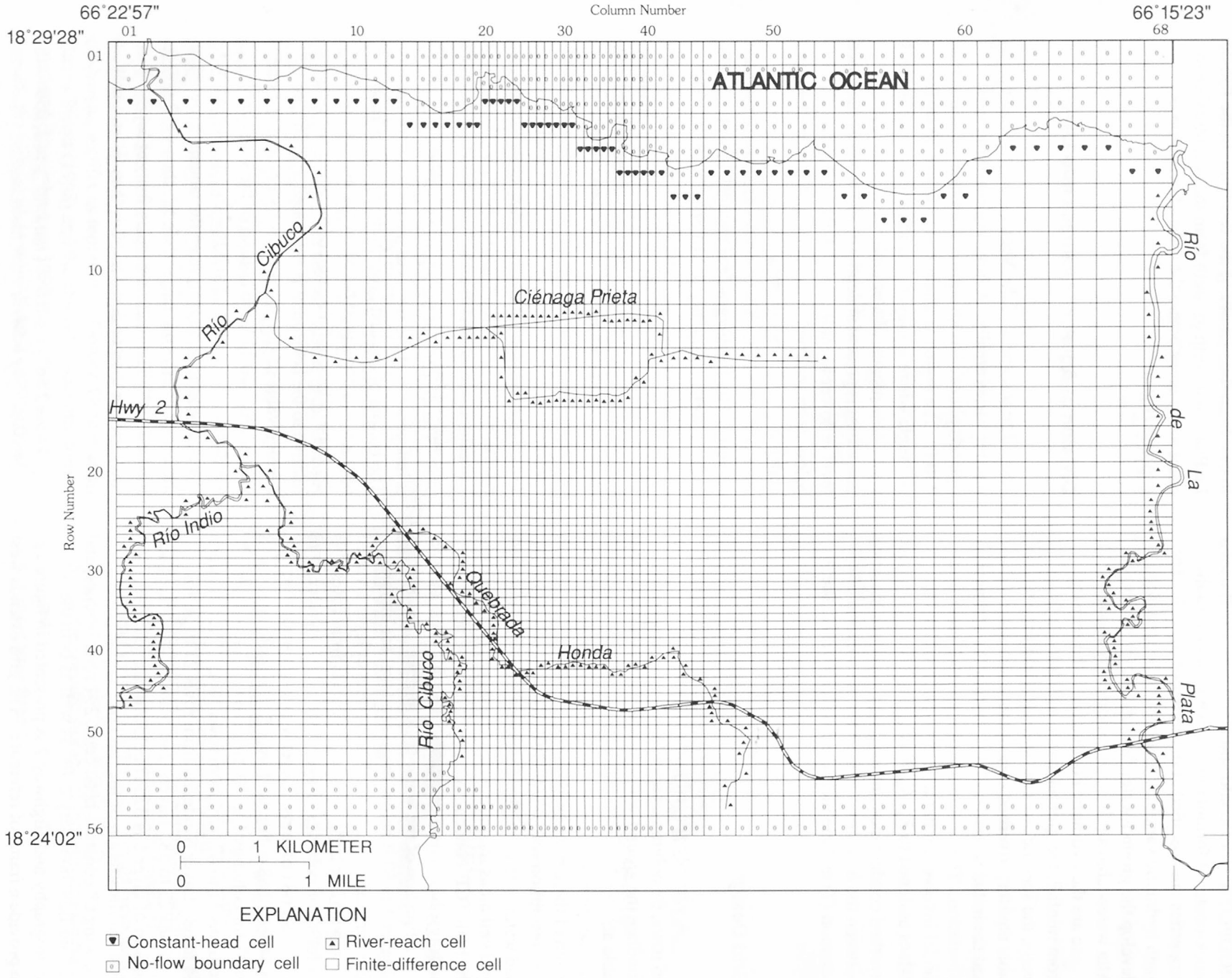

Figure 22. Constant head, no-flow boundary, river reach, and finite-difference cells in layer 1 of the grid used to develop the ground-water flow model.

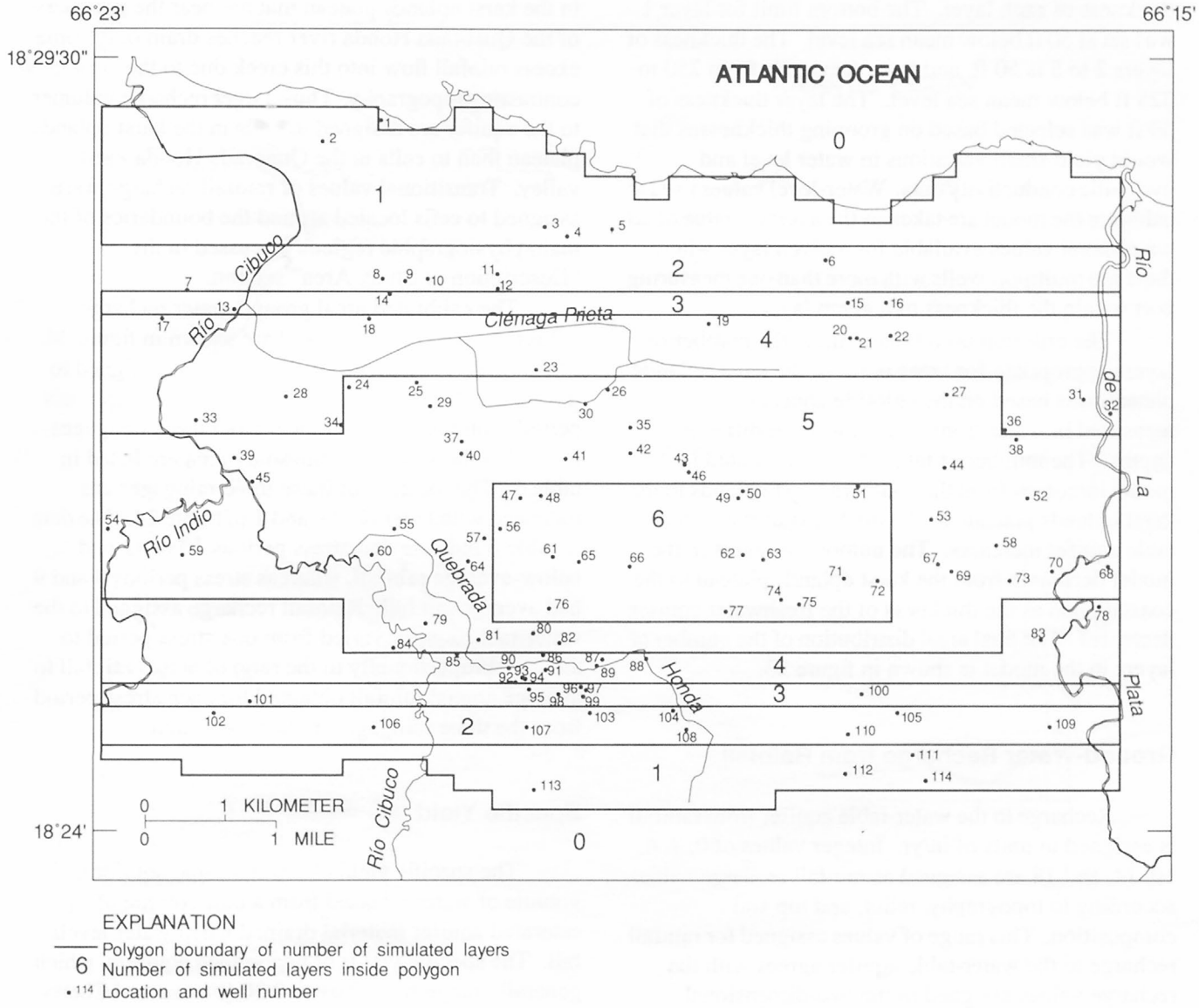

Figure 23. Areal distribution of number of simulated layers in the ground-water flow model area.

Boundaries and areal extent of layers 2 to 4 south of the karst uplands plateau were determined from this slope estimation, the distance between cells, and the thickness of each layer. The bottom limit for layer 1 was set at 50 ft below mean sea level. The thickness of layers 2 to 5 is 50 ft, and layer 6 extends from 250 to 325 ft below mean sea level. The layer thickness of 50 ft was selected based on grouping thicknesses that would yield small variations in water level and hydraulic conductivity data. Water-level values used to calibrate the model are taken as the average value of all water-level values available for a given layer where there are multiport wells with more than one measuring port within the thickness of a given layer.

The criterion used to determine the number of layers appropriate for areas north of the karst uplands plateau was based on the chloride concentrations measured in water from various wells at different depths. The number of layers being simulated in the model increases from the southern karst uplands to the karst uplands plateau, as the thickness of the water-table aquifer increases. The number of layers in the model decreases from the karst uplands plateau to the coastal plain as the thickness of the freshwater aquifer decreases. The final areal distribution of the number of layers in the model is shown in figure 23.

Ground-Water Recharge from Rainfall

Recharge to the water-table aquifer from rainfall is assigned in units of in/yr. Integer values of 0, 2, 6, 10, 14, and 18 are assigned as rainfall recharge values according to topography, relief, and top soil composition. This range of values assigned for rainfall recharge to the water-table aquifer agrees with the recharge values assigned in the two-dimensional USGS ground-water flow model developed by Gómez-Gómez and Torres-Sierra (1988). The value of 0 is used for no-flow boundary cells. River reach and neighboring cells are assigned a value of 2 in/yr. Coastal plain areas are assigned recharge values ranging from 6 to 10 in/yr. Assigned recharge values to cells generally increase as their distance from river reach cells increase. The Vega Alta and Dorado urban areas are assigned the value of 6 in/yr for rainfall recharge. Large sections of the southern karst uplands, the karst uplands plateau, and other areas of high elevation are assigned the recharge value of 18 in/yr. The shared boundary between the karst uplands plateau and the Quebrada Honda karst valley is delineated based on the surficial geology and the sharp contrast in land surface elevation along this boundary. Grid cells in the karst uplands plateau that are near the boundary of the Quebrada Honda river reaches drain only some excess rainfall flow into this creek due to the contrasting topography. Thus, larger recharge volumes to the aquifer are assigned to cells in the karst uplands plateau than to cells in the Quebrada Honda karst valley. Transitional values of rainfall recharge were assigned to cells located around the boundaries of the main physiographic regions discussed in the "Description of Study Area" section.

The calibrated areal ground-water recharge values to layer 1 of the model are shown in figure 24. The largest recharge value, 18 in/yr, was assigned to the karst uplands plateau. Rainfall data for the stress periods simulated in the model from three raingages located in the vicinity of the study area are listed in table 6. The location of these three raingages are indicated with letters D, G, and T in figure 24. The data in table 6 indicate that stress periods 10 to 12 had below-average rainfall, whereas stress periods 8 and 9 had average rainfall. Rainfall recharge assigned to the water-table aquifer varied from one stress period to another, proportionally to the ratio of actual rainfall to average annual rainfall obtained for each stress period from the three raingages in the model area.

Specific Yield

The specific yield of a water-table aquifer is the volume of water released from a unit volume of saturated aquifer material drained when water levels fall. The specific yields of unconfined aquifers, which generally range from 0.01 to 0.30 (Freeze and Cherry, 1979), could be orders of magnitude higher than the storativities of confined aquifers. The coefficient S_s in equation (7) becomes, for an unconfined water-table aquifer, the specific yield. Representative values of specific yields for some geologic materials are fine sand, 0.23; fine-grained sandstone, 0.21; clay, 0.03; silt, 0.08; and limestone, 0.14 (Todd, 1980).

For the model discussed in this report, different specific-yield values are assigned to alluvial deposits, to the transition zone between these alluvial deposits and limestone formations, to limestone formations, and to areas with high contents of clay. Alluvial valley terrains generally have higher interstitial porosity

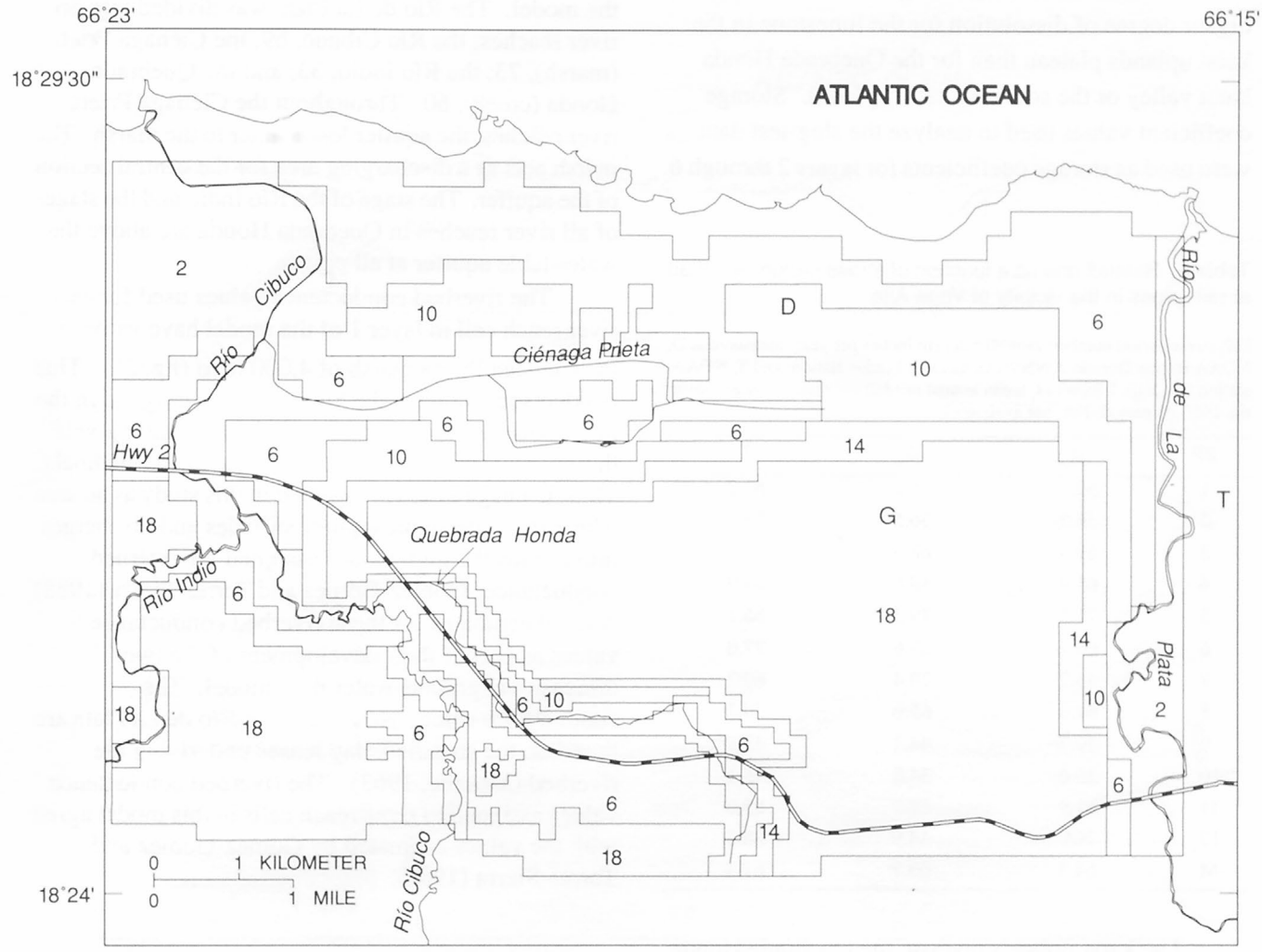

Figure 24. Areal variation of calibrated rainfall recharge rates.

values than limestone, thus alluvial materials can store more water. The specific yield of limestone increases with its state of dissolution. Slug-test results indicate a higher degree of dissolution for the limestone in the karst uplands plateau than for the Quebrada Honda karst valley or the southern karst uplands. Storage coefficient values used to analyze the slug-test data were used as storage coefficients for layers 2 through 6.

Table 6. Rainfall rate as a function of stress period recorded at raingages in the vicinity of Vega Alta

[SP, stress period number; rainfall rates (in inches per year) measured at D, NOAA station Dorado 2 WNW; G, Gramas Lindas station; and T, NOAA station Toa Baja 1 SSW; M, mean annual rainfall for each raingage during the 1960-93 period; NA, not available]

SP	D	G	T
1	52.1	56.2	62.2
2	54.3	56.5	58.1
3	69.4	68.5	72.3
4	65.4	59.6	69.9
5	71.2	79.3	86.1
6	64.7	69.6	77.0
7	63.7	70.4	69.2
8	64.6	65.0	70.7
9	59.7	44.2	48.1
10	35.6	34.8	43.1
11	51.9	58.2	55.0
12	NA	44.9	38.3
M	64.3	63.7	67.4

The karst uplands plateau, the Quebrada Honda karst valley, and the southern karst uplands were assigned specific-yield values ranging from 0.01 to 0.05. Due to the high clay content in the southern karst uplands, the specific-yield values in this area were chosen to reflect poorly confined conditions. The alluvial materials in the coastal plain were assigned specific-yield values ranging from 0.10 to 0.15. The transition zone from alluvial and beach deposits to the karst uplands plateau was assigned a value of 0.10. These values resulted from a calibration process that was based on reducing the differences between simulated and measured water levels. Figure 25 shows areal variations of the calibrated specific-yield values in the modeling area.

River Nodes

A total of 291 river reach cells are simulated in the model. The Río de La Plata was divided into 56 river reaches; the Río Cibuco, 69; the Ciénaga Prieta (marsh), 73; the Río Indio, 33; and the Quebrada Honda (creek), 60. Throughout the Ciénaga Prieta river reaches, the aquifer loses water to the marsh. The marsh acts as a discharging area for the central section of the aquifer. The stage of the Río Indio and the stages of all river reaches in Quebrada Honda are above the water-table aquifer at all points.

The riverbed conductance values used for each river reach cell in layer 1 of the model have values for the Ciénaga Prieta marsh of 4,000 ft^2/d (fig. 26). This conductance value is the highest value assigned in the flow model area. Wells 26 and 30 have water levels that coincide with the river stage in the marsh channels. Thus, Ciénaga Prieta is modeled in this study as an area where the water-table aquifer surfaces and discharges into it, thus the high values assigned for riverbed conductance. Gómez-Gómez and Torres-Sierra (1988) derived estimates for these riverbed conductance values as part of their development of the two-dimensional ground-water flow model. The conductance values assigned to the Río de La Plata are based on the stratified clay lenses underlying the riverbed (Monroe, 1963). The riverbed conductance values assigned to river-reach cells in this model agree with the values estimated by Gómez-Gómez and Torres-Sierra (1988).

General-Head Boundary Conditions

General-head boundary conditions (McDonald and Harbaugh, 1988) are imposed along the eastern and western boundaries of the simulated area. The grid cells where general-head boundary conditions are imposed lie along columns 1 and 68 (fig. 22) for all active cells along these columns in layers 1 through 5. Notice that there are no active cells in layer 6, which lie on columns 1 or 68. The conductance values of the general-head boundary sources at the left-hand side of column 1 and at the right-hand side of column 68 (fig. 22) were determined from the hydraulic conductivity of the general-head boundary cells (K_b), the thickness of each layer (M), and the width (W) and length (L) of each one of these general-head boundary

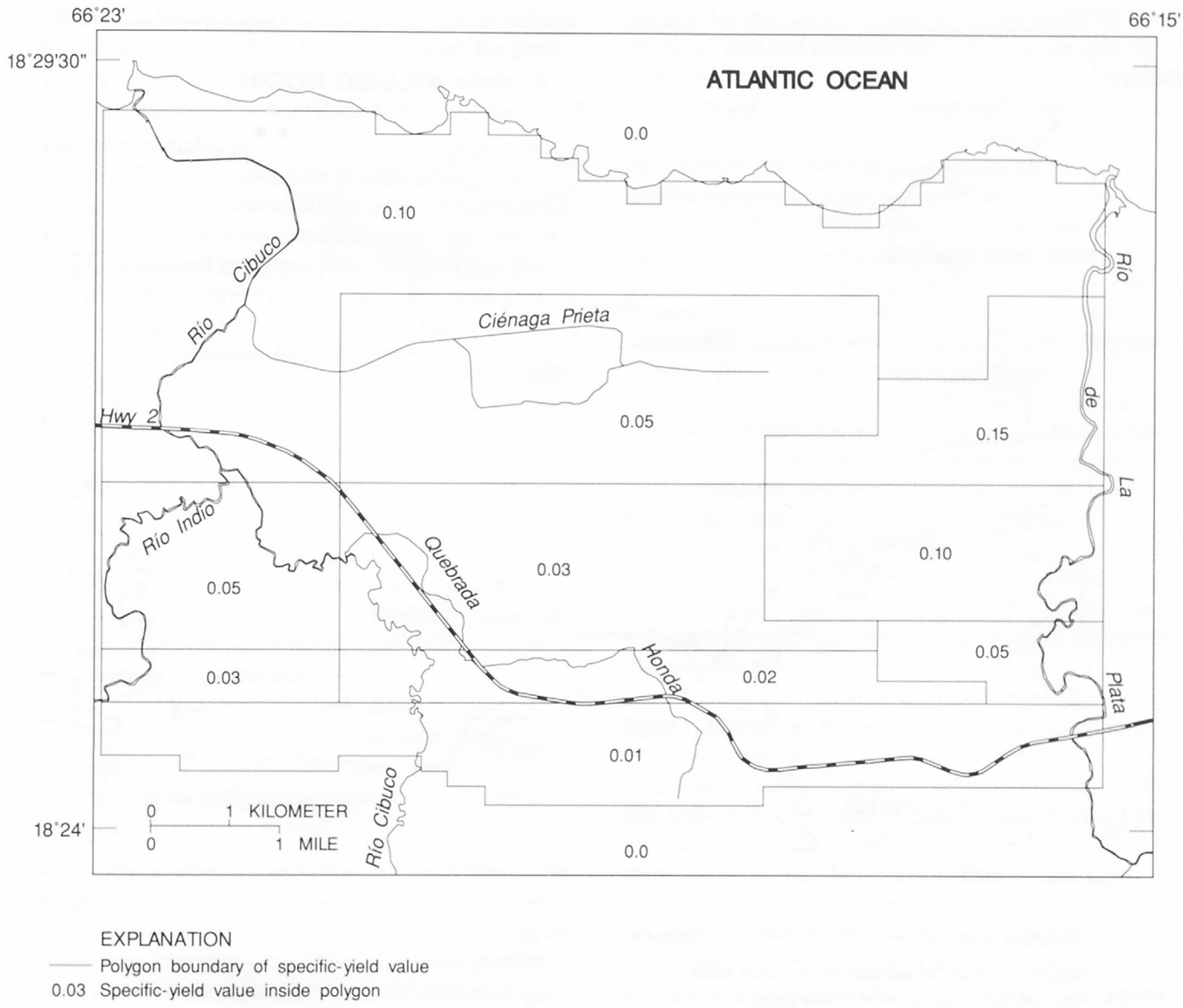

Figure 25. Areal variation of calibrated specific-yield values.

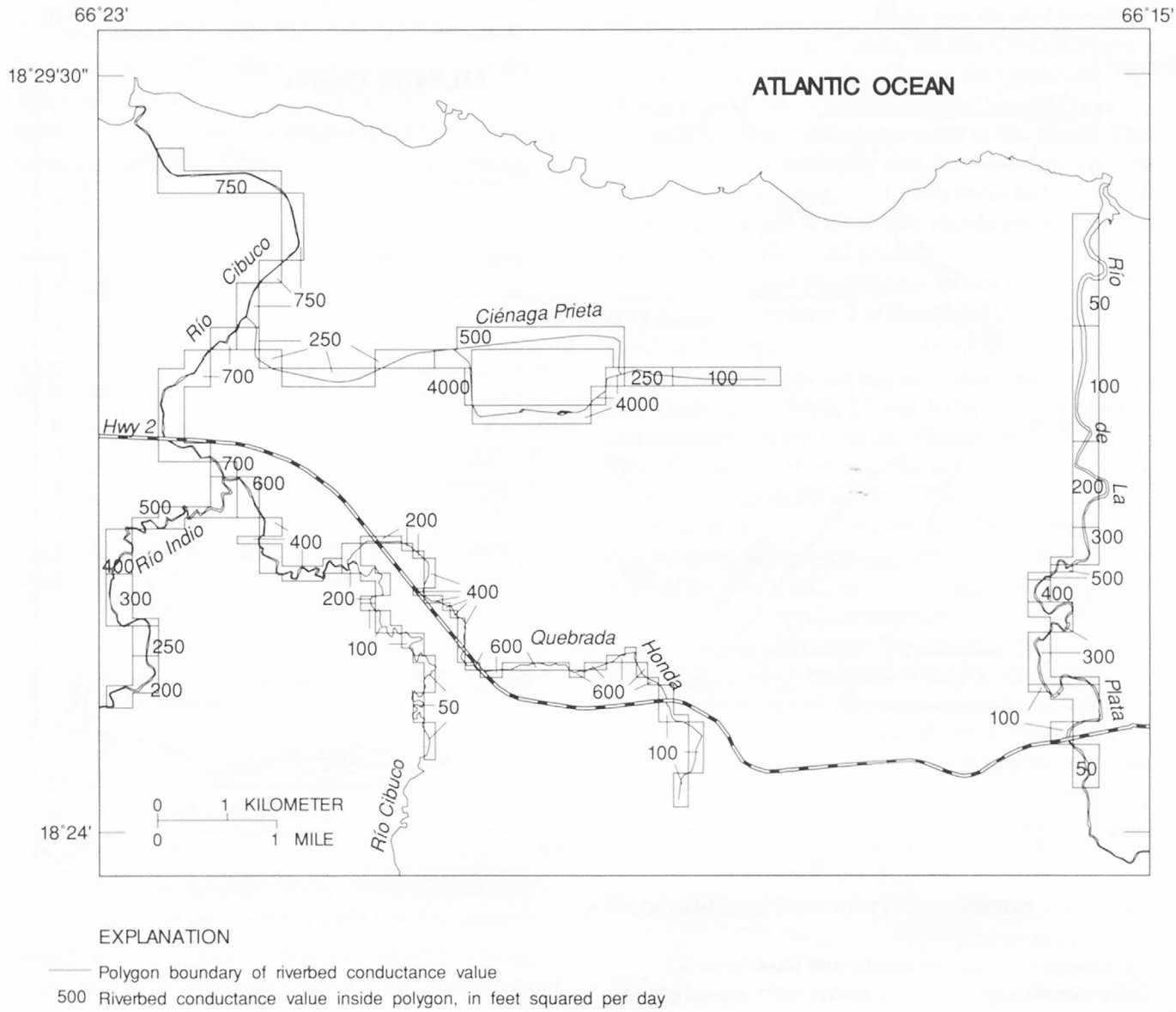

EXPLANATION

Polygon boundary of riverbed conductance value

500 Riverbed conductance value inside polygon, in feet squared per day

Figure 26. Riverbed conductance values of river reach cells simulated in the ground-water flow model.

source cells. The length, L, of each one of the general-head boundary source cells was taken to be 200 ft. The width, W, was taken to be equal to the corresponding width of columns 1 and 68, which varies from one row to another. The conductance value C used for these general-head boundary source cells was computed from the equation $C = K_b MW/L$. Notice that the role of variables M and L in this conductance equation is inverted for the computation of streambed conductances as horizontal flow is simulated in these general-head boundary conditions, whereas vertical flow is simulated in river-aquifer interactions. The boundary-head values used at the cells where general-head boundary conditions are imposed were the initial water levels computed from the steady-state prerun simulation.

Ground-Water Withdrawals

Withdrawal data from public water-supply wells were compiled, and estimated in some cases, from the Puerto Rico Aqueduct and Sewer Authority records for the period of February 1983 to April 1992. Withdrawals from privately-owned wells and industrial wells were estimated based on field measurements, pipe capacities, and time of use. Withdrawal rates from all discharging wells (and total withdrawals for each stress period) are listed in table 7 as a function of stress period.

The number of layers that each well taps in the aquifer are indicated in the second column of table 7. The withdrawal rates for each stress period during the simulation time of the model are also listed in table 7. Well withdrawals from each layer are proportional to the hydraulic conductivity values assigned to the layer in relation to the entire transmissivity of the well, as suggested in the documentation for MODFLOW (McDonald and Harbaugh, 1988). Thus, if K_i is the hydraulic conductivity of layer i, b_i is that thickness of layer i that the well penetrates, Q is the total well withdrawal rate, and T is the transmissivity of the entire thickness the well is penetrating, then the withdrawal rate Q_i for layer i is given by:

$$Q_i = \frac{Q b_i K_i}{T} . \qquad (9)$$

Calibrated Hydraulic Conductivity Maps

Calibration of hydraulic conductivity values, K, assigned at the center of each cell in the modeling area involved trial and error adjustments in some cells of unknown hydraulic properties, extrapolating values in groups of cells where the water levels behave similar to cells in multiport wells, applying general knowledge of the hydraulic behavior of geologic formations and aquifer materials, assigning equal values to blocks of cells rather than varying values linearly from cell to cell with distance, and establishing some degree of continuity among values of contiguous blocks. The starting values used for the hydraulic conductivity K were based on extrapolations made from the slug-test results. The calibration process consisted in making changes to these starting hydraulic conductivity values to reduce the error between measured and simulated water levels. Some of these values were changed according to the resulting changes in ground-water flow. The process of changing these hydraulic conductivity values was performed in the direction of the ground-water flow, starting from the southern karst uplands (upgradient) and ending with the coastal plain area (downgradient). Final calibrated values for layers 1 to 6 are shown in figures 27–32.

The first 10 columns in the western boundary of layer 1, just before the confluence of the Río Cibuco and Río Indio (fig. 27) occurs, show hydraulic conductivity values increasing as the confluence of the Río Indio and Río Cibuco is approached. North of the confluence of these two rivers, K values begin to decrease, reflecting the transition from limestone to alluvial deposits. In deeper layers, the K values also decrease because of a decreasing freshwater thickness. The lowest K values in layer 1 are assigned in the southern karst uplands because of the high clay content in this area. The vicinity of the uplands karst plateau has the highest K values, with values decreasing to the north, south, east, and west. Hydraulic conductivity values for the river reaches in the Río de La Plata are lower than neighboring values because of the mixture of alluvial and clay materials. K values decrease northward from the middle of the uplands karst plateau to the coastal plain (fig. 27).

At the end of the calibration process, there were discrepancies between the K values obtained from slug tests and the final calibrated values. These differences are listed in table 8. The fact that the screen openings of the multiport wells are relatively small compared to

Table 7. Ground-water well withdrawals for all simulated stress periods

[WN, well number; L, range of layer numbers from which the withdrawal occurred; Q_1, Q_2, ..., Q_{12}, withdrawal rates in cubic feet per second for all 12 simulated stress periods; TOT, total well withdrawals for each stress period in cubic feet per second]

WN	L	Q_1	Q_2	Q_3	Q_4	Q_5	Q_6	Q_7	Q_8	Q_9	Q_{10}	Q_{11}	Q_{12}
3	1	2.228e-2	2.228e-2	2.228e-2	2.228e-2	2.228e-2	2.228e-2	2.228e-2	2.228e-2	2.228e-2	2.228e-2	2.228e-2	2.228e-2
5	1	2.228e-2	2.228e-2	2.228e-2	2.228e-2	2.228e-2	2.228e-2	2.228e-2	2.228e-2	2.228e-2	2.228e-2	2.228e-2	2.228e-2
7	1-2	1.561	0.0	0.0	0.0	0.0	0.0	0.0	0.0	0.0	0.0	0.0	0.0
8	1-2	2.228e-1	2.228e-1	2.228e-1	0.0	0.0	0.0	0.0	0.0	0.0	0.0	0.0	0.0
9	1-2	1.557e-1	1.557e-1	1.557e-1	1.557e-1	1.557e-1	1.557e-1	1.557e-1	1.557e-1	1.557e-1	1.557e-1	1.557e-1	1.557e-1
10	1-2	1.112e-1	1.112e-1	1.112e-1	1.112e-1	1.112e-1	1.112e-1	2.228e-1	2.228e-1	2.228e-1	2.228e-1	2.228e-1	2.228e-1
11	1	8.475e-2	8.475e-2	8.475e-2	8.475e-2	8.475e-2	8.475e-2	8.475e-2	8.475e-2	0.0	0.0	0.0	0.0
13	1-2	2.228e-1	2.228e-1	2.228e-1	0.0	0.0	0.0	0.0	0.0	0.0	0.0	0.0	0.0
14	1	2.228e-1	2.228e-1	0.0	0.0	0.0	0.0	0.0	0.0	0.0	0.0	0.0	0.0
15	1	2.006e-1	2.006e-1	2.006e-1	1.670e-1	1.670e-1	1.670e-1	1.670e-1	1.670e-1	1.670e-1	1.670e-1	1.670e-1	1.670e-1
17	1-2	1.561	0.0	0.0	0.0	0.0	0.0	0.0	0.0	0.0	0.0	0.0	0.0
18	1-2	0.0	0.0	0.0	0.0	0.0	0.0	1.402e-1	1.402e-1	1.402e-1	1.402e-1	1.402e-1	1.402e-1
20	1-2	2.006e-1	2.006e-1	2.006e-1	1.670e-1	1.670e-1	1.670e-1	1.670e-1	1.670e-1	1.670e-1	1.670e-1	1.670e-1	1.670e-1
22	1-2	2.006e-1	2.006e-1	2.006e-1	1.670e-1	1.670e-1	1.670e-1	1.670e-1	1.670e-1	1.670e-1	1.670e-1	1.670e-1	1.670e-1
24	1-3	3.341e-1	3.341e-1	3.341e-1	3.341e-1	3.341e-1	3.341e-1	3.341e-1	3.341e-1	3.341e-1	3.341e-1	3.341e-1	3.341e-1
25	1-2	0.0	1.186e-1	2.822e-1	3.637e-2	1.285e-1	1.536e-1	2.666e-1	0.0	0.0	0.0	0.0	2.458e-1
27	1-2	1.462	1.540	1.533	1.511	1.508	1.444	1.734	1.730	3.464e-1	3.464e-1	3.464e-1	3.433e-1
28	1-2	1.561	0.0	0.0	0.0	0.0	0.0	0.0	0.0	0.0	0.0	0.0	0.0
29	2	4.767e-1	2.059e-1	5.085e-1	7.098e-1	4.556e-1	1.172e-1	7.593e-1	1.222	1.180	1.180	1.180	1.183
32	2	1.670e-1	1.670e-1	1.670e-1	1.670e-1	1.670e-1	1.670e-1	1.670e-1	1.670e-1	1.670e-1	1.670e-1	1.670e-1	1.670e-1
34	1-2	2.122e-1	2.698e-1	3.224e-1	2.811e-1	2.408e-1	2.698e-1	3.411e-1	3.206e-1	2.970e-1	2.970e-1	2.970e-1	3.076e-1
35	1-4	2.786e-1	2.786e-1	2.786e-1	2.786e-1	2.786e-1	2.786e-1	2.786e-1	1.448e-1	1.448e-1	1.448e-1	1.448e-1	1.448e-1
36	1-2	6.604e-1	4.909e-1	3.743e-1	7.663e-1	1.642	1.504	1.381	1.476	1.374	1.374	1.374	1.254
38	2-3	5.897e-1	7.169e-1	5.580e-1	8.299e-1	9.076e-1	9.605e-1	1.052	1.130	1.109	1.109	1.109	1.014
39	2-4	2.006	2.006	2.006	0.0	0.0	3.341e-1	3.341e-1	3.341e-1	3.341e-1	3.341e-1	3.341e-1	3.341e-1
42	1	2.228e-2	2.228e-2	2.228e-2	2.228e-2	2.228e-2	2.228e-2	2.228e-2	2.228e-2	2.228e-2	2.228e-2	2.228e-2	2.228e-2
44	1-3	3.464e-1	2.864e-1	2.606e-1	2.352e-1	8.263e-2	3.708e-1	4.591e-1	3.161e-1	4.132e-1	4.132e-1	4.132e-1	4.026e-1
45	2	9.288e-1	1.180	1.889	1.995	2.175	2.310	1.282	1.300	1.250	1.250	1.250	1.098
46	2-4	1.112e-1	1.112e-1	1.112e-1	1.112e-1	1.112e-1	1.112e-1	1.112e-1	1.112e-1	1.112e-1	1.112e-1	1.112e-1	1.112e-1
47	1-3	3.281e-1	3.637e-1	2.380e-1	2.013e-1	2.666e-1	3.708e-1	8.087e-2	0.0	0.0	0.0	0.0	0.0
49	3-5	3.884e-1	2.786e-1	1.427e-1	2.228e-1	2.786e-1	4.450e-1	3.779e-1	3.743e-1	3.341e-1	3.341e-1	3.341e-1	3.341e-1
50	2-4	0.0	0.0	1.865e-1	2.726e-1	3.334e-1	4.838e-1	4.167e-1	3.524e-1	3.531e-1	3.531e-1	3.531e-1	4.979e-1
52	2-3	2.228e-2	2.228e-2	2.228e-2	2.228e-2	2.228e-2	2.228e-2	2.228e-2	2.228e-2	2.228e-2	2.228e-2	2.228e-2	2.228e-2
53	1-4	8.898e-2	8.898e-2	8.898e-2	8.898e-2	8.898e-2	8.898e-2	8.898e-2	8.898e-2	8.898e-2	8.898e-2	8.898e-2	8.898e-2
55	1-3	8.334e-1	1.610e-1	0.0	0.0	0.0	0.0	0.0	0.0	0.0	0.0	0.0	0.0
56	1	1.338e-1	1.338e-1	1.338e-1	1.338e-1	1.338e-1	1.338e-1	1.338e-1	1.338e-1	1.338e-1	1.338e-1	1.338e-1	1.338e-1
57	1-3	1.338e-1	1.338e-1	1.338e-1	1.338e-1	1.338e-1	1.338e-1	1.338e-1	1.338e-1	1.338e-1	1.338e-1	1.338e-1	1.338e-1

Table 7. Ground-water well withdrawals for all simulated stress periods--Continued

WN	L	Q_1	Q_2	Q_3	Q_4	Q_5	Q_6	Q_7	Q_8	Q_9	Q_{10}	Q_{11}	Q_{12}
58	1-3	8.898e-2	8.898e-2	8.898e-2	8.898e-2	8.898e-2	8.898e-2	8.898e-2	8.898e-2	8.898e-2	8.898e-2	8.898e-2	8.898e-2
59	1-2	3.235e-1	3.637e-1	3.528e-1	2.285e-1	3.673e-1	3.221e-1	2.945e-1	2.829e-1	2.553e-1	2.553e-1	2.553e-1	2.468e-1
62	1-2	8.475e-2	8.475e-2	8.475e-2	8.475e-2	8.475e-2	8.475e-2	8.475e-2	8.475e-2	8.475e-2	8.475e-2	8.475e-2	8.475e-2
63	1-2	2.228e-1	2.228e-1	2.228e-1	2.228e-1	2.228e-1	2.228e-1	2.228e-1	2.228e-1	2.228e-1	2.228e-1	2.228e-1	2.228e-1
65	1-2	3.341e-1	3.341e-1	3.341e-1	3.341e-1	3.341e-1	3.341e-1	3.341e-1	3.341e-1	3.341e-1	3.341e-1	3.341e-1	3.341e-1
67	1-2	0.0	0.0	0.0	0.0	0.0	0.0	7.169e-1	1.434	1.571	1.571	1.571	1.158
68	1	3.340e-2	3.340e-2	3.340e-2	3.340e-2	3.340e-2	3.340e-2	3.340e-2	3.340e-2	3.340e-2	3.340e-2	3.340e-2	3.340e-2
69	2-3	0.0	0.0	0.0	0.0	0.0	0.0	6.498e-1	1.250	1.684	1.684	1.684	1.441
70	2-3	3.340e-2	3.340e-2	3.340e-2	3.340e-2	3.340e-2	3.340e-2	3.340e-2	3.340e-2	3.340e-2	3.340e-2	3.340e-2	3.340e-2
71	1-2	1.504	1.519	1.416	1.423	1.540	1.508	9.959e-1	7.981e-1	4.803e-1	4.803e-1	4.803e-1	1.095
72	1-2	0.0	0.0	0.0	0.0	0.0	2.493e-1	1.406	1.194	1.519	1.519	1.519	1.349
73	1	2.228e-2	2.228e-2	2.228e-2	2.228e-2	2.228e-2	2.228e-2	2.228e-2	2.228e-2	2.228e-2	2.228e-2	2.228e-2	2.228e-2
74	1-5	1.098	1.229	1.180	1.194	9.464e-1	1.342	1.402	1.324	1.342	1.342	1.342	1.257
75	1-2	1.367	1.448	9.570e-1	4.061e-1	5.262e-1	8.405e-1	9.252e-1	1.116	1.480	1.480	1.480	1.236
78	3	4.449e-2	4.449e-2	4.449e-2	4.449e-2	4.449e-2	4.449e-2	4.449e-2	4.449e-2	4.449e-2	4.449e-2	4.449e-2	4.449e-2
79	4	1.088	2.041	1.741	2.098	2.073	2.027	0.0	0.0	0.0	0.0	0.0	0.0
85	1-2	4.944e-1	1.334e-2	0.0	6.356e-2	0.0	0.0	0.0	0.0	0.0	0.0	0.0	0.0
86	1-4	6.780e-2	0.0	0.0	0.0	0.0	0.0	0.0	0.0	0.0	0.0	0.0	0.0
88	1-4	0.0	0.0	0.0	0.0	0.0	2.370e-1	4.344e-1	4.132e-1	3.920e-1	3.920e-1	3.920e-1	1.656e-1
89	1	4.449e-2	4.449e-2	4.449e-2	4.449e-2	4.449e-2	4.449e-2	4.449e-2	4.449e-2	4.449e-2	4.449e-2	4.449e-2	4.449e-2
90	1-3	6.533e-1	7.769e-1	7.028e-1	7.310e-1	6.498e-1	4.556e-1	0.0	0.0	0.0	0.0	0.0	0.0
92	1-3	1.112e-1	1.112e-1	1.112e-1	1.112e-1	1.112e-1	1.112e-1	1.112e-1	1.112e-1	1.112e-1	1.112e-1	1.112e-1	1.112e-1
95	1-3	1.112e-1	1.112e-1	1.112e-1	1.112e-1	1.112e-1	1.112e-1	1.112e-1	1.112e-1	1.112e-1	1.112e-1	1.112e-1	1.112e-1
98	1-3	1.112e-1	1.112e-1	1.112e-1	1.112e-1	1.112e-1	1.112e-1	1.112e-1	1.112e-1	1.112e-1	1.112e-1	1.112e-1	1.112e-1
101	1	0.0	0.0	0.0	0.0	0.0	0.0	0.0	0.0	0.0	1.914e-1	1.914e-1	1.914e-1
102	1-2	1.423e-1	1.992e-1	1.515e-1	1.963e-1	2.002e-1	1.910e-1	1.999e-1	1.699e-1	1.547e-1	1.547e-1	1.547e-1	1.201e-1
104	1-2	4.449e-2	4.449e-2	4.449e-2	4.449e-2	4.449e-2	4.449e-2	4.449e-2	4.449e-2	4.449e-2	4.449e-2	4.449e-2	4.449e-2
105	1	3.340e-2	3.340e-2	3.340e-2	3.340e-2	3.340e-2	3.340e-2	3.340e-2	3.340e-2	3.340e-2	0.0	0.0	0.0
106	1	1.003e-1	1.003e-1	1.003e-1	1.003e-1	1.003e-1	1.003e-1	1.003e-1	1.003e-1	1.003e-1	1.003e-1	1.003e-1	1.003e-1
107	1	3.855e-1	3.855e-1	3.855e-1	3.855e-1	4.139e-1	4.075e-1	3.638e-1	1.864e-1	4.455e-2	8.911e-2	8.911e-2	0.0
107	2	1.870e-1	1.870e-1	1.870e-1	1.870e-1	1.870e-1	2.000e-1	1.664e-1	3.390e-2	0.0	0.0	0.0	0.0
108	1	2.228e-2	2.228e-2	2.228e-2	0.0	0.0	0.0	0.0	0.0	0.0	0.0	0.0	0.0
109	1	1.003e-1	1.003e-1	1.003e-1	1.003e-1	1.003e-1	1.003e-1	1.003e-1	1.003e-1	1.003e-1	1.003e-1	1.003e-1	1.003e-1
111	1	1.112e-1	1.112e-1	1.112e-1	0.0	0.0	0.0	0.0	0.0	0.0	0.0	0.0	0.0
112	1	3.340e-2	3.340e-2	3.340e-2	0.0	0.0	0.0	0.0	0.0	0.0	0.0	0.0	0.0
114	1	2.228e-2	2.228e-2	2.228e-2	2.228e-2	2.228e-2	2.228e-2	2.228e-2	2.228e-2	2.228e-2	2.228e-2	2.228e-2	2.228e-2
TOT		24.89	20.45	19.82	17.71	18.65	20.28	20.02	20.61	19.68	19.88	19.88	19.01

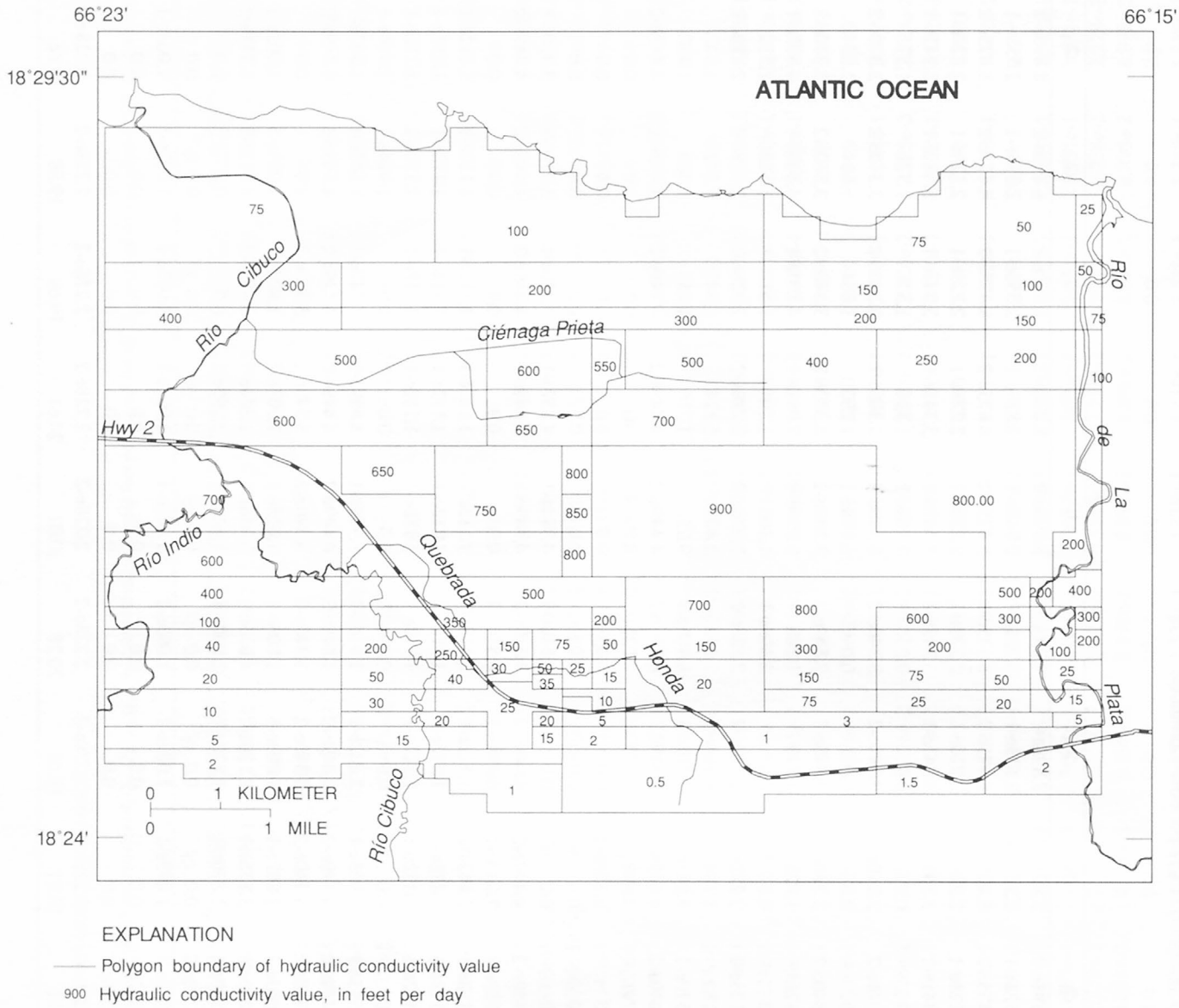

Figure 27. Calibrated hydraulic conductivity values for layer 1.

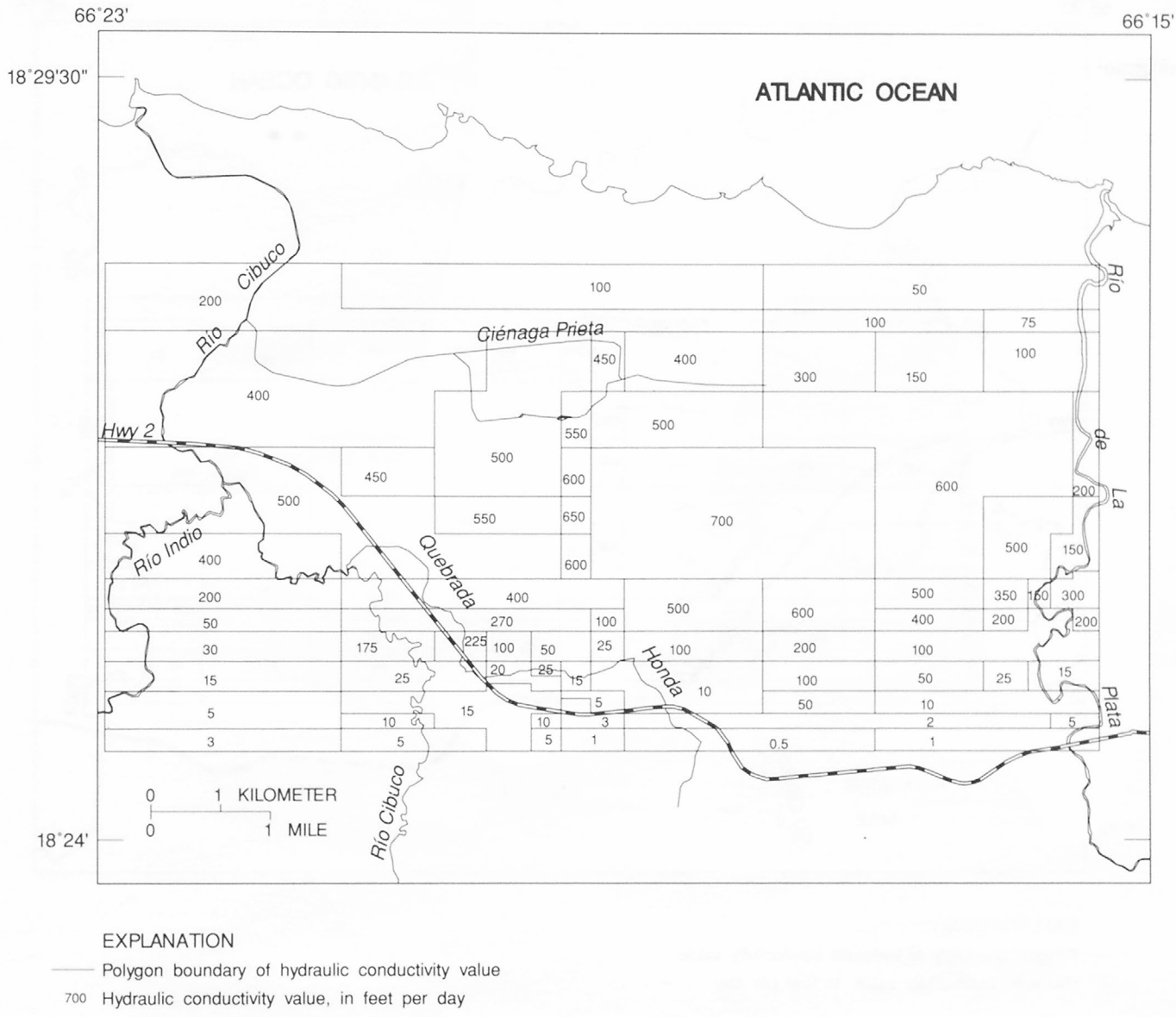

Figure 28. Calibrated hydraulic conductivity values for layer 2.

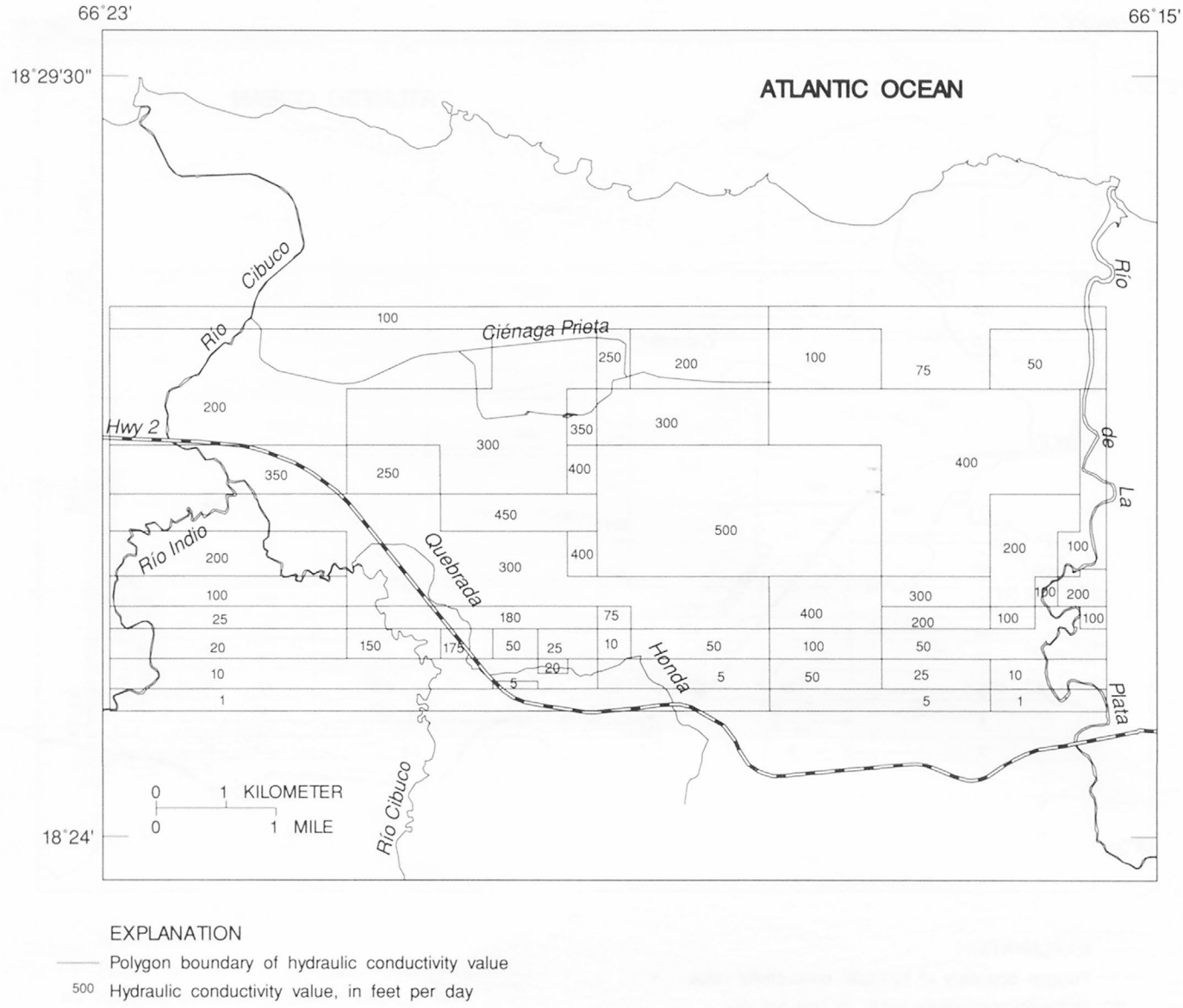

Figure 29. Calibrated hydraulic conductivity values for layer 3.

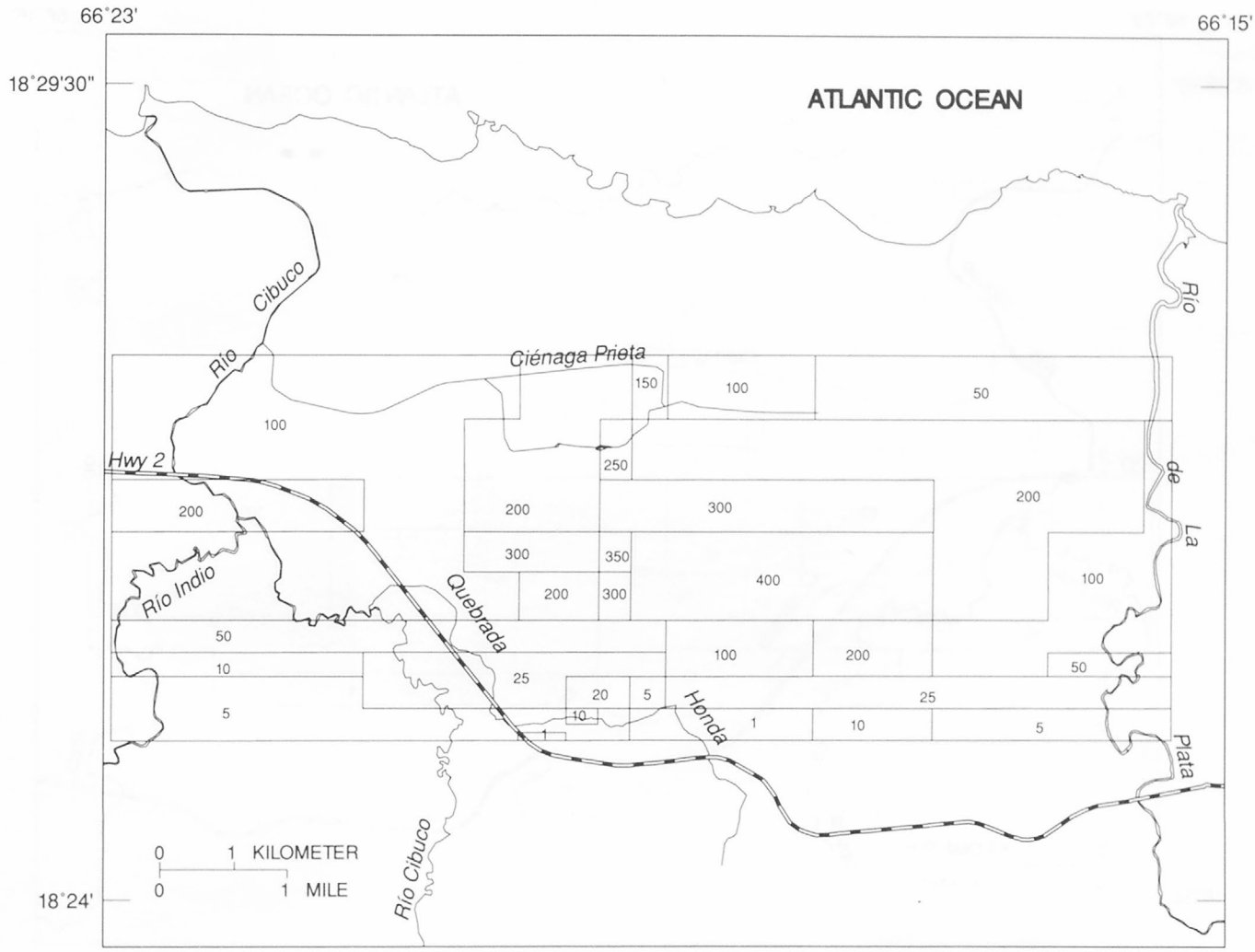

Figure 30. Calibrated hydraulic conductivity values for layer 4.

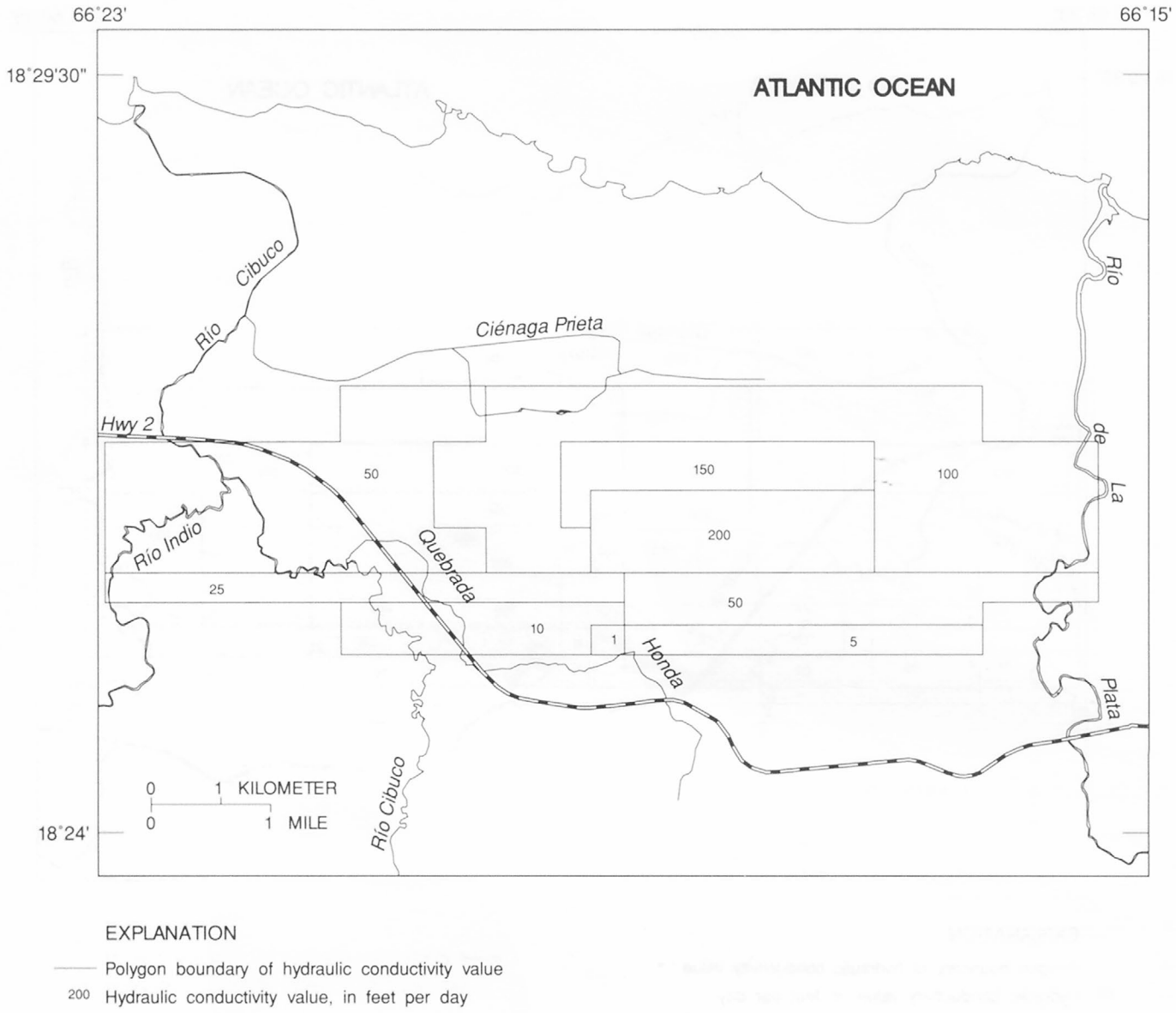

Figure 31. Calibrated hydraulic conductivity values for layer 5.

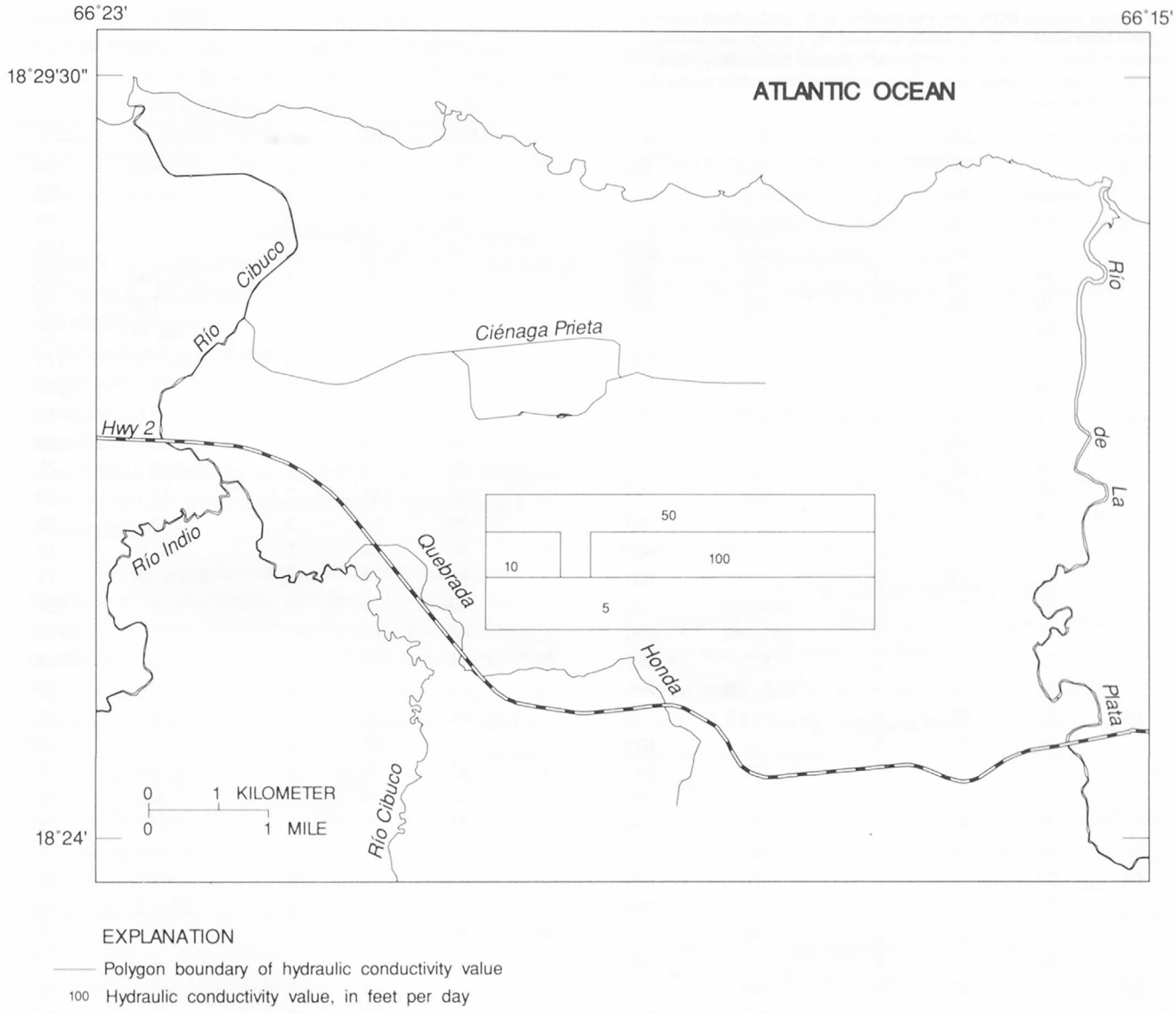

Figure 32. Calibrated hydraulic conductivity values for layer 6.

Table 8. List of average hydraulic conductivity values obtained from slug tests and calibrated values for all multiport wells in the aquifer

[WN, well number; ROW, grid row number; COL, grid column number; L, grid layer number; SL, hydraulic conductivity value (in feet per day) obtained from slug test; CAL, calibrated hydraulic conductivity value (in feet per day); multiple hydraulic conductivity zone values within the same layer are separated by commas]

WN	ROW	COL	L	SL	CAL
23	14	30	3	370	300
	14	30	1	620	600
40	19	20	5	160, 200	100
	19	20	4	200	200
	19	20	3	280	300
	19	20	2	490	500
	19	20	1	760	750
41	19	34	4	240	200
	19	34	3	390	300
	19	34	1	550, 830	750
43	19	47	5	520	150
	19	47	4	120	300
	19	47	3	340	500
	19	47	2	290	700
	19	47	1	790, 400	900
48	21	31	5	1.6	100
	21	31	4	290, 230	300
	21	31	3	380, 440	450
	21	31	2	510	550
	21	31	1	660, 720	750
61	28	32	6	1.2	10
	28	32	5	290	100
	28	32	4	130	200
	28	32	3	250	300
	28	32	2	250	500
	28	32	1	690	700
64	29	21	4	120	100
	29	21	3	130	300
	29	21	2	240	500
	29	21	1	960	700
66	29	42	6	230	100
	29	42	5	180	200
	29	42	4	90	400
	29	42	3	110	500
	29	42	2	320	700
	29	42	1	1,030	900
76	35	32	4	2.2	25
	35	32	3	170, 180	180
	35	32	2	270	270
	35	32	1	830	350
77	35	49	6	3.2	5
	35	49	5	300	50
	35	49	4	590	100
	35	49	2	610	500
	35	49	1	730, 820	700
80	38	30	4	150, 160	25
	38	30	3	9.4	50
	38	30	2	22	100
	38	30	1	240, 260	150
81	39	23	5	1.8	10
	39	23	4	80, 74	25
	39	23	3	140, 160	175
	39	23	1	180	250
82	39	33	5	0.6	10
	39	33	4	82	20
	39	33	3	240	25
	39	33	2	41	50
	39	33	1	210	75
84	40	14	5	1.6	10
	40	14	4	2, 0.5, 88	25
	40	14	3	120	150
	40	14	2	150	175
86	41	31	4	30	10
	41	31	3	120	20
	41	31	2	27	25
	41	31	1	200	50
87	41	39	3	16, 140	5
	41	39	2	8.6	10
	41	39	1	110	15
91	43	31	4	0.8	5
	43	31	3	15	10
	43	31	1	69, 0.2	35
94	44	29	4	3.8	1
	44	29	3	7	5
	44	29	2	5	15
	44	29	1	7.6	25
96	45	36	3	3	1
	45	36	2	4.8	5
	45	36	1	1.7, 50, 53	10
97	45	37	3	10	1
	45	37	2	4.6	5
	45	37	1	41	10
99	46	36	3	12	1
	46	36	2	2, 3.7	3
	46	36	1	2, 7.2	5
103	48	37	2	1.9, 1.2	3
	48	37	1	1.8, 11, 1.8	5
113	54	30	1	0.6, 0.7	1

the thickness of a layer in the model could lead to local responses in slug tests instead of more global responses from the entire thickness of the multiport zone. This sometimes results in an overestimation or underestimation of the appropriate K values for the layers in which the well is completed. The impact of local heterogeneities on well-aquifer responses obtained from slug tests tends to become smaller as the length of the screen opening increases because inertial effects increase as the screen opening increases.

The distribution of the calibrated K values for layers 2 to 6 is similar to the way values are distributed for layer 1. In general, the karst uplands plateau vicinity has the largest K values. These values decrease to the east, west, and north for the alluvial deposits and to the south for the less-dissolved limestone. Values were assigned to layer 6 to reflect that this layer simulates the beginning of a transition zone from the water-table aquifer to the underlying confined aquifer. This transition zone is characterized by a rather low permeability.

Vertical conductance values were assigned as a function of the hydraulic conductivity values for each layer. The vertical component of the hydraulic conductivity, K_z, assigned to cells in this model was one percent of its horizontal hydraulic conductivity value K for rows 1 to 40. The ratio of horizontal to vertical hydraulic conductivity assigned to cells in rows 41 to 44 was 20:1. The value of K_z for rows equal to or higher than 45 was 0.05 ft/d. If K_1 and K_2 are the vertical hydraulic conductivity values assigned to specific cells in layers 1 and 2, respectively, and b_1 and b_2 are the corresponding thicknesses of the cells, then the vertical conductance, V_c, between these cells is computed from the equation:

$$V_c = \frac{2K_1K_2}{K_1b_2 + K_2b_1}. \qquad (10)$$

There are areas, however, where hydraulic information is needed to avoid the need to incorporate tedious trial and error iterations into the calibration process. Examples of these areas are located to the east and northeast of the karst uplands plateau. Extrapolation was used to quantitatively describe the hydraulic flow in these areas. Future work in these areas could focus on measuring vertical gradients of water levels and hydraulic conductivity.

Ground-Water Flow Budget

The water budget sections from the output of MODFLOW include the estimation of inflows, outflows, and changes in ground-water storage. The continuity equation establishes that inflows are equal to outflows, plus changes in storage for the water-table aquifer. The discrepancy among inflows, outflows, and changes in storage varies from one stress period to another and reflects the accuracy of the strongly implicit procedure used to solve the system of equations resulting from the application of the finite-difference technique to equation (7). Total volumetric flow rates at the end of each of the 12 stress periods contained in this transient simulation are listed in table 9.

For example, for stress period 12, the discrepancy among inflows, outflows, and changes in storage was -0.18 percent. Inflows to the modeling area, in units of ft^3/s, for stress period 12 include storage (2.6123e+5), constant head cells along the Atlantic Ocean coast (198), recharge from rainfall (1.6854e+6), seepage from rivers (1.3592e+5), and head-dependent boundaries (1.7094e+5). Total inflows for this stress period are 2.2537e+6. Constant head cell inflows from freshwater equivalent heads are the volumes of water needed for a balance of pressures as the moving freshwater/saltwater interface reaches equilibrium conditions.

Outflows from the modeling area, in units of ft^3/s, for stress period 12 include storage (9,484), freshwater outflow at the Atlantic Ocean coast boundary (2.5618e+5), pumping wells (1.6450e+6), seepage to rivers (86,559), and head-dependent boundaries (2.6042e+5). Total outflows for this stress period are 2.2577e+6. A breakdown of the flow budget by layer indicates that the flow to constant heads occurs in layer 1, a result that is consistent with the conceptualization of the system.

Table 9. Volumetric flow rates at the end of each stress period

[SP, stress period number; IN and OUT, volumetric inflow and outflow rates to the aquifer in cubic feet per day; ST, flow due to aquifer storage changes; CH, flow through constant head cells; WE, flow from wells; RE, flow due to aquifer recharge; RL, flow due to aquifer interactions with river reach cells; HD, flow through head dependent boundaries; TOT, total flows in or out of the aquifer; PD, percent discrepancy between total inflows and total outflows]

SP		ST	CH	WE	RE	RL	HD	TOT	PD
1	IN	23,668	0	0	2.4365e+6	1.4319e+5	2.7840e+5	2.8818e+6	
1	OUT	47,691	2.9175e+5	2.1509e+6	0	91,561	2.9791e+5	2.8798e+6	0.07
2	IN	0	0	0	2.4513e+6	1.3650e+5	1.0424e+5	2.6920e+6	
2	OUT	31,437	3.1187e+5	1.7667e+6	0	1.4557e+5	4.1326e+5	2.6689e+6	0.86
3	IN	0	0	0	3.0112e+6	1.2922e+5	56,349	3.1968e+6	
3	OUT	1.0976e+5	3.9084e+5	1.7125e+6	0	2.8325e+5	6.9509e+5	3.1914e+6	0.17
4	IN	12,490	0	0	2.7202e+6	1.2602e+5	55,433	2.9142e+6	
4	OUT	1,736	3.8339e+5	1.5299e+6	0	2.7813e+5	7.2762e+5	2.9208e+6	-0.23
5	IN	0	0	0	3.3205e+6	1.1859e+5	38,497	3.4776e+6	
5	OUT	86,680	4.4544e+5	1.6118e+6	0	3.8702e+5	9.4272e+5	3.4737e+6	0.11
6	IN	53,176	0	0	2.9972e+6	1.2367e+5	51,784	3.2258e+6	
6	OUT	0	4.0884e+5	1.7519e+6	0	3.1824e+5	7.5449e+5	3.2335e+6	-0.24
7	IN	16,684	0	0	2.9189e+6	1.1716e+5	66,068	3.1188e+6	
7	OUT	476	3.8386e+5	1.7300e+6	0	3.0621e+5	7.1307e+5	3.1337e+6	-0.47
8	IN	33,699	0	0	2.7625e+6	1.1874e+5	86,996	3.0019e+6	
8	OUT	41	3.5916e+5	1.7806e+6	0	2.6921e+5	5.9682e+5	3.0058e+6	-0.13
9	IN	1.8687e+5	0	0	2.3348e+6	1.2283e+5	1.0289e+5	2.7474e+6	
9	OUT	0	3.2966e+5	1.7003e+6	0	2.1741e+5	5.0295e+5	2.7503e+6	-0.11
10	IN	4.4529e+5	0	0	1.7717e+6	1.2952e+5	1.4119e+5	2.4877e+6	
10	OUT	2,549	2.8872e+5	1.7207e+6	0	1.3957e+5	3.4144e+5	2.4929e+6	-0.21
11	IN	1,838	0	0	2.3115e+6	1.2788e+5	1.3813e+5	2.5794e+6	
11	OUT	28,325	2.9640e+5	1.7207e+6	0	1.5387e+5	3.6909e+5	2.5683e+6	0.43
12	IN	2.6123e+5	198	0	1.6854e+6	1.3592e+5	1.7094e+5	2.2537e+6	
12	OUT	9,484	2.5618e+5	1.6450e+6	0	86,559	2.6042e+5	2.2577e+6	-0.18

SIMULATED WATER-LEVEL CONTOURS

Several key elements are important in the performance evaluation of a ground-water flow model. These elements include the ability of the flow model to simulate water-level variations for both dry and wet periods, near river reach cells, and areas of steep hydraulic gradients. Other important derivates of a flow model include flow-budget estimation, determination of aquifer-river flow directions, and an assessment of the impact on water levels due to ground-water withdrawals.

The simulated water-level contours corresponding to 1, 2, 3, 4, 5, 6, 7, 8, 9, 10, 20, 25, 50, and 100 ft above mean sea level at the end of stress period 8 (January 15, 1991) are shown in figure 33. Water-level contours at the end of stress periods 9, 10, 11, and 12 are shown in figures 34–37. Only the simulated water-level contours from stress periods 8 through 12 are presented in this study because measured water levels were available only at these times. The measured and simulated water levels for each one of the last five stress periods are listed in table 10. Simulated water-level contours shown in figures 33–37 were generated using water levels from MODFLOW output as input data for the linear option of ARCTIN (ARC/INFO, 1992) to generate the TIN coverage. The extent of the simulated water-level contours for 50 and 100 feet shown in these figures is limited by no-flow boundary cells.

Simulated water-level contours of 1 to 4 ft near the coastal plain were generally equally spaced from one another (figs. 33–37). The errors between these simulated contours and the measured water levels are minimal. Measured water levels just west of the Río de La Plata indicate a decreasing hydraulic gradient with decreasing distance from the river boundary. Simulated contours reflect regional drawdowns caused by large ground-water withdrawal volumes from the Maguayo wells (wells 67, 69, 71, 72, 74, and 75) and from the San Antonio wells (wells 27, 36, and 38). In general, simulated water levels are lower than measured for the San Antonio and Maguayo well areas. The opposite occurs for the uplands karst plateau area, where the simulated water levels are slightly higher than measured water levels (figs. 33–37). The largest error between the measured and the simulated water levels in the Quebrada Honda karst valley and southern karst uplands areas was less than 5 ft. This error is mainly due to the fact that rainfall recharge from the outcrop creates large vertical hydraulic gradients around the Quebrada Honda karst valley water levels in the third and fourth layers of the model. Being able to simulate ground-water flow with reasonable accuracy in the Quebrada Honda karst valley is of particular importance because this is the area where the ground water contains high TCE concentrations (Geraghty & Miller, 1992). Future applications of this model depend on its ability to accurately describe the hydraulic behavior for this area.

Sensitivity Analysis

The overall performance of a ground-water flow model can be better analyzed through a sensitivity analysis. Increments and decrements of 10 and 25 percent were applied to values of hydraulic conductivity, rainfall recharge, well withdrawals, specific yield, both general-head boundary conductance areas, riverbed conductances of all five rivers in the simulation area, and anisotropy. The root mean square error *(RMSE)* is used as the overall criterion for determining if the hydraulic variable in question should be decreased or increased. If N is the total number of measured water-level values, h_{oi} are the measured water levels, and the simulated water-level values are denoted by h_{si}, then the *RMSE* is computed from the equation:

$$RMSE = \sqrt{\frac{1}{N}\sum_{i=1}^{N}(h_{oi} - h_{si})^2}. \qquad (11)$$

The values of N for stress periods 8 through 12 are 125, 121, 118, 119, and 118, respectively, as shown at the end of table 10. Table 11 lists the overall *RMSE* for stress periods 8 through 12 for all variable changes listed above.

The sensitivity analysis indicates that the model is most sensitive to changes in hydraulic conductivity values, rainfall recharge, anisotropy ratio, and well withdrawals and least sensitive to changes in specific yield, riverbed conductance values, and conductance and boundary-value heads used for general-head boundaries. The general-head boundaries assumed at the eastern and western boundaries of the study area were tested for changes in assumed water level and conductance values and showed small changes from one applied change to another, indicating stability with respect to these general-head boundaries.

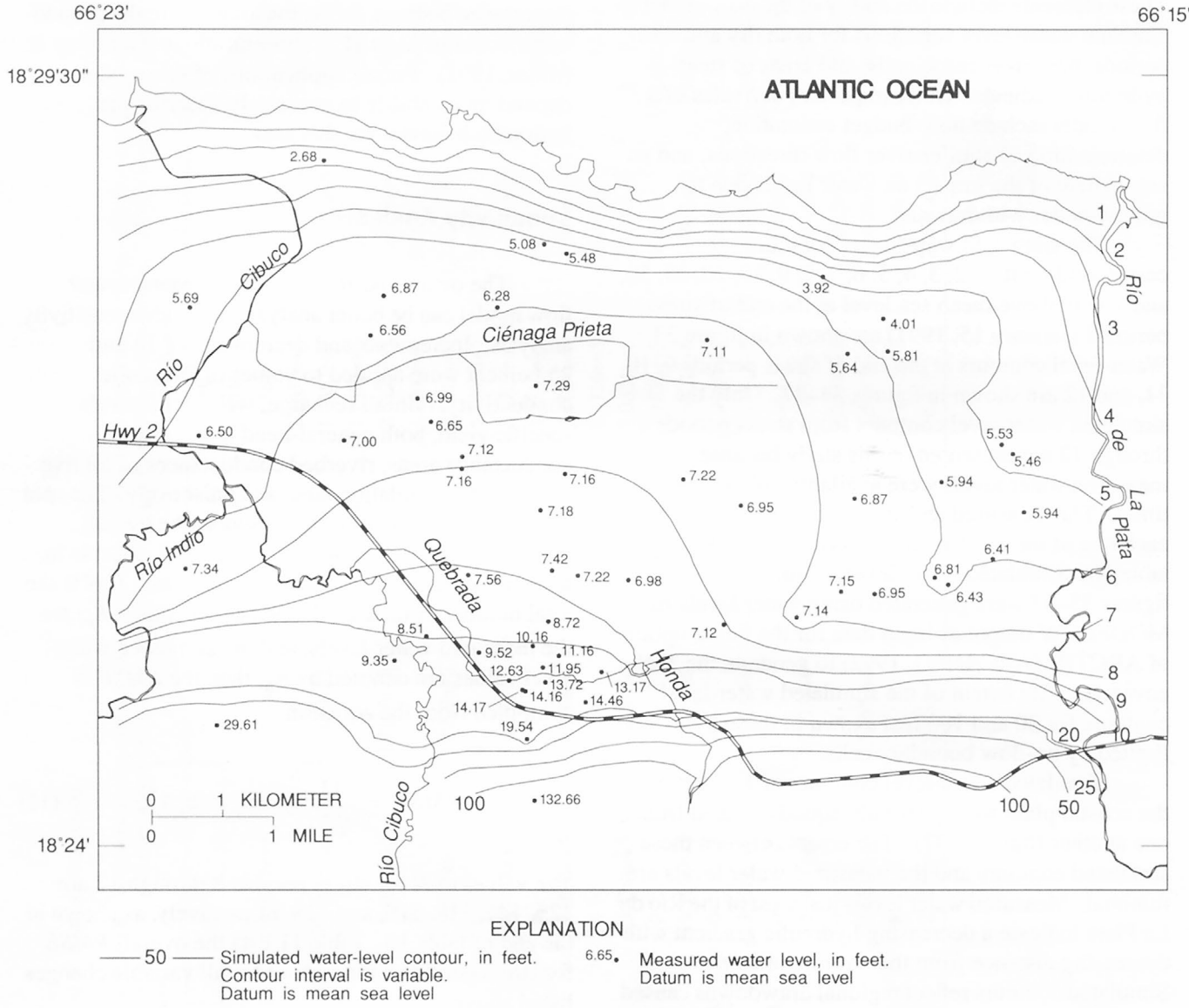

Figure 33. Simulated water-level contours and measured water levels, January 1991.

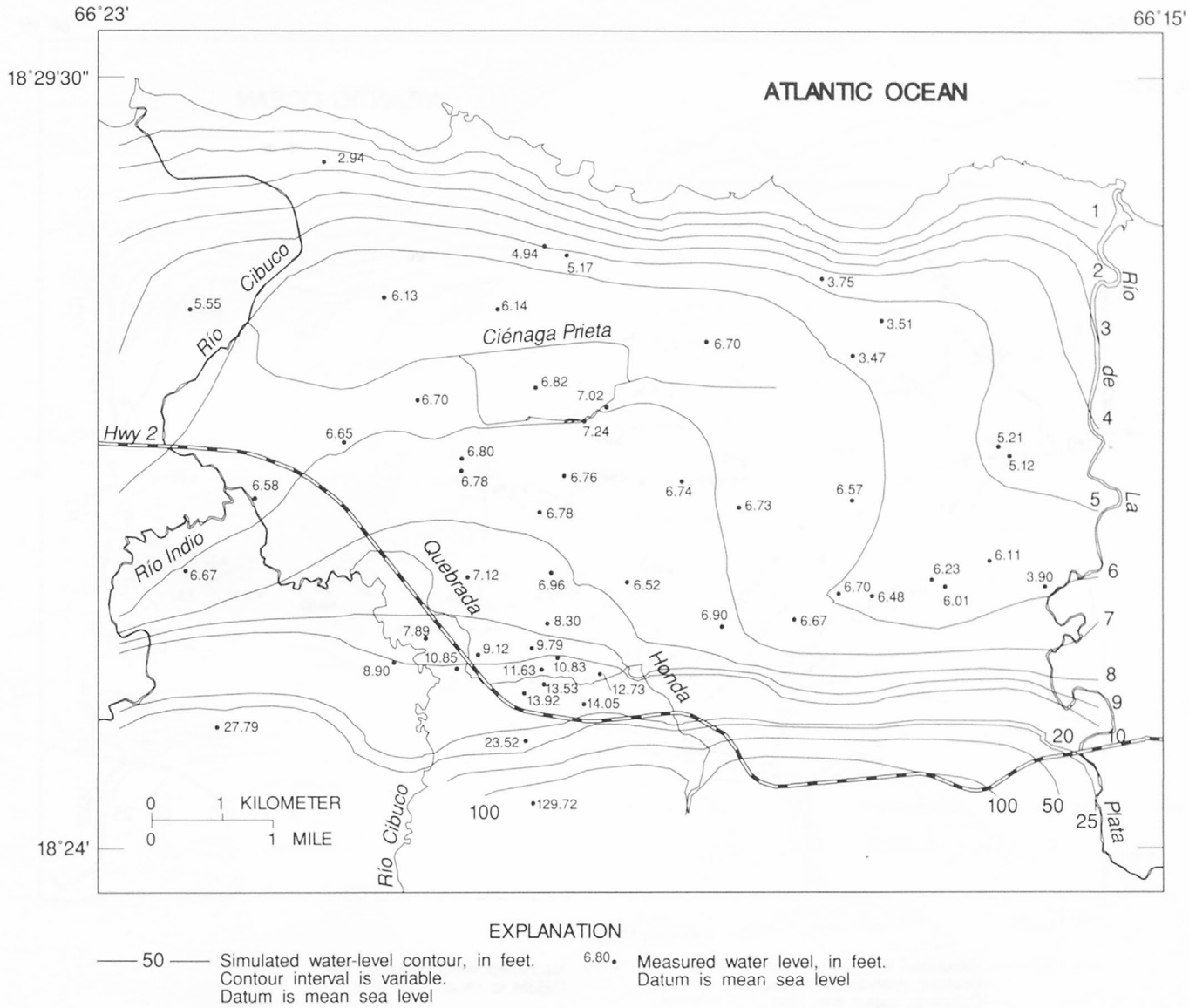

Figure 34. Simulated water-level contours and measured water levels, May 1991.

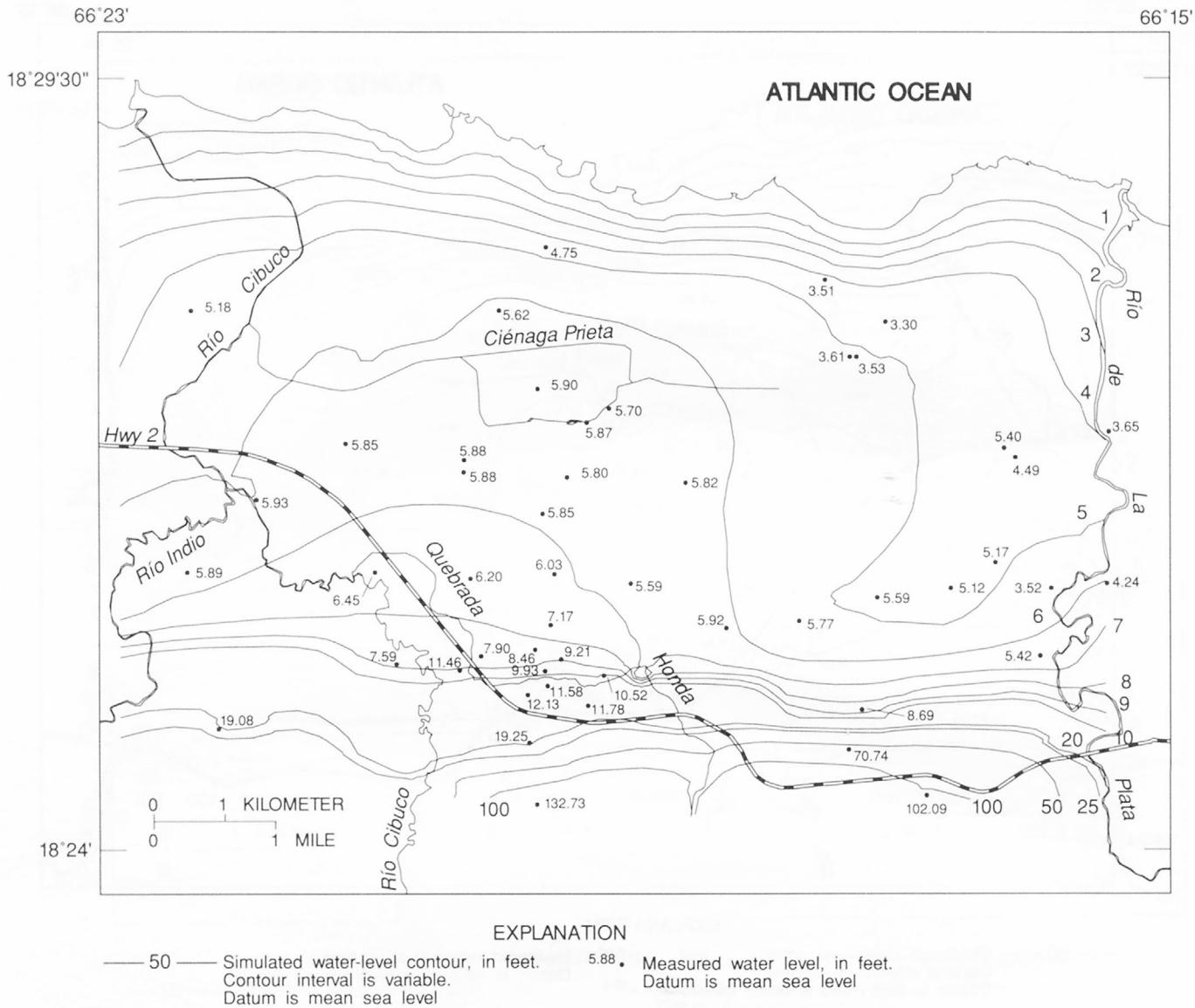

EXPLANATION

—— 50 —— Simulated water-level contour, in feet. Contour interval is variable. Datum is mean sea level

5.88 • Measured water level, in feet. Datum is mean sea level

Figure 35. Simulated water-level contours and measured water levels, August 1991.

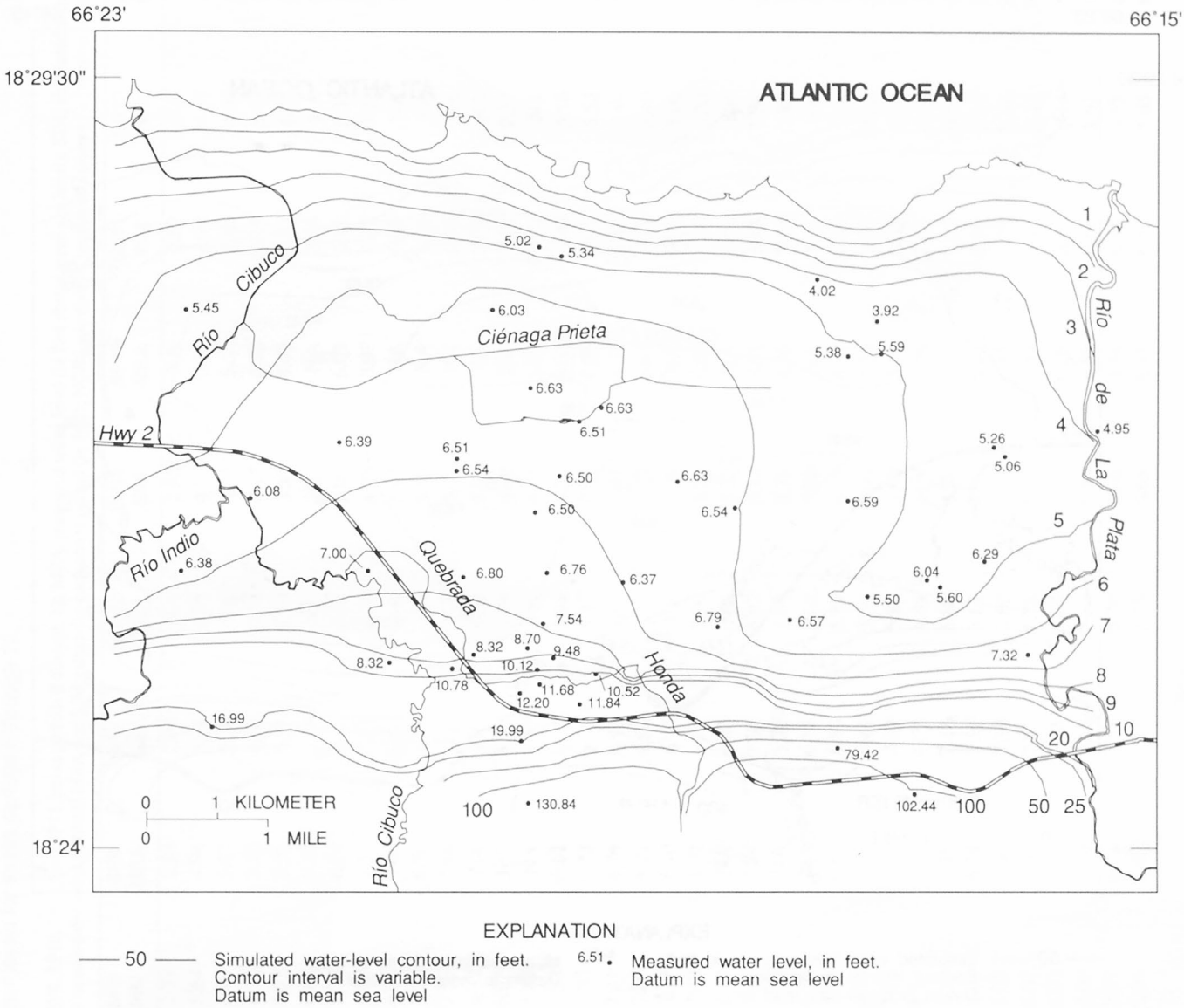

Figure 36. Simulated water-level contours and measured water levels, January 1992.

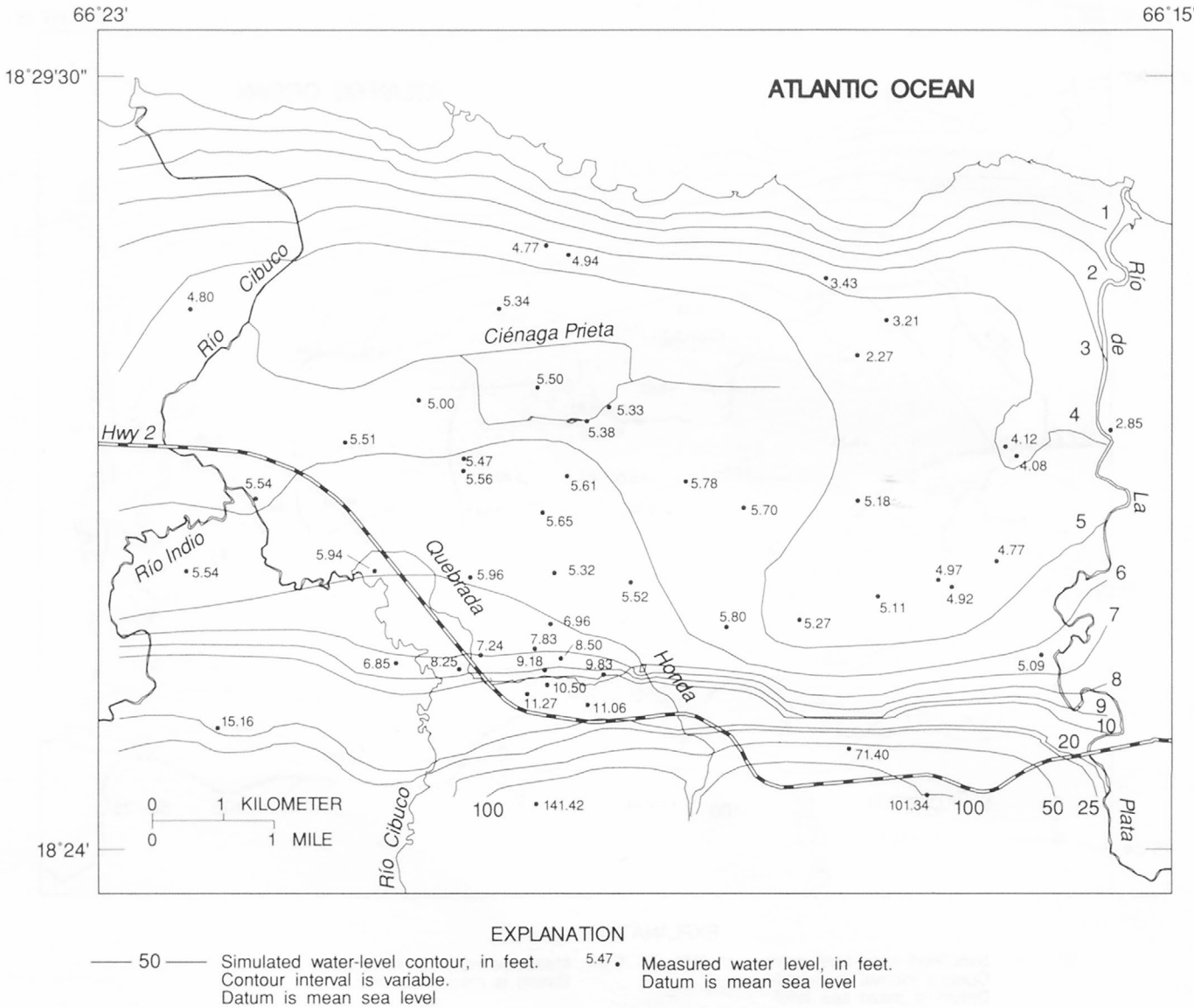

Figure 37. Simulated water-level contours and measured water levels, April 1992.

Table 10. Measured and simulated water levels for stress periods 8 through 12

[WN, well number; L, grid layer number; SP8, SP9, SP10, SP11, and SP12, stress periods 8 through 12; MEA, measured water level (in feet above mean sea level); SIM, simulated water level (in feet); NA, water level not available; RMSE, root mean square error between MEA and SIM values for each stress period (in feet); NOBS, number of measured values as a function of stress period]

WN	L	SP8 MEA	SP8 SIM	SP9 MEA	SP9 SIM	SP10 MEA	SP10 SIM	SP11 MEA	SP11 SIM	SP12 MEA	SP12 SIM
2	1	2.68	2.79	2.94	2.68	NA	2.55	NA	2.59	NA	2.45
3	1	5.08	5.64	4.94	5.34	4.75	4.89	5.02	4.92	4.77	4.49
4	1	5.48	5.49	5.17	5.20	NA	4.77	5.34	4.80	4.94	4.39
6	1	3.92	4.90	3.75	4.62	3.51	4.15	4.02	4.18	3.43	3.78
7	1	5.69	5.72	5.55	5.57	5.18	5.35	5.45	5.37	4.80	5.16
8	1	6.87	6.82	6.13	6.44	NA	5.88	NA	5.98	NA	5.40
12	1	6.28	6.78	6.14	6.61	5.62	6.02	6.03	6.11	5.34	5.53
16	2	4.01	5.69	3.51	5.43	3.30	4.78	3.92	4.82	3.21	4.31
18	1	6.56	6.87	NA	6.50	NA	5.93	NA	6.05	NA	5.46
19	1	7.11	7.17	6.70	6.68	NA	5.93	NA	6.03	NA	5.39
19	2	7.07	7.16	6.68	6.68	NA	5.92	NA	6.02	NA	5.39
20	2	5.64	6.12	NA	5.77	3.61	5.02	NA	5.08	NA	4.52
21	1	NA	6.03	3.47	5.72	3.53	4.99	5.38	5.04	2.27	4.50
22	1	5.81	5.83	NA	5.57	NA	4.87	5.59	4.90	NA	4.38
23	1	7.29	7.33	6.82	6.92	5.90	6.27	6.63	6.40	5.50	5.80
23	2	7.24	7.33	6.78	6.92	5.88	6.27	6.59	6.40	5.52	5.80
23	3	7.17	7.34	6.74	6.92	5.82	6.27	6.52	6.40	5.49	5.80
23	4	7.12	7.34	6.71	6.92	5.79	6.27	6.41	6.40	5.49	5.80
25	1	6.99	7.17	6.70	6.75	NA	6.09	NA	6.25	5.00	5.46
26	1	NA	7.40	7.02	6.95	5.70	6.26	6.63	6.39	5.33	5.80
29	2	6.65	6.44	NA	6.03	NA	5.35	NA	5.52	NA	4.78
30	1	NA	7.46	7.24	7.01	5.87	6.33	6.51	6.47	5.38	5.87
32	1	NA	3.94	NA	3.91	3.65	3.78	4.95	3.76	2.85	3.71
33	1	6.50	6.33	NA	6.15	NA	5.86	NA	5.93	NA	5.67
34	1	7.00	7.18	6.65	6.80	5.85	6.19	6.39	6.35	5.51	5.73
36	1	5.53	4.50	5.21	4.44	5.40	3.94	5.26	3.90	4.12	3.73
37	1	7.12	7.88	6.80	7.39	5.88	6.62	6.51	6.83	5.47	6.08
38	1	5.46	4.70	5.12	4.59	4.49	4.08	5.06	4.04	4.08	3.86
40	1	7.16	8.10	6.78	7.58	5.88	6.78	6.54	7.00	5.56	6.23
40	2	7.15	8.09	6.74	7.57	5.86	6.77	6.45	6.99	5.41	6.22
40	3	7.08	8.07	6.69	7.56	5.80	6.76	6.39	6.98	5.46	6.21
40	4	7.06	8.07	6.67	7.55	5.78	6.76	6.32	6.97	5.44	6.21
40	5	7.01	8.07	6.62	7.55	5.76	6.75	6.28	6.97	5.44	6.21
41	1	7.16	8.09	6.76	7.53	5.80	6.68	6.50	6.89	5.61	6.13
41	2	7.13	8.07	6.71	7.52	5.78	6.66	6.44	6.87	5.65	6.12
41	3	7.13	8.06	6.69	7.51	5.76	6.65	6.43	6.86	5.65	6.11

Table 10. Measured and simulated water levels for stress periods 8 through 12--Continued

WN	L	SP8 MEA	SP8 SIM	SP9 MEA	SP9 SIM	SP10 MEA	SP10 SIM	SP11 MEA	SP11 SIM	SP12 MEA	SP12 SIM
41	4	7.10	8.05	6.62	7.50	5.75	6.65	6.40	6.85	5.64	6.11
41	5	7.06	8.05	6.58	7.49	5.71	6.64	6.34	6.85	5.67	6.10
43	1	7.22	7.74	6.74	7.14	5.82	6.20	6.63	6.38	5.78	5.62
43	2	7.18	7.72	6.66	7.12	5.80	6.18	6.56	6.36	5.76	5.60
43	3	7.16	7.71	6.62	7.10	5.76	6.17	6.50	6.35	5.76	5.59
43	4	7.12	7.70	6.63	7.10	5.73	6.17	6.48	6.34	5.74	5.59
44	1	5.94	5.70	NA	5.40	NA	4.71	NA	4.68	NA	4.35
45	2	NA	6.25	6.58	5.98	5.93	5.52	6.08	5.64	5.54	5.31
48	1	7.18	8.38	6.78	7.79	5.85	6.89	6.50	7.13	5.65	6.32
48	2	7.19	8.36	6.74	7.78	5.84	6.88	6.48	7.11	5.62	6.31
48	3	7.18	8.35	6.73	7.77	5.83	6.87	6.46	7.10	5.60	6.31
48	4	7.14	8.35	6.69	7.77	5.80	6.86	6.44	7.10	5.68	6.30
48	5	7.12	8.34	6.65	7.76	5.79	6.86	6.37	7.09	5.68	6.30
50	3	6.95	7.21	6.73	6.60	NA	5.63	6.54	5.79	5.70	4.99
51	1	6.87	6.70	6.57	6.18	NA	5.30	6.59	5.34	5.18	4.80
52	1	5.94	5.38	NA	5.17	NA	4.70	NA	4.67	NA	4.50
58	1	6.41	6.00	6.11	5.52	5.17	4.85	6.29	4.83	4.77	4.60
59	1	7.34	7.40	6.67	7.13	5.89	6.69	6.38	6.84	5.54	6.43
60	3	NA	8.91	NA	8.38	6.45	7.52	7.00	7.74	5.94	6.96
61	1	7.42	8.81	6.96	8.19	6.03	7.18	6.76	7.43	5.32	6.58
61	2	7.46	8.79	7.01	8.17	6.10	7.16	6.83	7.42	5.42	6.57
61	3	7.50	8.77	7.03	8.15	6.13	7.15	6.82	7.40	5.43	6.56
61	4	7.67	8.74	7.20	8.13	6.24	7.13	6.76	7.37	5.42	6.54
61	5	7.93	8.72	7.47	8.11	6.48	7.11	7.01	7.36	5.81	6.52
61	6	7.94	8.69	7.49	8.08	6.50	7.09	6.98	7.33	5.80	6.50
64	1	7.56	9.11	7.12	8.53	6.20	7.56	6.80	7.81	5.96	6.96
64	2	7.46	9.10	7.06	8.52	6.16	7.55	6.76	7.80	5.98	6.95
64	3	7.47	9.09	7.01	8.51	6.13	7.54	6.74	7.79	5.93	6.95
64	4	7.60	9.06	7.18	8.48	6.30	7.51	6.83	7.76	6.14	6.92
64	5	7.88	9.03	7.44	8.46	6.50	7.50	7.02	7.74	6.34	6.90
65	1	7.22	8.52	NA	7.88	NA	6.85	NA	7.09	NA	6.25
66	1	6.98	8.45	6.52	7.79	5.59	6.75	6.37	6.98	5.52	6.17
66	2	6.94	8.43	6.48	7.77	5.54	6.73	6.30	6.96	5.52	6.15
66	3	6.94	8.41	6.48	7.75	5.53	6.72	6.33	6.95	5.55	6.14
66	4	7.38	8.37	6.90	7.72	5.89	6.69	6.66	6.92	5.96	6.11
66	5	7.80	8.35	7.36	7.70	6.23	6.68	6.84	6.90	6.26	6.10

Table 10. Measured and simulated water levels for stress periods 8 through 12--Continued

WN	L	SP8 MEA	SP8 SIM	SP9 MEA	SP9 SIM	SP10 MEA	SP10 SIM	SP11 MEA	SP11 SIM	SP12 MEA	SP12 SIM
66	6	7.97	8.32	7.50	7.67	6.37	6.66	6.93	6.88	6.50	6.07
67	1	6.81	5.57	6.23	4.82	NA	4.00	6.04	4.01	4.97	3.87
68	1	NA	6.07	NA	6.05	4.24	6.00	NA	6.00	NA	5.99
69	1	6.43	5.72	6.01	4.95	5.12	4.13	5.60	4.14	4.92	3.96
70	1	NA	6.12	3.90	5.86	3.52	5.46	NA	5.45	NA	5.30
71	1	7.15	6.46	6.70	5.86	NA	4.85	NA	4.93	NA	3.99
72	1	6.95	6.20	6.48	5.35	5.59	4.39	5.50	4.44	5.11	3.95
75	1	7.14	6.56	6.67	5.57	5.77	4.48	6.57	4.61	5.27	4.02
76	1	8.72	9.40	8.30	8.80	7.17	7.70	7.54	7.95	6.96	7.10
76	2	8.66	9.36	8.25	8.75	7.14	7.67	7.54	7.92	6.95	7.07
76	3	8.68	9.33	8.22	8.73	7.17	7.65	7.56	7.89	6.98	7.05
76	4	9.65	9.34	9.16	8.75	7.94	7.67	8.23	7.91	7.66	7.08
77	1	7.12	8.06	6.90	7.31	5.92	6.19	6.79	6.39	5.80	5.60
77	2	7.19	8.03	6.92	7.29	5.92	6.17	6.80	6.36	5.72	5.59
77	3	7.20	8.01	6.90	7.26	5.92	6.15	6.79	6.34	5.78	5.57
77	4	7.80	7.98	7.49	7.24	6.35	6.14	7.14	6.33	6.33	5.55
77	5	7.92	7.96	7.62	7.22	6.47	6.12	7.20	6.30	6.40	5.54
77	6	7.97	7.91	7.60	7.17	6.46	6.08	7.16	6.27	6.53	5.50
79	4	8.51	9.99	7.89	9.40	NA	8.34	NA	8.59	NA	7.69
80	1	10.16	10.13	9.79	9.58	8.46	8.43	8.70	8.68	7.83	7.85
80	2	10.25	10.07	9.84	9.52	8.54	8.38	8.76	8.63	8.02	7.80
80	3	10.24	10.02	9.88	9.47	8.55	8.34	8.82	8.59	8.00	7.77
80	4	10.30	10.01	9.84	9.46	8.53	8.34	8.81	8.58	8.08	7.77
81	1	9.52	10.30	9.12	9.74	7.90	8.63	8.32	8.88	7.24	8.01
81	2	9.42	10.25	9.03	9.68	7.84	8.58	8.28	8.83	7.14	7.97
81	3	9.34	10.21	8.96	9.64	7.78	8.54	8.24	8.79	7.13	7.93
81	4	9.08	10.20	8.66	9.63	7.55	8.53	8.06	8.78	6.94	7.92
81	5	9.14	10.14	8.69	9.57	7.56	8.48	8.07	8.73	7.07	7.87
82	1	11.16	10.56	10.83	10.04	9.21	8.84	9.48	9.07	8.50	8.29
82	2	10.82	10.46	10.47	9.93	8.93	8.75	9.26	8.98	8.54	8.21
82	3	10.75	10.40	10.35	9.88	8.84	8.70	9.12	8.93	8.29	8.17
82	4	10.70	10.32	10.29	9.79	8.75	8.62	9.04	8.85	8.26	8.09
82	5	10.87	10.17	10.56	9.63	8.90	8.48	9.14	8.71	8.34	7.94
83	1	NA	7.68	NA	7.19	5.42	6.54	7.32	6.57	5.09	6.25
84	2	9.35	10.58	8.90	9.94	7.59	8.79	8.32	9.05	6.85	8.08
84	3	9.13	10.49	8.68	9.86	7.44	8.73	8.01	8.98	6.75	8.02

Table 10. Measured and simulated water levels for stress periods 8 through 12--Continued

WN	L	SP8 MEA	SP8 SIM	SP9 MEA	SP9 SIM	SP10 MEA	SP10 SIM	SP11 MEA	SP11 SIM	SP12 MEA	SP12 SIM
84	4	9.28	10.51	8.82	9.87	7.58	8.74	7.98	8.99	6.96	8.03
84	5	9.54	10.39	9.27	9.76	7.75	8.64	8.07	8.90	7.12	7.95
85	2	NA	10.94	10.85	10.36	11.46	9.19	10.78	9.47	8.25	8.56
86	1	11.95	11.43	11.63	11.02	9.93	9.76	10.12	9.99	9.18	9.29
86	2	12.02	11.33	11.75	10.91	10.07	9.66	10.19	9.89	9.35	9.19
86	3	11.70	11.27	11.43	10.85	9.75	9.60	9.88	9.83	9.08	9.13
86	4	11.84	11.19	11.57	10.77	9.88	9.53	9.96	9.76	9.22	9.06
87	1	13.17	11.44	12.73	10.85	10.52	9.58	10.52	9.77	9.83	9.22
87	2	12.90	11.34	12.50	10.75	10.33	9.49	10.30	9.68	9.75	9.14
87	3	12.19	11.27	11.88	10.69	9.86	9.43	9.98	9.62	9.24	9.08
87	4	11.42	11.15	11.97	10.57	9.96	9.32	9.88	9.51	9.39	8.96
90	1	12.63	12.18	NA	11.96	NA	10.56	NA	10.83	NA	10.22
91	1	13.72	12.63	13.53	12.44	11.58	11.05	11.68	11.28	10.50	10.77
91	2	13.53	12.53	13.23	12.33	11.43	10.95	11.50	11.18	10.47	10.66
91	3	13.27	12.40	12.90	12.18	11.22	10.81	11.22	11.04	10.34	10.50
91	4	13.67	12.30	13.37	12.06	11.64	10.70	11.56	10.93	10.77	10.38
93	1	14.17	12.57	NA	12.57	NA	11.04	NA	11.31	NA	10.88
94	1	14.16	12.64	13.92	12.66	12.13	11.14	12.20	11.39	11.27	11.00
94	2	14.16	12.51	13.90	12.50	12.13	11.01	12.23	11.27	11.37	10.86
94	3	14.54	12.40	14.23	12.34	12.58	10.88	12.60	11.13	12.14	10.68
94	4	15.03	12.30	14.69	12.18	13.09	10.75	13.05	11.00	12.47	10.51
97	1	14.46	15.61	14.05	15.16	11.78	13.66	11.84	13.82	11.06	13.32
97	2	18.06	15.23	18.07	14.78	15.20	13.31	14.90	13.49	14.36	13.02
97	3	20.40	15.11	20.33	14.66	17.02	13.20	16.40	13.39	15.90	12.92
100	1	NA	11.93	NA	10.51	8.69	8.78	NA	9.35	NA	8.06
102	1	29.61	28.77	27.79	27.79	19.08	18.26	16.99	17.33	15.16	15.38
107	1	NA	18.07	NA	22.19	19.25	19.43	19.99	19.72	NA	22.44
107	2	19.54	18.31	23.52	21.61	NA	19.47	NA	19.78	NA	21.15
110	1	NA	91.84	NA	81.61	70.74	71.57	79.42	78.33	71.40	71.67
113	1	132.66	132.59	129.72	129.30	132.73	132.82	130.84	131.71	141.42	141.57
114	1	NA	124.23	NA	118.27	102.09	103.44	102.44	102.74	101.34	100.72
RMSE			1.08		1.11		0.98		0.79		0.78
NOBS			125		121		118		119		118

Table 11. Sensitivity analysis based on root mean square error

[RMSE8 through RMSE12, root mean square error values for stress periods 8 through 12 (in feet); *K*, hydraulic conductivity; R, recharge; *Q*, ground-water well withdrawal rate; *S*, specific yield; CON and BHV, conductance and boundary-head values used for the general-head boundary conditions; GHBE and GHBW, general-head boundaries on eastern and western limits of simulation area; RP, RC, CP, RI, and QH, riverbed conductance values for river reach cells of Río de La Plata, Río Cibuco, Ciénaga Prieta marsh, Río Indio, and Quebrada Honda creek, respectively]

Applied change	RMSE8	RMSE9	RMSE10	RMSE11	RMSE12
Final calibration	1.08	1.11	0.98	0.79	0.78
10 percent increase in *K*	1.34	1.41	1.37	1.29	1.28
25 percent increase in *K*	2.02	2.10	2.50	2.44	2.41
10 percent decrease in *K*	1.33	1.30	1.68	1.44	1.42
25 percent decrease in *K*	2.61	2.55	3.86	3.57	3.52
10 percent increase in R	1.54	1.45	1.71	1.49	1.52
25 percent increase in R	2.93	2.70	3.38	3.27	3.25
10 percent decrease in R	1.60	1.63	1.53	1.62	1.52
25 percent decrease in R	3.14	3.08	3.41	3.66	3.51
10 percent increase in *Q*	1.23	1.26	1.05	1.04	0.91
25 percent increase in *Q*	1.77	1.77	1.56	1.70	1.47
10 percent decrease in *Q*	1.20	1.18	1.18	0.86	0.96
25 percent decrease in *Q*	1.71	1.61	1.74	1.41	1.54
10 percent increase in *S*	1.08	1.11	1.00	0.78	0.79
25 percent increase in *S*	1.09	1.11	1.03	0.78	0.81
10 percent decrease in *S*	1.08	1.11	0.98	0.79	0.78
25 percent decrease in *S*	1.08	1.11	0.98	0.80	0.78
10 percent increase in BHV of GHBE	1.10	1.12	1.03	0.75	0.81
25 percent increase in BHV of GHBE	1.15	1.16	1.14	0.75	0.89
10 percent decrease in BHV of GHBE	1.09	1.11	0.96	0.85	0.78
25 percent decrease in BHV of GHBE	1.12	1.16	0.96	0.97	0.83
10 percent increase in BHV of GHBW	1.12	1.13	1.03	0.82	0.85
25 percent increase in BHV of GHBW	1.21	1.21	1.15	0.92	0.99
10 percent decrease in BHV of GHBW	1.07	1.10	0.98	0.80	0.78
25 percent decrease in BHV of GHBW	1.09	1.14	0.97	0.86	0.77
10 percent increase in CON of GHBE	1.08	1.11	0.98	0.79	0.78
25 percent increase in CON of GHBE	1.08	1.11	0.98	0.79	0.78
10 percent decrease in CON of GHBE	1.08	1.11	0.98	0.79	0.78
25 percent decrease in CON of GHBE	1.08	1.11	0.98	0.79	0.78
10 percent increase in CON of GHBW	1.08	1.11	0.98	0.79	0.78
25 percent increase in CON of GHBW	1.08	1.11	0.98	0.79	0.78
10 percent decrease in CON of GHBW	1.08	1.11	0.98	0.79	0.78
25 percent decrease in CON of GHBW	1.09	1.11	0.99	0.79	0.78
10 percent increase in RP	1.08	1.11	0.98	0.80	0.79
25 percent increase in RP	1.08	1.11	0.99	0.82	0.81
10 percent decrease in RP	1.08	1.11	0.98	0.79	0.78
25 percent decrease in RP	1.08	1.11	0.98	0.79	0.78
10 percent increase in RC	1.08	1.11	0.98	0.79	0.78
25 percent increase in RC	1.08	1.11	0.98	0.79	0.79
10 percent decrease in RC	1.08	1.11	0.98	0.79	0.78
25 percent decrease in RC	1.08	1.11	0.98	0.79	0.79
10 percent increase in CP	1.07	1.10	0.97	0.81	0.82
25 percent increase in CP	1.06	1.10	0.96	0.82	0.83
10 percent decrease in CP	1.10	1.11	0.99	0.79	0.79
25 percent decrease in CP	1.12	1.13	1.01	0.79	0.79
10 percent increase in RI	1.08	1.11	0.98	0.79	0.78

Table 11. Sensitivity analysis based on root mean square error--Continued

Applied change	RMSE8	RMSE9	RMSE10	RMSE11	RMSE12
25 percent increase in RI	1.08	1.11	0.98	0.80	0.78
10 percent decrease in RI	1.08	1.11	0.98	0.79	0.78
25 percent decrease in RI	1.07	1.11	0.98	0.79	0.79
10 percent increase in QH	1.11	1.14	1.00	0.81	0.79
25 percent increase in QH	1.14	1.14	1.05	0.86	0.81
10 percent decrease in QH	1.09	1.12	0.99	0.80	0.79
25 percent decrease in QH	1.15	1.19	1.03	0.85	0.81
10 percent increase in anisotropy ratio	1.34	1.39	1.37	1.29	1.29
25 percent increase in anisotropy ratio	2.00	2.06	2.49	2.45	2.43
10 percent decrease in anisotropy ratio	1.28	1.27	1.64	1.42	1.40
25 percent decrease in anisotropy ratio	2.45	2.41	3.72	3.48	3.42

SUMMARY AND CONCLUSIONS

A transient three-dimensional ground-water flow model of the water-table aquifer in Vega Alta, Puerto Rico, has been developed using MODFLOW, the finite-difference modular model developed by the USGS (McDonald and Harbaugh, 1988). The ground-water flow model presented in this report simulates the period extending from February 1983 to April 1992. Areal and vertical variations in hydraulic conductivity and hydraulic gradients in the Vega Alta water-table aquifer were estimated from slug tests and water-level measurements conducted in pumping and measurement ports of multiport wells.

The hydraulic gradients obtained from measurement ports and the hydraulic conductivity values obtained from slug tests performed on pumping ports in multiport wells provided information regarding prevalent areal and vertical variations in hydraulic properties in the southern karst uplands, Quebrada Honda karst valley, Río Cibuco alluvial valley, uplands karst plateau, and the coastal plain. The initial distribution of water levels was computed from the water-level contours generated for February 1983 during the beginning of the transient simulation period. These water-level contours were generated using water levels measured for the study area during February 1983. A comparison of ground-water flow velocities among the southern karst uplands, the Quebrada Honda karst valley, and the uplands karst plateau areas was possible through water level and hydraulic conductivity measurements in these multiport wells. This comparison led to the initial assessment of areal and vertical distributions of spatial gradients of hydraulic properties based on the multiport well locations. A calibration process that took into account the general behavior of the aquifer materials transformed this initial assessment into a calibrated ground-water flow simulator, as indicated by a low *RMSE* for all stress periods for which water-level data at wells were available.

The numerical grid designed to develop the ground-water flow model took into account the extent of the freshwater aquifer, assigning appropriate areal variations to the aquifer thickness. Ground-water recharge from rainfall as well as streambed conductance values were derived from a USGS-developed two-dimensional ground-water flow model for the study area. Specific-yield values were calibrated according to the physiographic regions present in the model area. From the Quebrada Honda karst valley north to the karst uplands plateau, the hydraulic conductivity values generally increase, indicating a higher level of karstic dissolution.

The simulated period of the transient ground-water flow model presented in this report was divided in 12 stress periods of variable duration. The last five of these stress periods were chosen to end in January 1991, May 1991, August 1991, January 1992, and April 1992, coinciding with five rounds of water-level measurements performed in the area. The reasonable agreement between the measured and simulated water levels obtained for these five stress periods assesses the reliability of the values assigned to the hydraulic properties that characterize the ground-water flow of the Vega Alta water-table aquifer.

REFERENCES

ARC/INFO, 1992, Environmental Systems Research Institute, version 6.1: Redlands, Calif., ARC/INFO.

Bechtel Environmental, Inc., 1990, Caribe General Electric Groundwater Investigation Report: Bechtel Environmental, Inc., v. 1–5.

Black, W.H., Smith, H.R., and Patton, F.D., 1986, Multiple-level ground water monitoring with the MP system: Proceedings of the Surface and Borehole Geophysical Methods and Ground Water Instrumentation Conference and Exposition, NWWA, Denver, p. 41–61.

Bouwer, Herman, and Rice, R.C., 1976, A slug test for determining hydraulic conductivity of unconfined aquifers with completely or partially penetrating wells: Water Resources Research, v. 12, no. 3, p. 423–428.

Conte, S.D., and de Boor, Carl, 1980, Elementary numerical analysis, an algorithmic approach (3d ed.): New York, McGraw-Hill, 432 p.

Freeze, R.A., and Cherry, J.A., 1979, Groundwater: Englewood Cliffs, N.J., Prentice Hall, 604 p.

Geraghty & Miller, Inc., 1991, Transient electromagnetic geophysical investigation of the freshwater/saltwater interface near Vega Alta, Puerto Rico: Geraghty & Miller, Inc., 12 p.

____1992, A ground-water flow and transport model of the Vega Alta area: Geraghty & Miller, Inc., v. 1–2.

Giusti, E.V., 1978, Hydrogeology of the karst of Puerto Rico: U.S. Geological Survey Professional Paper 1012, 68 p., 2 pls.

Giusti, E.V., and Bennett, G.D., 1976, Water resources of the north coast limestone area, Puerto Rico: U.S. Geological Survey Water-Resources Investigations Report 75-42, 42 p.

Gómez-Gómez, Fernando, and Torres-Sierra, Heriberto, 1988, Hydrology and effects of development on the water-table aquifer in the Vega Alta quadrangle, Puerto Rico: U.S. Geological Survey Water-Resources Investigations Report 87-4105, 54 p.

Guzmán-Ríos, Senén, and Quiñones-Márquez, Ferdinand, 1984, Ground-water quality at selected sites throughout Puerto Rico, September 1982-July 1983: U.S. Geological Survey Open-File Report 84-058, 1 sheet.

McDonald, M.G., and Harbaugh, A.W., 1988, A modular three-dimensional finite-difference ground-water flow model: U.S. Geological Survey Techniques of Water-Resources Investigations, book 6, chap. A1, 586 p.

Monroe, W.H., 1963, Geology of the Vega Alta quadrangle, Puerto Rico: U.S. Geological Survey Geologic Quadrangle Map GQ-191, 1 sheet.

____1980, Geology of the middle Tertiary Formations of Puerto Rico: U.S. Geological Survey Professional Paper 953, 93 p., 1 pl.

NUS Corporation, 1986, Remedial Investigation Report, vol. 1—Vega Alta Site, Vega Alta, Puerto Rico: U.S. Environmental Protection Agency Work Assignment Number 44-2LA1.0, Pittsburgh, Penn., 200 p.

Sepúlveda, Nicasio, 1992, Computer algorithm for the analysis of underdamped and overdamped water-level responses in slug tests: U.S. Geological Survey Water-Resources Investigations Report 91-4162, 20 p.

Theis, C.V., 1963, Estimating the transmissivity of a water-table aquifer from the specific capacity of a well: U.S. Geological Survey Water-Supply Paper 1536-I, p. 332–338.

Todd, D.K., 1980, Groundwater hydrology (2d ed.): New York, John Wiley & Sons, 535 p.

Torres-González, Arturo, and Díaz, J.R., 1984, Water resources of the Sabana Seca to Vega Baja area, Puerto Rico: U.S. Geological Survey Water-Resources Investigations Report 82-4115, 53 p.

Torres-Sierra, Heriberto, 1985, Potentiometric surface of the upper limestone aquifer in the Dorado-Vega Alta area, north-central Puerto Rico, February 1983: U.S. Geological Survey Water-Resources Investigations Report 85-4268, 1 sheet.

van der Kamp, Garth, 1976, Determining aquifer transmissivity by means of well response tests—the underdamped case: Water Resources Research, v. 12, no. 1, p. 71–77.

☆ U.S. GOVERNMENT PRINTING OFFICE: 1996 - 774-216 / 00100 REGION NO. 8